UNIVERSIDADE DE LISBOA

FACULDADE DE CIÊNCIAS

DEPARTAMENTO DE ENGENHARIA GEOGRÁFICA, GEOFÍSICA E ENERGIA

The role of different crucible materials on silicon ingots contamination

Gonçalo Rafael Ferreira Dias

Mestrado Integrado em Engenharia da Energia e do Ambiente

Dissertação orientada por:
João Manuel de Almeida Serra [FCUL], Marisa di Sabatino [NTNU]

2017

Acknowledgments

The present work is part of a common effort between NTNU, SINTEF, IFE - Institutt For Energiteknikk, REC Solar, REC Silicon, Steuler Solar and The Quartz Corp to understand how impurities can be better controlled in high performance multicrystalline silicon for solar cells, gathering more knowledge about their sources, transport mechanisms and the repercussions in cell performance.

Throughout it, the encouragement and guidance of my supervisor at NTNU, Prof. Marisa di Sabatino, has been fundamental. I deeply appreciate her recommendations and the trust put in me for working and learning in Trondheim, at a prestigious university where I have been well received and supported.

I would also like to express my appreciation towards my supervisor at FCUL, Prof. João Serra for his advice and aid on being able to do this dissertation in Norway. Furthermore, I am thankful to Dr. Gaute Stokkan, for his constructive criticism and suggestions, and Dr. Kai Erik Ekstrøm, for his sympathy and time spent when training me on lab equipment. The help from the technical staff of the Department of Materials Science and Engineering and SINTEF has also allowed me to develop skills in sample preparation and heat treatment, making this experience more fruitful and enjoyable.

In addition, I want to mention my friends, colleagues and the good people I have met in Norway for their kindness, opinions and motivation. Lastly, I am extremely grateful to my parents, who have been tireless when providing me with this opportunity.

Resumo

Esta dissertação apresenta uma revisão sobre a influência do material constituinte do cadinho, entre outros componentes, na quantidade de impurezas presente em lingotes de silício multicristalino, obtidos por solidificação direcional. Seguidamente, são apresentadas medidas propostas para a sua mitigação.

Na obtenção de lingotes com baixas concentrações de impurezas, parâmetros como o nível de pureza do cadinho e do filme de nitreto de silício são apontados. O filme é tipicamente aplicado nesta prática de para evitar a adesão do lingote ao cadinho. Juntamente, as condições de escoamento do silício em fase líquida e da atmosfera circundante são assinaladas como relevantes.

Também neste trabalho, é desenvolvido um procedimento experimental através de tratamentos térmicos de pares de difusão, realizado na NTNU. O seu objetivo é a caraterização das difusividades de ferro e titânio num cadinho comercial de nitreto de silício. Este é uma alternativa reutilizável que tem vindo a ser proposta aos mais estabelecidos cadinhos de quartzo, que sofrem transições de fase na gama de temperaturas do processo, levando a uma súbita redução de volume que põe em causa a sua integridade. Para além do nitreto de silício permitir o crescimento de vários lingotes, é ainda, tipicamente, melhor condutor de calor. Tais aspetos levam a considerar uma redução dos custos de produção dos lingotes, do ponto de vista do investimento em cadinhos, bem como do gasto energético durante o processo.

É, porém, necessário assegurar que as células fotovoltaicas sintetizadas a partir destes lingotes não são afetadas no ponto de vista da sua eficiência de conversão. Face a células de silício monocristalino, tem vindo a ser demonstrado que as perdas em silício multicristalino se devem à presença de defeitos na rede cristalina, que promovem a recombinação dos portadores de carga, principalmente sob a forma de deslocações e impurezas eletricamente ativas, onde se destacam o ferro e outros metais de transição.

Por forma a reduzir a sua presença, diversas práticas são aplicadas durante a sintetização de matéria-prima e componentes auxiliares de elevada pureza, no decorrer da recristalização e nas seguintes etapas. No contexto do trabalho experimental, o mecanismo de difusão de impurezas do cadinho para o silício ocorre durante a solidificação direcional. O estudo das difusividades no cadinho, por intermédio de pares de difusão, evita a deposição do filme antiaderente, assim como os gastos relativos à obtenção de lingotes.

Estes são constituídos por uma amostra do cadinho, em contato com outra de silício monocristalino. Os materiais foram facultados pela STEULER SOLAR e o SINTEF, respetivamente. Para se manterem unidos durante o tratamento térmico, os pares são envolvidos com fio de kanthal, numa fase preliminar, permitindo o estudo do titânio, enquanto que para o ferro este fio é substituído por um peso de silício, obtido da porção do lingote de Czochralski, de onde se cortam as referidas amostras.

As espessuras adequadas para as amostras de silício foram estimadas de acordo com a 2ª lei de Fick para temperaturas até 1350 ºC, com base na difusividade e solubilidade dos elementos referidos, descrita em silício por vários autores. Todavia, tal não se verifica para nitreto de silício, para o qual as publicações geralmente abordam filmes, resultantes da deposição química de vapor em substratos de silício, onde atuam como barreiras de difusão. Consequentemente, a sua estrutura cristalográfica difere consideravelmente da cerâmica em análise, levando a por em causa a sua aplicabilidade neste caso de estudo. Além disso, estes coeficientes ainda não foram publicados tanto para ferro, como para titânio.

Após o tratamento térmico, os perfis de concentração das impurezas são analisados em corrente contínua através de espetrometria de massa por descarga luminescente (GD-MS), ao longo da espessura das amostras de silício. O mesmo não é feito para o cadinho que, por tratar-se de um isolante elétrico, requer outro método não disponível no decorrer dos trabalhos. Deste modo, com um ajuste à 2ª lei de Fick é

possível estimar quantidade de impureza transportada para a amostra de silício, a partir da qual se obtém indiretamente o coeficiente de difusão na cerâmica. Eventualmente, pode também ser verificado o limite de solubilidade e a difusividade à temperatura do tratamento.

Outro aspeto preponderante para determinar a difusividade no cadinho, é sua composição elementar, principalmente no que toca a ferro e titânio. A análise por espetrometria de massa por plasma acoplado indutivamente (ICP-MS) adequa-se ao limite de deteção exigido, pelo menos na ordem das ppbm. Todavia, a dissolução do nitreto de silício em soluções de ácido nítrico e fluorídrico resulta numa quantidade de sólidos superior à imposta pela técnica. Por esse motivo foi considerada a ficha técnica do fabricante.

Os requisitos para estudos semelhantes com pares de difusão são sublinhados, seguidos de uma melhor descrição do mecanismo de difusão de titânio no cadinho. Os resultados sugerem que o procedimento experimental ainda carece de ajustes por forma a estudar ferro com sucesso, uma vez que há indícios de contaminação por fontes indesejáveis.

A observação das amostras aponta para a presença duma fonte desconhecida, desde o instante anterior ao tratamento térmico. Esta possibilidade surge já que a difusão para as amostras ocorre a uma taxa muito mais rápida com temperaturas elevadas, do que durante o período de arrefecimento. Questionando se os refratários no interior do forno fossem a fonte, a contaminação deveria ser mais percetível nos tratamentos com períodos mais longos, devido à exposição prolongada. No entanto, este não é sempre o caso. Como causas mais prováveis assinalam-se a hipotética presença de partículas com ferro nas superfícies do laboratório, onde se realizam outros tratamentos térmicos. O contato com os pares de difusão ocorreu antes do aquecimento, devido às medidas de segurança impostas pelas elevadas temperaturas, justificando o uso de luvas de proteção e pinça.

Um método de diferenças finitas foi criado para estimar a difusividade de titânio a partir dos perfis de concentração em função da espessura. Este simula o efeito das condições de tratamento no par de difusão, de acordo com a 2ª lei de Fick, até que a quantidade de titânio encontrada na amostra de silício corresponda à contaminação estimada a partir dos valores detetados pela técnica de pulverização catódica. No entanto, a importância duma análise de reprodutibilidade emerge da possibilidade de existir uma fonte de contaminação não considerada e da ocorrência de fraturas nas amostras do cadinho, coincidentes com o uso do fio de kanthal.

Partindo das especificações do fabricante para a composição do cadinho (1 ppmm para titânio), três cenários são propostos para obter coeficientes de difusão de titânio. Um primeiro cenário, de estimativa por defeito, considera a concentração média de titânio no silício segundo as medições de GD-MS e assume regiões não detetadas como zeros. Deste calculam-se coeficientes de difusão entre 10^{-15} e 10^{-13} m^2/s, na faixa de 1200 a 1350 °C. Isto significa que a difusão de titânio no cadinho é provavelmente superior a esses valores, caso o seu conteúdo no cadinho se situe entre 0,5 e 1,5 ppmm. Tal deve-se à quantidade de impurezas não contabilizada numa secção junto à interface, removida durante a pré-pulverização, que visa excluir contaminantes que possam ter vindo a depositar-se após o tratamento térmico. Um segundo cenário usa o primeiro valor detetado, o mais próximo da interface, para descrever pontos em falta junto à superfície, sendo conservador relativamente ao perfil decrescente sugerido pela 2ª lei de Fick. Finalmente, o terceiro recorre a um ajuste dos perfis de GD-MS com a solução particular desta lei para uma fonte inesgotável. De ambos resultam difusividades entre 10^{-14} e 10^{-12} m^2/s, no mesmo intervalo de temperatura.

Palavras-chave: solidificação direcional; impurezas; difusão; nitreto de silício; silício multicristalino.

Abstract

This work reviews the role of crucibles made from different materials in the addition of impurities to multicrystalline silicon ingots produced by the directional solidification technique. Moreover, it comprises efforts made on the characterization of the solid-state diffusion mechanism of iron and titanium impurities in a slip-cast silicon nitride crucible, as a substitute for the currently used silica crucibles. This is done by heat-treating diffusion couples at NTNU, with samples from the crucible, without coating, behaving as an impurity source, and from Czochralski silicon, provided by SINTEF.

Glow discharge mass spectrometry (GD-MS), also facilitated by NTNU, is employed to obtain concentration vs depth profiles of the impurities. By this means, the intent is to figure out indirectly how the impurities diffuse inside the crucible material.

The requisites for future similar diffusion couple studies are underlined, followed by a better understanding of the titanium diffusion in this silicon nitride crucible. A finite difference method, simulating the effect of the treatment conditions in the diffusion couple, solves Fick's 2nd law until the resulting amount of titanium found in the silicon sample matches the contamination estimated through the sputtering technique.

Challenges regarding crucible cracking and eventually unaccounted contamination call for a reproducibility analysis, preferably comprising annealing periods longer than 1 hour at 1200 ºC or higher.

Relying on deductions from the manufacturer's specifications for the crucible's composition, three scenarios are proposed to achieve diffusivity estimates for titanium in the crucible material. A first low end scenario, considering the average titanium concentration in silicon, based on the GD-MS measurements and assuming non-detected regions as zeros, suggests diffusion coefficients among, at least, 10^{-15} and 10^{-13} m^2/s, in the range of 1200 to 1350 ºC.

A second scenario uses the detected value nearest to the interface to describe the missing data near the surface, being conservative regarding the decreasing profile suggested by Fick's 2nd law. Finally, the third resources to curve fitting of the GD-MS profiles with the particular solution of this law for an inexhaustible source. Both lead to diffusivities of 10^{-14} and 10^{-12} m^2/s, for the same temperature interval.

Keywords: directional solidification; impurities; diffusion; silicon nitride; multicrystalline silicon.

Table of contents

List of tables

List of figures

1 Introduction

1.1 Motivation

The objective is to characterize the impact of different crucible materials on the contamination of directionally solidified, p-type silicon ingots and study the solid-state diffusion of iron and titanium in a commercial reaction bonded silicon nitride (Si_3N_4) crucible, a substitute for fused silica crucibles, currently used in directional solidification (DS).

Silica crucibles are often limited to a single use, since they crack due to a phase transformation while cooling down. Si_3N_4 crucibles however, can withstand reutilization, present a thermal expansion coefficient more similar to silicon and are more thermally conductive, which may lessen the energy requirements.

If the crucible is put in contact with other materials, e.g. molten and solid silicon, it may act as a contamination source. When defects such as transition metals are introduced in the silicon crystal lattice, they can enable trap levels between the conduction and valence bands of the semiconductor, promoting the recombination of light generated charge carriers and leading to a curtailment in the conversion efficiency. So far, the knowledge for the diffusion of impurities in Si_3N_4 is lacking when compared to more widespread materials. Therefore, achieving data regarding this crucible can support its application in the photovoltaic industry and provide more information for future studies.

1.2 Aim of this work

The study aims to review the current literature on the contamination of DS ingots originating from different crucibles and to determine diffusion coefficients for Fe and Ti in the stated crucible for a range of temperatures by heat treatment of diffusion couples, with Si_3N_4 and monocrystalline silicon from a Czochralski ingot, according to Fick's 2^{nd} law. This method works around ingot casting, while still aiding the description of the contamination in the solid phase of the ingot during crystallization and subsequent cooling. Concentration vs depth profiles are obtained through direct current - glow discharge mass spectrometry for the silicon sample. The data is taken as an indirect measurement of the amount of impurities originating from the crucible. The resulting profiles are analysed in order to estimate the diffusivities.

2 Theory

2.1 Silicon solar cells

The Earth's crust is mainly constituted by oxygen, followed by silicon, representing 26% of its weight. Its free form does not occur in nature, being instead associated with oxides and silicates, such as in quartz and sand. For solar cells, silicon is preferred with low impurity amounts. Currently, the Siemens deposition can yield 9N (99.9999999%) electronic grade silicon, although purity grades of 6-7N [1] are also produced by feeding monosilane (SiH_4) into a fluidised bed reactor with heated silicon particles. The gas is continuously decomposed, covering each particle's surface with more silicon, increasing their diameter. These granules can be extracted and added to the bed continuously, while the Siemens deposition is batch reliant, allowing decreased costs [2].

The current methods for silicon feedstock recrystallization are quite extensive and often present specific designs. Nonetheless, silicon based photovoltaic (PV) cells can be solidified in monocrystalline (mono-Si), multicrystalline (mc-Si) or amorphous (a-Si) forms. Mono-Si is presently the most efficient solution (25.3% - FhG-ISE), above mc-Si (21.9% - Fraunhofer-ISE), while excluding concentrator or heterostructure technologies [3].

Single crystal cells derive from the Czochralski (Cz) process, where an ingot is grown by slowly pulling a previously dipped seed in molten silicon. This production rate can be about 2 kg h^{-1}, making the directional solidification of mc-Si an attractive method, since its overall productivity rounds 7 kg h^{-1}. Other advantage of using DS is lower energy consumption, about 10 kWh kg^{-1} with Cz surpassing it by more than three times. This incentivizes interest towards mc-Si solar cells due to cost-effectiveness and it is, in fact, the highest market share holder (about 70% of the global PV production in 2015) [4].

To stay competitive, mono-Si needs improvements in the energy demanding manufacture or in the solar cells conversion efficiency, where an increase of 1% could reduce the cell production cost about 7%. The efforts usually focus around hot-zone designs, multiple charges, cheaper and long-lasting crucibles and reduced argon consumption [5].

2.2 Directionally solidified silicon

DS follows the principles of the Bridgman crystallization and is how most mc-Si ingots are produced, in quartz crucibles coated with a mix of α and β-Si_3N_4 to avoid ingot sticking. This method consists in inductively heating the silicon charge inside the crucible, followed by a nucleation stage starting at the bottom of the crucible, which is regulated by slowly lowering the crucible out of the hot zone. Mean grain size increases along the ingot height, as result of the competitive growth between adjacent grains, parallel to the thermal gradient (Figure 2.1). Other techniques are also used to make the liquid silicon solidify in a single direction due to a temperature gradient [6].

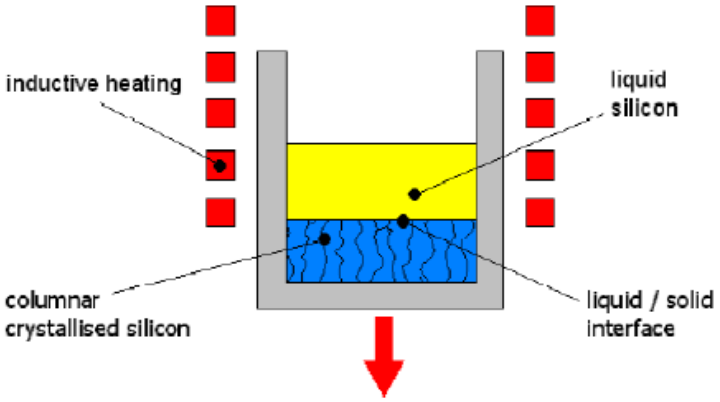

Figure 2.1 - Directional solidification of a mc-Si ingot by the Bridgman technique [6].

Defects in mc-Si from DS can originate from the feedstock, crucible and coating or due to process conditions. These can induce dangling bonds and deep states in the silicon bandgap, promoting the recombination of light generated charge carriers and, therefore, curtailing the conversion efficiency [7].

Dislocations can be found in clusters formed at grain boundaries, spreading into considerable areas of the ingot due to thermal stress while solidifying [6]. They constitute the main source of recombination centres, while stacking faults and twins are usually negligible [7]. Engineering techniques to decrease their amount, during and after crystal growth, were summarized in [7]. The correlation between grain size and minority carrier lifetime is also uncertain, since the grain diameters in mc-Si are usually in the order of mm to cm, larger than the typical minority carrier diffusion length of 100 μm [7].

High performance multicrystalline silicon (hpmc-Si) focuses on generating smaller grains, in the mm^2 range, by controlling the nucleation stage. These provide relaxation under thermal stress, supressing the generation and proliferation of dislocations [8]. Fewer dislocation clusters, which improve the gettering efficacy [9], a high fraction of random angle boundaries and a lower twin proportion, contribute to an increase of at least 0.5% in efficiency over traditional mc-Si [10].

2.3 Contaminants in mc-Si

The lower efficiency in mc-Si solar cells, comparatively to mono-Si, is often associated to the limited charge carrier diffusion length, consequence of the increased recombination effect brought by crystalline structural defects and a higher amount of electrically active impurities.

The prevalent impurities are oxygen, carbon and nitrogen [11], but metallic atoms are also common. Sometimes these associate with other defects, aggravating the electrical performance of the cells even further [7], so that the studies focus not only in reduction of the impurity amounts, but also on the density of crystalline defects. As the presently available solar grade silicon feedstock and argon gas, which is employed to provide an inert atmosphere, meet the high purity requirements, the crucible and its coating are regarded the primary sources of contamination for DS mc-Si ingots [12]. Boron doped ingots typically present low minority carrier lifetimes in the top, edge zone and bottom (Figure 2.2):

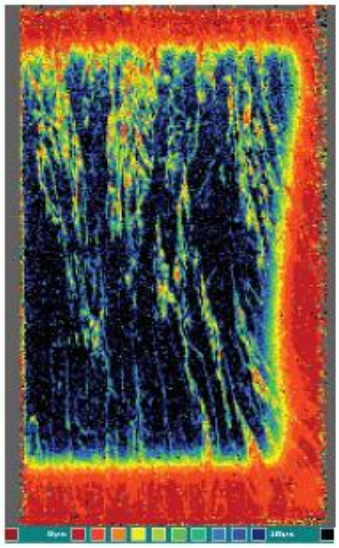

Figure 2.2 - Lifetimes in a cross section of a mc-Si ingot. The red colour highlights areas with shorter lifetimes [13].

At the top, the reduced lifetime is caused by the segregation of transition metals [14], resulting from their typically higher solubility in liquid rather than in solid silicon. As the solid-liquid interface progresses, the concentration in the melt increases, carrying the majority of the impurities towards the top of the solidified ingot [15]. The segregation of substitutional impurities (B and Al) has been reported to depend on the grain morphology, according to Scheil's equation (presented in page 7), whilst the melt and the grain boundaries were described as diffusion enhancing paths for interstitial impurities (Fe, Ti, Cu, and Ni), increasing their effective segregation and concentration in irregular grains [16].

Recombination activity at the edges is given by dissolved or diffused impurities, from the crucible walls and coating [14]. When these are kept at high temperatures, faster diffusers, including Fe, are known to migrate into the solid phase [17]. While cooling, both contaminants can spread further into nearby regions, depending on the cooling rate and respective diffusion coefficients [18]. The affected zone also broadens towards the bottom (see Figure 2.2), implying that the earlier solidified sections are subjected to impurity diffusion for longer periods.

Interstitial iron, as well as iron complexes, introduce deep levels in the band gap, increasing the carrier recombination rate. However, the first is more detrimental. Dissolved iron in boron doped silicon primarily occurs as interstitial iron - at temperatures above 200 ºC and boron concentrations below 10^{16} at/cm^3 - and Fe-B pairs - at room temperature and boron concentrations above 10^{14} at/cm^3. Interstitial iron precipitates on high angle grain boundaries and dislocations by internal gettering, depleting adjacent areas [14]. In the border region, the dislocation density is much lower than in the vicinity, therefore the content of Fe-B is significantly higher, possibly explaining the low lifetime [7].

A reduction in contamination of fast or moderately fast diffusers, such as Fe, can be achieved by gettering techniques. However, posterior removal is more difficult for slow diffusers incorporated in the ingot, like Ti [13].

In the bottom, lifetime is often affected by oxygen-related defects [14]. Single interstitial oxygen atoms are not electrically active [11], but oxygen precipitates damage the electrical performance, act as internal gettering sinks for other impurities and affect the mechanical properties of the silicon wafers [19]. Oxygen and carbon incorporation has been described to occur according to the following sequence [19]:

i. Dissolution of the silica (SiO_2) crucible by the melt, introducing oxygen and silicon atoms;
ii. The dissolved oxygen reaches the gas/melt interface, evaporating as silicon monoxide (SiO);
iii. The argon gas flow brings SiO to react with the graphite components in the furnace, producing gaseous carbon monoxide (CO);
iv. These return to the melt surface by diffusion or convection, followed by dissolution;
v. Lastly, the dissolved C and O atoms are segregated into the crystal.

Although there are several furnace configurations, the cited graphite components participating in the previous process are usually the heaters, crucible covers and a box that serves to mechanically stabilize the silica crucible, as it softens above 1200 ºC [20], before reaching the silicon melting temperature [21].

The concentration of carbon can influence oxygen precipitation, although, it has been demonstrated that carbon is not detrimental for recombination in substitutional sites [19]. On the other hand, nitrogen has been reported to result from the partial dissolution of the silicon nitride coating by the liquid silicon. It may form lifetime limiting complexes with oxygen near the crucible walls and bottom [11], even though it is usually electrically inactive [19].

The melt flow influences their distribution and also whether the solubility limit of carbon and nitrogen is reached. At that stage, precipitation of silicon carbide (SiC) and Si_3N_4 can occur [11], eventually promoting the nucleation of new grains [19]. SiC can cause severe ohmic shunts in solar cells and sometimes grow several mm along the direction of crystallization, therefore harming several wafers. Due to their hardness, they can also affect the sawing process and the production yield. Si_3N_4 precipitates are insulating, but might be decorated by impurities and surrounded by decorated dislocations, affecting the electric performance of solar cells [21].

2.3.1 Schockley-Read-Hall recombination

When introduced in the silicon crystal lattice, defects can enable trap levels between the conduction and valence bands of the semiconductor.

Research in interstitial titanium has identified an acceptor level at $E_c - (0.08 - 0.09)$ eV with the charge state $Ti_i^{-/0}$ and two donor levels at $E_c - (0.27 - 0.28)$ eV with $Ti_i^{0/+}$ and at $E_v + (0.25 - 0.28)$ eV with $Ti_i^{+/++}$. Interstitial iron introduces a donor level at $E_v + (0.39 - 0.40)$ eV for the charge state $Fe_i^{0/+}$ and in p-type silicon, mobile atoms with positive charge are captured by negatively charged substitutional acceptor atoms to form iron-acceptor pairs. The frequent Fe-B pairs introduce a donor level at $E_v + 0.19$ eV [22]. These states promote an indirect recombination mechanism of electron-hole pairs, designated as Shockley-Read-Hall (SRH), where an electron (or hole) is captured at the trap level and a hole (or electron) moves into the same energy level, before the first carrier thermally returns to its previous state. Figure 2.3 illustrates the recombination in four parts [23]:

i. Electron capture – an electron from the conduction band moves to the trap level;
ii. Electron emission – an electron from the trap level jumps to the conduction band;
iii. Hole capture - an electron from the trap level moves to the valence band (the hole disappears);
iv. Hole emission – an electron from the valence band jumps to the trap level (a hole is formed).

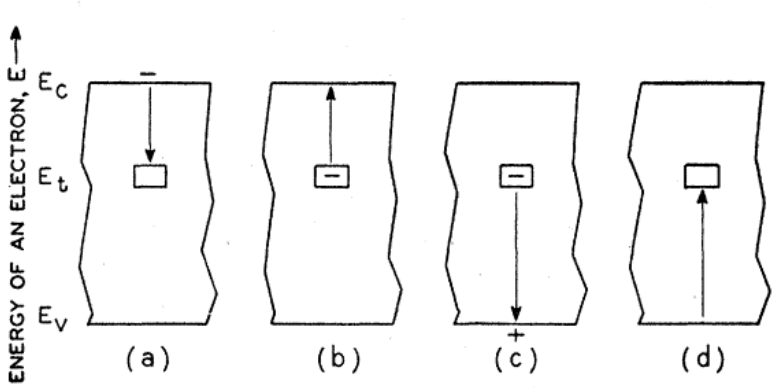

Figure 2.3 - Scheme of the processes in SRH recombination [23].

When light is absorbed in the solar cell, within or at a certain distance from the depletion region, electron-hole pairs are generated. For a p-n junction in a steady state, this depletion region is formed by the diffusion of holes towards the n-doped side (excess of free electrons), leaving their respective negative acceptors behind, whilst electrons move in the opposite sense, towards the p-doped side (excess of holes), also leaving their respective holes. These diffused oppositely charged carriers eventually meet in their way across the junction and recombine, creating an interface without free holes and electrons, designated depletion region (Figure 2.4).

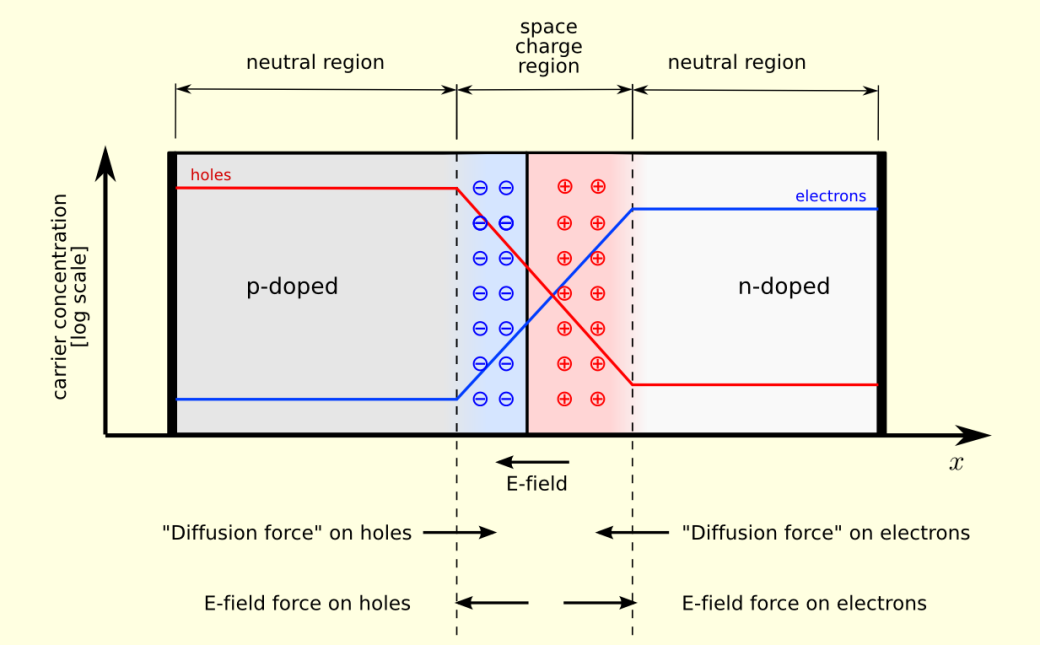

Figure 2.4 - A p–n junction in steady state with no applied voltage. The grey regions represent neutrally charged parts of the semiconductor [24].

The remaining charges stay separated by this region, since they create an electric field that provides enough opposing force to stop recombination and is responsible for the built-in voltage [25].

To contribute to the useful current, these carriers must then be collected by the p-n junction. If the pair splits within the depletion region, the electric field quickly pulls them apart and collection occurs. However, in the other sections the charge carriers must diffuse towards the p-n junction. The average length they are able to cross within the material until recombining is termed diffusion length, a parameter influenced by carrier lifetime, which is partially affected by the recombination rate. Therefore, the

presence of SRH recombination centres, diminishes the likelihood of a carrier reaching the junction and consequently decreases the conversion efficiency of the solar cell [26].

2.3.2 Impact of Fe and Ti in feedstock for DS mc-Si

Several ingots were prepared to evaluate the impact of transition metals on solar cell performance, including iron and titanium [27]. A reference ingot was doped with boron (0.13 ppmw) and compared to others, to which certain amounts of impurities were added intentionally. Unintentional contamination was assumed to be minimal and the same for every ingot, since high purity polysilicon feedstock, fused quartz crucibles and silicon nitride coating were used.

Fe was introduced before melting with the feedstock but Ti was added after complete melting, given its susceptibility to form oxides at lower temperatures.

The contamination levels were chosen targeting typical amounts present in silicon ingots. Two ingots, labelled Fe 50 and Fe 200, were grown with added concentrations of 53 ppmw and 200 ppmw of Fe, respectively. Similarly, another was prepared with 9.3 ppmw of Ti and labelled Ti 10. Wafers were cut from selected positions of the ingots and went through similar state-of-the-art solar cell industrial processing, regardless of the contamination.

The experimental data was fit successfully to two validated models based on Scheil's distribution[1], to describe the whole ingots. Cell performance was determined as a function of base-bulk and emitter-bulk recombination, as shown in Figure 2.5.

All contaminated cells, including others prepared with Cr, Cu, and Ni, have performances comparable to the reference in the 40-70% ingot height section. The regions below (ingot bottom) and above (ingot top) present lower efficiencies.

Contaminated ingots present an extended degradation near the bottom, while in the reference it reaches about 10% of the height. In a previous report for Fe 50 [28], smaller grains and highly dislocated areas were detected. This work went further, demonstrating that it also happens with Cr, Ni and Cu, with higher feedstock concentrations accentuating the degradation. The performance at the top of the ingots also suffers due to this increase and is result of the phenomena described above. Ti was so detrimental to the efficiency that the curtailments were difficult to discern. Based on the analysis, it was summarized that 8 ppmw of Cr, 11 ppmw of Fe, 0.1 ppmw of Ti, 4 ppmw of Ni or 8 ppmw of Cu resulted in solar cells with similar performances when prepared in the same conditions, regardless of the influence of other parameters. The lower amount of Ti illustrates the need to avoid contamination of the ingot, given the limited getterability brought by the slow diffusivity.

[1] Solute concentration profile along the ingot, according to the following equation, which describes the segregation during solidification, assuming that no diffusion exists in the solid phase once it is formed, infinitely fast diffusion occurs in the liquid phase and that the solid-liquid interface is in equilibrium:

$$C_s = k\, C_m (1 - f_s)^{k-1}$$

C_s and C_m stand for the concentration in the solid phase and in the melt, respectively, k is the effective segregation coefficient and f_s represents the mass fraction of the melt being solidified [109].

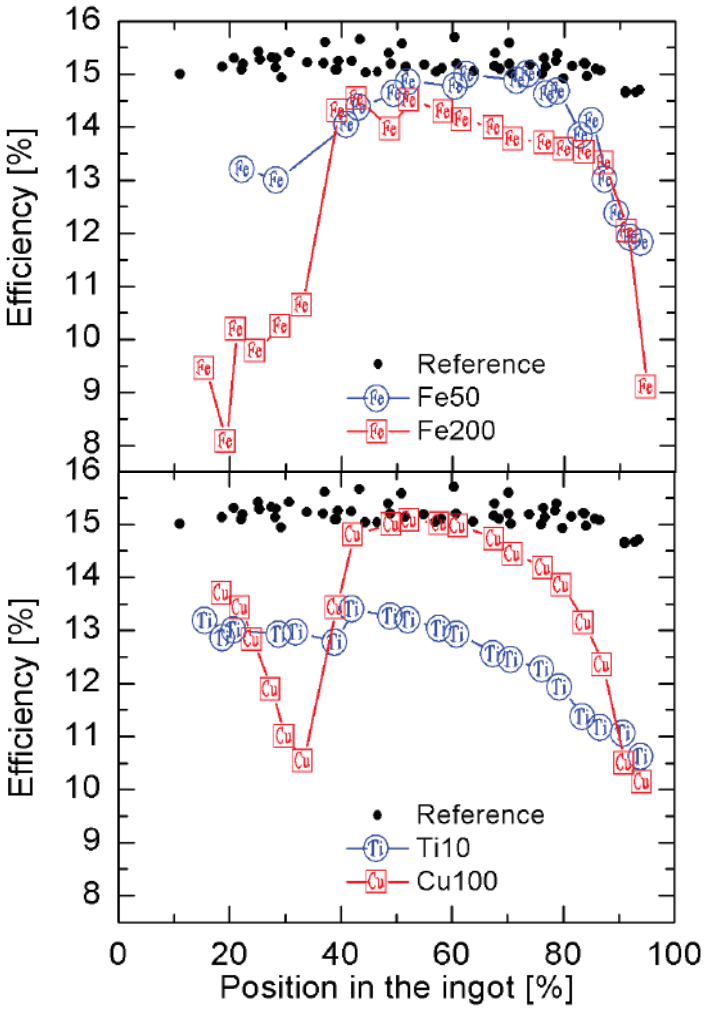

Figure 2.5 - Solar cell efficiency versus ingot position from the bottom: a) Cells from the ingots contaminated with 53 and 200 ppmw of Fe; b) Cells from the ingot contaminated with 10 ppmw of Ti. Cu 100 was also studied in the work, an ingot contaminated with 100 ppmw of Cu (adapted from [13]).

2.4 Directional solidification crucibles

2.4.1 Silica

As of the day, silica crucibles, also often designated as quartz or amorphous silica, are the most used in solar cell manufacture, due to the requirements put on by the high melting point (1412 ºC) of silicon, the reactivity of its molten phase, the heat induced stress and the availability of high purity feedstock [29].

They can be synthesized by many procedures, most of them confidential, especially for crucibles not used for directional solidification. For DS crucibles, the chain starts at the extraction of high purity crystalline quartz, usually followed by processing to increase this purity even further. The sand is electrically fused into silica glass which is afterwards turned into a powder that is sintered, meaning that it is mixed with water and a binder to form fused silica slurry [30]. The slurry is moulded and goes through several moisture absorption steps and annealing at high temperatures finalizing the production of the crucibles with the aspect seen in Figure 2.6.

Figure 2.6 - Fused silica ceramic crucible manufactured by SOLAR CERA Co., Ltd. for directional solidification of mc-Si [31].

Although in Cz production the ingot is not contact with the crucible, that does not happen for DS. It solidifies in contact with silica, which might be wetted by the molten silicon, creating such a strong adherence, that the crucible must be broken to free the contained ingot (Figure 2.7).

Figure 2.7 - A small mc-Si ingot grown in a fused silica crucible without coating. The wetting by molten silicon caused considerable sticking [32].

Furthermore, silicon has a higher thermal expansion coefficient in comparison with silica, which while cooling translates into a more pronounced shrinkage in silicon, than in the crucible. If simultaneously met by wetting, both may induce enough stress to form cracks in the ingot [33]. To avoid this, it is a common practice to apply a uniform coating of silicon nitride (α or β-Si_3N_4), with specific particle size and distribution, that decreases the wetting effect and also lowers the contamination from the crucible. The latter justifies its use in crucibles for Cz pulling, in order to achieve better quality ingots [29].

Another factor contributing to crucible failure while cooling is the phase transformation occurring in silica. In the melting stage, with temperatures over 1470 ºC, or others depending on the pressure, part of the silica is transformed from a glassy α-quartz phase into a more stable layer of another silica polymorph in those conditions, β-cristobalite (Figure 2.8). This layer has a cubic crystal structure and a melting point of 1713 ºC, above the peak registered in the furnace, aiding the integrity of the crucible. In the post-solidification cooling, this phase undergoes a new transition, from β to α-cristobalite, with a tetragonal structure, leading to a decrease in volume of around 5% and cracking the layer. In normal conditions, the crucible also deforms due to the cooling stage, both contributing to break the crucible so that it cannot be reutilized [29, 34].

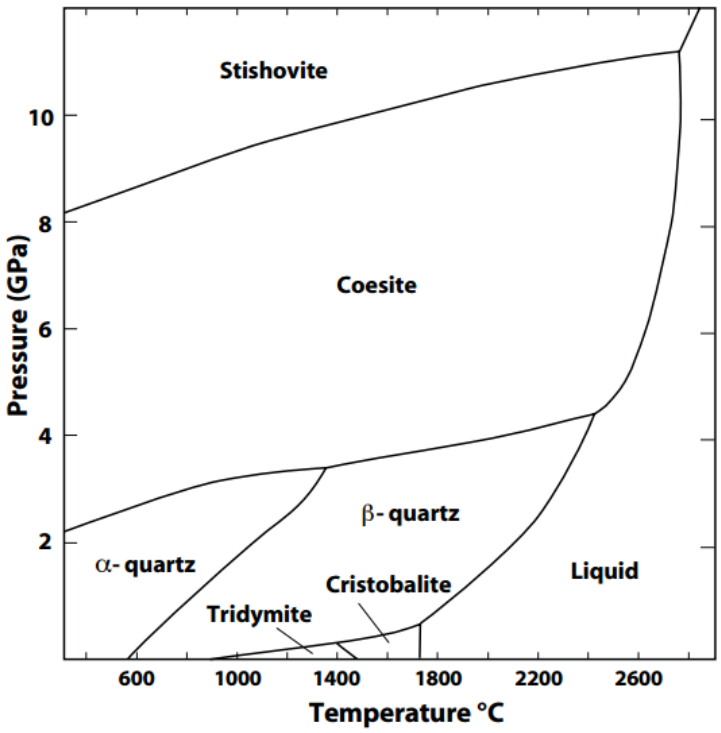

Figure 2.8 - Phase diagram of the silica polymorphs, based on Swamy and Saxena (1994) [35].

2.4.1.1 Decreasing contamination during DS in SiO_2 crucibles

Several efforts accounting for O and C contamination in DS mc-Si have been published, considering for instance heater positioning and heating power, crucible rotation, argon atmosphere pressure and crucible covers. In addition, the role of crucible and coating purity level and the effect of an alternating magnetic field on metallic elements distribution have been analysed.

Melt convection and diffusion are said to be relatable to the oxygen distribution, both in the silicon melt and ingot [36]. A simulation was carried, suggesting that melt content would be smaller for a side heating system, as opposed to a system with only top heating. This was explained to be consequence of an upwards melt flow near the crucible wall when side heating is used. The dissolved oxygen from the silica crucible quickly reaches the melt surface, followed by evaporation [37].

Another numerical study refers to the influence of the temperatures inside the furnace, during the holding phase, on the melt contents of carbon and oxygen. An increased temperature enhances oxygen evaporation from the melt surface, promoting the reaction of SiO with the graphite components, forming CO. If this gas is not drawn out before reaching the liquid silicon, the carbon content will be higher. An accordingly warmer crucible also accelerates the oxygen dissolution by the melt. This increase is not compensated by the enhanced evaporation rate, leading to a superior oxygen amount in the molten phase. Hence, the furnace temperature should be kept as low as possible to minimize the contamination of the ingot by these elements [38].

The effect rotation speed of the crucible rotation on oxygen concentration was also studied numerically [36, 39] and reported in a cylindrical ingot, with 10 cm of diameter and height [36]. The results show that increasing crucible rotation leads to higher oxygen content in the melt, when taking into account the balance between evaporation from the melt surface and crucible dissolution. The evaporation slows down at a quicker rate than the dissolution, so that the oxygen present in the melt increases [39].

Regarding the oxygen distribution in the cylindrical ingot, increasing crucible rotation yields higher concentrations near the top and middle of the ingot, although the distribution should be inhomogeneous among the radial direction. When an ingot was grown at a rotation rate of 1 rpm, the oxygen concentration was homogenized throughout the radius and minimized in the whole ingot, in comparison with another prepared with a rotation rate of 30 rpm [36].

The use of a crucible cover was suggested to reduce the carbon contamination. Based on the multiple previous numerical models for the transport of O and C in DS [40], comprised a transient global simulation of these mechanisms in the melt, furnace atmosphere and the segregation during the solidification, to estimate the impurity distribution in an industrial-size ingot. The numerical predictions illustrated that applying an inert coating to a pure graphite cover could reduce the C concentration in the ingot by about 60%, although there was no significant difference for oxygen. Afterwards, comparisons were made with the C concentration in a prepared ingot, agreeing to a reasonable extent with the simulation results [40]. Additionally, cover usage was reported to diminish the oxygen amount near the top of the ingot, due to an enhanced gas flow promoting the evaporation of oxygen from the melt surface. This was concluded accounting a gradually decreasing distribution, from top to bottom, obtained without cover [19].

Other numerical analysis, verified experimentally, sought to explain the influence of pressure in an industrial furnace. It was found that it affects the argon flow above the melt surface, altering the transport of the SiO and CO gases. Lower pressure yields less O concentration in the grown ingot, while for C it shows a decreasing trend until 200 mbar. For lower pressures, it starts increasing due to CO diffusion through a gap between the crucible and respective cover, present in this furnace. It is then worthy to determine at what point the pressure may be decreased avoiding drawbacks [41].

Not only oxygen is introduced in the melt by dissolution, but also nitrogen and other impurities are likely to be dissolved or diffuse out from the coating and crucible [20]. Addressing crucible and coating purity levels, [15] elucidated that this property is relevant for minority carrier lifetime in the ingot, with experiments depicting a doubled lifetime when a highly-pure quartz crucible and coating were chosen instead of the industrial standard. Applying a sufficiently thick layer of high-purity silica on standard-purity crucible, prior to the deposition of silicon nitride coating, may provide a diffusion barrier and thence improved lifetime measurements. Other configuration was tested with a silica film deposited over of the silicon nitride coating, aiming to supply producers with already coated crucibles. The silicon melt was able to dissolve more oxygen, due to contact with the silica coating, leading to ingots with acceptable lifetimes and higher oxygen content [15].

Increased carrier lifetimes were also achieved in ingots grown with high-purity silica crucibles, as opposed to standard industrial crucibles, using similar silicon nitride coatings. The thickness of the low-lifetime edge region was decreased and the improved regions coincided with lower concentrations of interstitial iron. The Fe content in the crucible seemed to influence diffusion from the silicon nitride coating, determining whether it behaved as an infinite source, for the standard crucible, or depletable source, when using the high-purity alternative [12].

At last, in research done for metallurgical grade silicon, multicrystalline ingots were obtained with and without an alternating magnetic field during an industrial DS process. The less contaminated areas of the ingots showed lower concentration of metallic impurities when the alternating magnetic field was used, since it induced a convection capable of limiting the diffusion of those impurities in the melt, resulting in decreased effective segregation coefficients [42].

The stated cons for fused silica crucibles brought attempts to find alternatives that may be reused in DS, ensuring high purity, low chemical reactivity with molten silicon and a thermal expansion coefficient that does not generate mechanical tensions between ingot and crucible while cooling down. The research started decades ago, with interest in many materials, some among them were graphite crucibles coated with SiC or Si_3N_4 [43], moulded graphite sheets coated with silicon oxynitride [44], Si_3N_4 crucibles [33, 45, 46, 47] and recently a composite of Si_3N_4 and SiO_2 [48].

The reports on these alternative crucible materials for the DS of silicon ingots do not address the contamination by distinct elements, placing more focus on crystalline structure and resistivity analysis, hindering the comparison with silica crucibles and their role on the electrical performance of the resulting ingots. The graphite crucibles [43, 44] refer to earlier stages of development in the industry, both in terms of material purity and solidification technique. Meanwhile, the composite of Si_3N_4 and SiO_2 [48] comprises a simulation of the growth process, according to the thermophysical properties of the crucible, and photoluminescence analysis of the grain structures from prepared ingots. Hence, besides SiO_2, most knowledge comprises Si_3N_4 crucibles.

2.4.2 Silicon nitride

The wide array of configurations aiming to achieve desirable characteristics is evident for quartz based products at our disposal these days. Silicon nitride is not different, as many routes can be taken to meet requirements and multiple inventors came up with their own versions. For this subject, interest is turned towards Si_3N_4 options who can fulfil the previously enounced requirements.

Most often, reaction bonded silicon nitride (RBSN) is selected for fabrication of crucibles, as these can be produced without requiring a binding agent, thereby avoiding a reported contamination source [20]. It is produced by casting a slurry with silicon powder and heating it in a controlled nitrogen atmosphere at around 1200 ºC [49]. Nitrogen permeates the pores between the grains and reacts with the silicon. Afterwards, the temperature is increased close to the silicon melting point. The process can take up to two weeks, resulting in a ceramic weighing 60% more than the original powder due to the added nitrogen, with almost no volume change. The use of sintering aids in its processing may also provide strength and creep resistance at high-temperatures [49].

The development of RBSN was summarized in [33], started by JP-59-162199, where RBSN crucibles were designed to achieve coefficients of thermal expansion comparable to the silicon ingots. These had 85% of the theoretical maximum density for silicon nitride and good mechanical strength. However, problems with wetting and consequent adherence led to crucible cracking.

This was addressed by [45] where regulated particle size distribution of the silicon particles and pressure during nitriding allowed to produce silicon nitride with a density between 40 and 60% of the theoretical maximum and at least 50% of the pores of the crucible surface with larger diameter than the mean particle size of the Si_3N_4 particles.

These crucibles showed no tendency for wetting phenomena, except for regions with open porosity below 40%, allowing a relatively easy release of the ingot from the crucible. Reusability was also reported in [46] for 30 cm x 30 cm square cross section RBSN crucibles, with a wall 25 mm thick and a Si_3N_4 release coating. Sixteen crack-free ingots were cast in a heat exchange method furnace using the same mould.

The potential of silicon nitride crucibles was studied in [50], verifying the influence of their thermal properties during mc-Si solidification in a Bridgman furnace, demonstrating that the lower thermal resistivity of the silicon nitride, in comparison with silica, led to more heat loss through the crucible

bottom, prolonging melting time but accelerating solidification. This conclusion led to the replacement of the two carbon fibre discs underneath the crucible by better insulating alumina fibre material, shortening the melting and solidification times in favour of lower energy requirements. Allied with reusability, as seen in Figure 2.9, a so sought cost reduction might be possible.

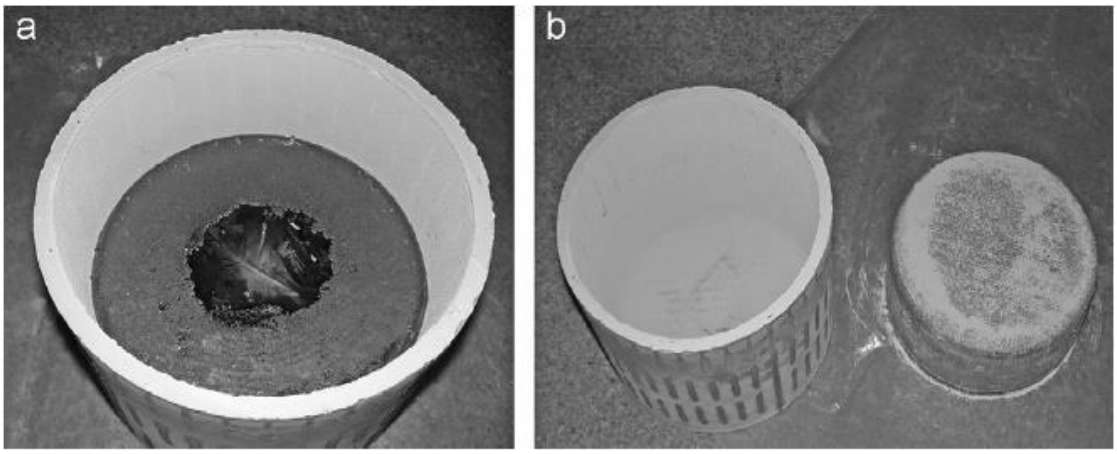

Figure 2.9 - a) Ingot solidified in the silicon nitride crucible, under the optimized thermal conditions; b) shows the detachment was successful, without major signs of wetting [50].

Similar results have been also claimed in [51], but it was also observed that using a crucible with large thermal conductivity may be responsible for a more pronounced concave shape in the melt-crystal interface and a high temperature gradient in the ingot, increasing the chance of thermal stress and propagation of dislocations. Based on further analysis, [48] presented the Si_3N_4 and SiO_2 composite design based on the knowledge that the crucible bottom wall regulates the vertical heat release, whereas the side wall influences the horizontal heat flux, related to the stated melt-crystal interface shape.

Analysis of ingots prepared with Si_3N_4 crucibles with different purity grades, Si_3N_4 coating firing procedures and holding temperatures in the melting stage can be found in [52]. The results were compared to reference ingots cast in silica crucibles, accounting for the dissolved oxygen and dopant elements distributions along the ingot height.

It has been reported that the dissolved oxygen concentration in the bottom of the ingots depends directly on the holding temperature when melting the silicon charge, but no relationship was found between the bottom contamination and the crucible material used. There were although other parameters that could contribute to this, such as the thermal gradient, given that silicon nitride crucibles are more heat conductive than others made of silica. The concentration decreased towards the top in all ingots, however, the decrease was steeper for the silicon nitride crucibles, in comparison with SiO_2 crucibles. The authors' reasoning for this is the possibility of having different sources for oxygen in the two crucible materials, a silicon oxynitride layer in Si_3N_4 crucibles, as diffusion seemed to decline over solidification time, and a silicon oxide layer in the silica counterparts, where the diffusion was more stable.

To avoid wetting, the coating is applied and fired in an oxidizing atmosphere. Trying to keep the oxygen content in the coating layer low, the experiments included firing at 900 and 1100 ºC in a mixture of air and N_2, while the remaining parameters were as close to each other as possible. The resulting ingot contamination made it evident that lower firing temperatures decreased the dissolved oxygen concentration, supporting the claims of [53], however this happened at the cost of severe sticking.

The boron and phosphorous contents in the Si_3N_4 crucibles were considered before applying the coating. Boron is believed to be present at this stage as boron-nitrides. After coating, the firing can oxidize them partially, forming boron-oxides. Phosphorus oxides should also occur. Both are volatile at the melting temperature of silicon, therefore may diffuse through the coating into the ingot. Conversely, the remaining boron-nitrides should stay solid below 3000 K. The vapour pressure of the phosphorus-oxides is described as significantly superior to the boron-nitrides, respectively in the order of 10^{-3} atm and 1 atm, so that after some runs, the phosphorus ingot contamination is drastically reduced, due to evaporation from the crucible. Meanwhile, boron is less prone to evaporation, so the variation in the ingot should be less noticeable, justifying the choice of a crucible material with less boron content to limit ingot contamination throughout the crucible reutilization [52].

Improvement of the raw material purity was also pointed out in [20], regarding a nitride bonded silicon nitride (NBSN) crucible. Changes to the crucible manufacturing or a cleaning run were also proposed as alternatives. Six ingots of undoped DS mc-Si were produced, demonstrating similar concentrations of interstitial oxygen and substitutional carbon in comparison to a standard fused silica crucible. The authors underlined that those six runs almost reached the cost efficiency of the fused silica crucibles.

The level of ingot contamination also decreased after re-running. In this case, the dominant impurities were boron, aluminium and phosphorus, based on a comparison of measured and calculated resistivities. An estimate of their diffusion length during the growth process ruled out solid state diffusion as the dominant mechanism of contamination for the ingot bulk. Additionally, the volume change, prior and after to the growth process, was too small be responsible for the introduction of the measured impurities, thereby, the dissolution of the crucible by the melt was also not the major form of contamination. It was attributed instead to out-diffusion from the NBSN crucible into the molten silicon, relying in a model, with the melt behaving as an infinite sink. The B, Al and P atoms were transported in the melt by diffusion and convection, followed by segregation into the ingot. Noticeably, the literature lacks data regarding the diffusivity of these elements for materials similar to the NBSN crucible, so the simulation reached those diffusion coefficients considering the impurity concentrations in the ingot. Although the estimated orders of magnitude were plausible, a comparison with more data could further support their claim.

Currently, the silicon nitride crucibles have not been implemented industrially. This is probably because there is no clear evidence that reusability can lead to a cost reduction, in comparison with the widespread fused silica, or due to the effect of these crucibles on ingot contamination [20].

2.5 Impurity Transport

2.5.1 Macroscopic diffusion

In solids, atomic positions are dictated by the most energetically favourable sites. At 0 K, the atoms remain at their lattice sites, but if temperature increases, they will vibrate around the sites due to thermal agitation. Eventually there is enough available energy to allow atoms to move into other energetically favourable site.

In a homogeneous distribution, without applied external forces, this random migration does not disturb the equilibrium, since on average the fluctuations cancel out. Nonetheless, for an inhomogeneous placement, atoms gradually rearrange themselves following the chemical potential gradient until equilibrium is established. This mechanism has been designated diffusion and described both with phenomenological (or macroscopic) and atomistic (or microscopic) approaches.

The cited phenomenological route derives from Adolf Fick's analysis in 1855, where an analogy with Josef Fourier's law for thermal conduction was established. The fact that heat transfer by conduction is also dictated by random molecular motions sets a deep connection between both laws [54, 55, 56]. Fick suggested the definition of a diffusion coefficient, also termed diffusivity, to depict the linear response between the concentration gradient and the diffusion flux of a substance. Similarly, Fourier defined conductivity, relative to the temperature differential and the heat flux.

Taking the example of a solution, the net flux of a mass dM [kg] of solute across a section A [m^2] of solvent, during a period dt [s], is designated by diffusion flux J [kg m^{-2} s^{-1}] [57]:

$$J = \frac{1}{A}\frac{dM}{dt} \tag{2.1}$$

2.5.1.1 Fick's 1st Law – steady state diffusion

If J, which might also be expressed in [atoms m^{-2} s^{-1}], does not change with time it is said that the system is in steady-state conditions. In that state and considering an isotropic medium i.e. a medium where physical and chemical properties don't change with direction, Fick's first law states that J_x, the flux in the *x* dimension, is given by:

$$J_x = -D\frac{\partial C}{\partial x} \tag{2.2}$$

where the diffusivity, D [m^2 s^{-1}], is a scalar factor of proportionality between J_x and $\frac{\partial C}{\partial t}$ which stands for the gradient of concentration [mol m^{-3}] across the *x* dimension. The negative sign means that the solute atoms tend to move towards locations where concentration is lower [54, 55, 56, 57]. If the system is allowed to evolve for enough time, diffusion will lead it to a state of equilibrium, where the concentration is equal in every location.

2.5.1.2 Fick's 2nd law - non-steady state diffusion

However, steady-state conditions are not often present because the diffusion flux and the concentration gradient may vary with time [54, 56]. Let us take a volume defined by Δx, Δy and Δz as well as a point P in an (*x*, *y*, *z*) arbitrary position, as seen in Figure 2.10 [56]. The diffusion flux has the J_x, J_y and J_z components for each dimension and changes within the defined volume. If the net balance of incoming and exiting flux at point P is negative, it means that the amount of particles is being depleted. Otherwise, the concentration at point P might increase if there are more particles moving in than leaving. This relationship can be expressed by:

$$inflow - outflow = accumulation\ or\ loss\ rate \tag{2.3}$$

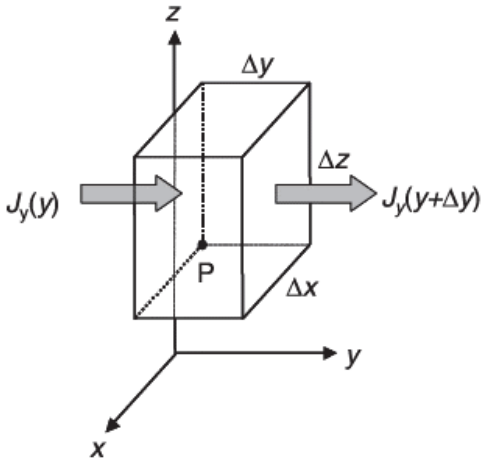

Figure 2.10 - Infinitesimal test volume, with the incoming and exiting diffusion fluxes in the y component [56].

This balance can also be defined in the *x* component by:

$$J_x(P)\Delta y\,\Delta z - J_x(P+\Delta x)\Delta y\,\Delta z = [J_x(P) - J_x(P+\Delta x)]\Delta y\,\Delta z \tag{2.4}$$

that is the incoming flux through the left plane with section $\Delta y\,\Delta z$ and exiting flux through the right plane with the same area. The other components are analogous. Putting them together we end up with:

$$\begin{aligned}[J_x(P) - J_x(P+\Delta x)]\Delta y\,\Delta z + [J_y(P) - J_y(P+\Delta y)]\Delta x\,\Delta y + \\ [J_z(P) - J_y(P+\Delta z)]\Delta x\,\Delta y = \frac{\partial C}{\partial t}\,\Delta x\,\Delta y\,\Delta z\end{aligned} \tag{2.5}$$

where the particle accumulation or loss rate in the test volume is expressed by the partial time derivative of the concentration. Applying Taylor's theorem to expand the components in square brackets to their linear terms, we have:

$$\begin{aligned}f(x) = f(a) + f'(a)(x-a) + \cdots <=> \\ <=> f(x) - f(a) = f'(a)(x-a) <=> \\ <=> J_x(P) - J_x(P+\Delta x) = -\Delta x\frac{\partial J_x}{\partial x}\end{aligned} \tag{2.6}$$

The same goes to the other components, yielding:

$$-\left[\frac{\partial J_x}{\partial x} + \frac{\partial J_y}{\partial y} + \frac{\partial J_z}{\partial z}\right]\Delta x\,\Delta y\,\Delta z = \frac{\partial C}{\partial t}\,\Delta x\,\Delta y\,\Delta z \tag{2.7}$$

Reducing the test volume to infinitesimal size, the above equation can also be written with $\boldsymbol{\nabla}.$, the divergence vectorial operator, which acts on the vector of the diffusion flux $\boldsymbol{J}$:

$$-\boldsymbol{\nabla}.\boldsymbol{J} = \frac{\partial C}{\partial t} \tag{2.8}$$

This expression is denoted as the continuity equation. The previous deduction is useful when combined with Fick's first law for the three dimensions:

$$\boldsymbol{J} = -D\boldsymbol{\nabla}C \tag{2.9}$$

Here the vector of diffusion flux $\boldsymbol{J}$ is antiparallel to the direction of the concentration gradient field $\boldsymbol{\nabla}C$ which points to where the concentration increases the most. The conjugation of equations (2.8) and (2.9) leads to Fick's 2nd law, a second-order partial differential equation also known as the diffusion equation:

$$\frac{\partial C}{\partial t} = \boldsymbol{\nabla}.(D\boldsymbol{\nabla}C) \tag{2.10}$$

We can see that these parameters are part of the general diffusion-convection equation, where $-\boldsymbol{\nabla}.(\boldsymbol{v}C)$ describes the contribution of convection or advection to the change in concentration and R accounts for generation or depletion of the diffusing particles in each point, that can be interpreted as the production or consumption of a chemical species in reactions with the surrounding material:

$$\frac{\partial C}{\partial t} = \boldsymbol{\nabla}.(D\boldsymbol{\nabla}C) - \boldsymbol{\nabla}.(\boldsymbol{v}C) + R \tag{2.11}$$

If we keeping considering no convection, $R = 0$ and a constant D in every direction, usually a good assumption for diffusion in solids, one might use:

$$\frac{\partial C}{\partial t} = D\nabla^2 C \tag{2.12}$$

$\nabla^2 C$ is the Laplacian operator of the concentration, which generalises the second derivative. Otherwise, if the medium is anisotropic such as in some crystals, textile fibres and polymer films, D must be studied in every direction, as presented in [54].

When equation (2.12) is simplified to one dimension, it becomes:

$$\frac{\partial C}{\partial t} = D\frac{\partial^2 C}{\partial x^2} \tag{2.13}$$

J. Crank has proposed many ways of solving equation (2.12) while applying physically meaningful boundary conditions [54]. One of the most useful for this work is the diffusion mechanism in a semi-infinite bar, whenever the source of the diffusing species has a constant concentration C_s over time (equation (2.14)). The bar is considered semi-infinite only when no diffusing atom is able to reach the opposite extremity over the considered diffusion time [57]. For the sake of better understanding, let us take similar solid with a source of atoms diffusing in one single direction. Before they are even put in contact, the solid is a state of equilibrium, so that if it has any atoms of the same element as the solute, they are homogeneously distributed in every point with a C_0 concentration. At the precise time they are placed together, the interface is at $x = 0$ and right after the atoms begin migrating towards the bulk of the solid, along the positive side of the x axis. Summarizing, the boundary conditions are:

i. For $t = 0$, $C = C_0$ at $0 \leq x \leq \infty$;
ii. For $t > 0$, $C = C_s$ at $x = 0$ and $C = C_0$ at $x = \infty$.

That when applied to equation (2.13) results in:

$$\frac{C_x - C_0}{C_s - C_0} = 1 - erf\left(\frac{x}{2\sqrt{Dt}}\right) \tag{2.14}$$

This equation relates concentration, position, and time. C_x is the concentration at depth x measured at time t, that can be computed if the other parameters are specified, using the Gaussian error function erf, commonly described in mathematical tables [54]. Figure 2.11 demonstrates the effect of diffusion time on the concentration profile, in the conditions cited above. This behaviour is also typical for diffusion coefficients.

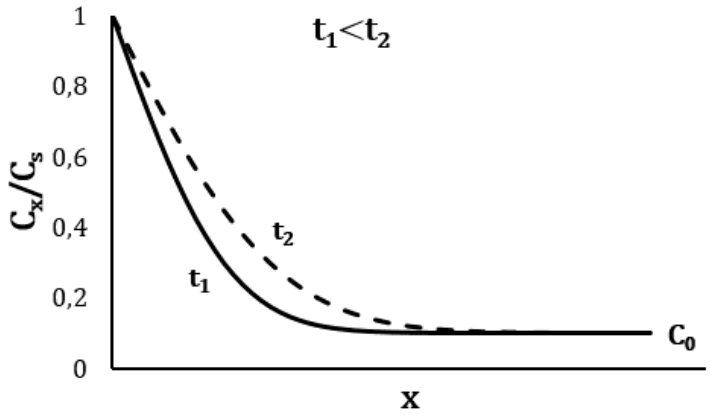

Figure 2.11 - Relationship between concentration profile and diffusion time.

So far, the diffusion coefficient has always been admitted as constant, however such condition rarely occurs due to the influence of other factors [57]. The Arrhenius equation describes its dependency on nature of the host and diffusing species, as well as temperature:

$$D = D_0 exp\left(-\frac{H_M}{k_B T}\right) \tag{2.15}$$

D_0 is the temperature independent diffusion coefficient [m^2 s^{-1}], H_M quantifies the migration enthalpy required to diffuse one atom [eV], k_B is Boltzmann's constant [eV K^{-1}] and T the absolute temperature [K].

2.5.2 Solubility

A factor that definitely is relevant when evaluating solid diffusion of an atom species is the solubility limit. It defines the maximum concentration that can be dissolved in a host material, at a certain temperature and equilibrium conditions, above which value the excess solute will precipitate and form another solid phase or a compound with different composition. Solubility may be determined through an expression similar to equation (2.15) [57, 58]:

$$S = S_0 exp\left(S_s - \frac{H_s}{k_B T}\right) \qquad T < T_{eut} \tag{2.16}$$

where the S_s and H_s parameters are the solution entropy and enthalpy, respectively, and S_0 is, like D_0, the temperature independent pre-exponential factor. Note that this holds only for values of temperature below eutectic temperature, the lowest temperature at which a certain mixture of materials solidifies.

3 Method

The diffusivity of impurities in the crucible is investigated by heat treating diffusion couples, comprising Cz silicon and the Si_3N_4 crucible as a source of contamination.

This method aims to use direct current - glow discharge - mass spectrometry (GD-MS) depth profiles, since it is easily accessible and an effective way of dissolving the crucible material, so that the amount of solid particles is low enough for elemental analysis through high resolution - inductively coupled plasma - mass spectrometry (ICP-MS) is yet to be determined, as nitric and hydrochloric acid mixtures were unsuccessful.

3.1 GD-MS

Glow discharge mass spectrometry is a direct technique of elemental analysis, relying on the application of a potential difference between two electrodes, in an inert gas environment at low-pressure. Certain conditions of pressure, current and voltage result in a brilliant discharge [59].

The general process is illustrated in Figure 3.1. Electrons are emitted and accelerated in the discharge electric field, causing excitation and ionization of atoms of the working gas (usually argon). Gas ions (Ar^+) bombard the cathode (sample) inducing ion-electron emission and sputtering atoms (Sa) from its surface. These then participate in various collisions in plasma, leading to their excitation and ionization. Light emission from the excited atoms allows atom-emission spectroscopy, while ions (Sa^+) are detected by mass spectrometry [60].

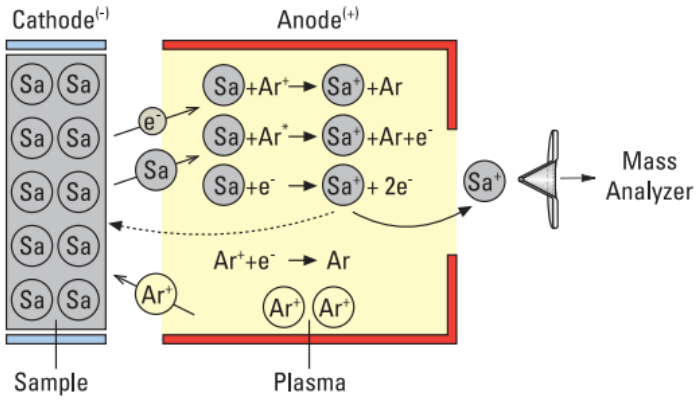

Figure 3.1 - Schematic of the glow discharge process [61].

Relatively to ICP-MS, GD-MS has lower interference levels for almost the same limits of detection, higher ion source stability, better reproducibility, simpler calibration and weaker matrix effects due to the separate processes of sputtering and ionization [60].

3.1.1 Quantification method

Most often, ion beam ratio (IBR) is the quantification method employed GD-MS. Except for the signal arising from the discharge support gas, it assumes that the ratio of ion current for any isotope, I_X, in relation to the total ion current, I_M, is representative of the ratio of the number of atoms of that isotope to the other constituent atoms of the sample.

For trace analysis on high-purity materials, the ion signal for the matrix is assumed to be large, relative to individual trace species, therefore, the matrix has a concentration of 100%. The concentration of an isotope K_X is obtained from the product of the IBR and the concentration of the matrix, K_M [59]:

$$K_X = \left(\frac{I_X}{I_M}\right) K_M \tag{3.1}$$

If one considers instead multiple isotopes of the detected element and the matrix, their respective abundances A_X and A_M should be taken and used as follows [62]:

$$K_X = \left(\frac{I_X}{I_M}\right) K_M \left(\frac{A_M}{A_X}\right) \tag{3.2}$$

For quantitative results, the variation in analytical sensitivity that occurs between different elements must be accounted by the relative sensitivity factors (RSF), which can be determined for an element in a given matrix. The correct concentration of the species in the matrix is computed through [62]:

$$C_X = K_X \, RSF_X \tag{3.3}$$

3.1.2 Insulator analysis

In addition to the difficult dissolution, the Si_3N_4 crucible electrically non-conductive and may charge-up when acting as the cathode of the glow discharge. Although unavailable during the period of the experiments, insulator analysis is possible [63]:

i. by grinding the sample and mixing the powder with a conducting binder, which is pressed into a pellet prior to analysis. It has the drawback of the loss of spatial information, since the material must be ground into powder and contamination through the binder;
ii. by placing a metallic diaphragm (secondary cathode) on top of the sample with an opening smaller than the diameter of the glow discharge cell. Hence, it is also exposed to the discharge and part of these sputtered atoms are redeposited on the non-conducting material. This creates a conducting surface so that the sample does not charge-up while being sputtered. The blank contribution due to the sputtering of the secondary cathode material constitutes a major drawback of this technique, which increases the detection limits.

Consequently, external sources are avoided as much as possible and the contamination is instead detected in the silicon samples, serving as an indirect measurement. In this context, the glow discharge parameters applied for Cz silicon sample analysis are listed in Table 3.1. Such conditions were also applied to determine the GD-MS limits of detection, for similar equipment, matrix [62] and the RSFs in Table 3.2. Subsequently, the concentrations of Fe and Ti were quantified resourcing to equation (3.4) and expressed in mol/m^3 based on equation (3.5).

Table 3.1 - GD-MS discharge parameters used for analysis of silicon samples

Discharge voltage	1000 V
Discharge current	60 mA
Discharge gas	300 mL/min
Matrix signal intensity (^{28}Si)	10^{10} cps

Table 3.2 - RSF and abundance factors employed in the quantification of GD-MS analysis of silicon samples

Element	RSF	Abundance (Isotope)
Fe	1.16	91.66 (^{56}Fe)
Ti	0.99	73.94 (^{48}Ti)
Si (matrix)	-	92.21 (^{28}Si)

$$C_X\left[\frac{mol_X}{m_{Si}^3}\right] = \frac{C_X\left[\frac{kg_X}{kg_{Si}}\right]}{M_X\left[\frac{kg_X}{mol_X}\right] \times \rho_{Si}\left[\frac{kg_{Si}}{m_{Si}^3}\right]} \tag{3.4}$$

The stated limits of detection, LoD, are 0.2 ppbw for Ti and 0.9 ppbw for Fe. These were described in terms of mol/m^3, by the following expression:

$$LoD_X\left[\frac{mol_X}{m_{Si}^3}\right] = 10^{-12}\frac{LoD_X\,[ppbw]}{M_X\left[\frac{kg_X}{mol_X}\right] \times \rho_{Si}\left[\frac{kg_{Si}}{m_{Si}^3}\right]} \tag{3.5}$$

where X represents the impurity species, M_X is its molar mass and ρ_{Si} is the volumetric mass of silicon at room temperature.

3.2 Diffusivity and solubility data

To estimate the resulting concentration profiles according to the heat treatment conditions, as well as the adequate thickness for the mono-Si samples, one must consider the diffusion and solubility properties of these transition metals for the temperature interval to which the samples are submitted.

It is known that iron and titanium predominantly occupy interstitial sites in silicon, diffusing from one interstitial site its nearest-neighbour [22]. Data regarding their diffusion and solubility is available and was considered for this work, as stated in Appendix A. However, information relative to the diffusion in Si_3N_4 is scarce, without results for Fe and little is known about Ti. This calls for an alternative approach, which is described in 3.5.

In most literature, Si_3N_4 is used on silicon substrates as a dielectric which supresses the diffusion of B, P and Al dopants. Given that it often relates to different configurations of amorphous or crystalline α-Si_3N_4 and β-Si_3N_4, at temperatures below 1000 ºC, this suggests that such data may not be an accurate approach for a crucible. The data found during this work is summarized in [55, 64].

3.3 Heat treatment

The resulting amount of impurity in silicon after heat treatment might be related to a certain diffusivity in the material, according to the treatment conditions defined by three temperature curves, as represented in Figure 3.2:

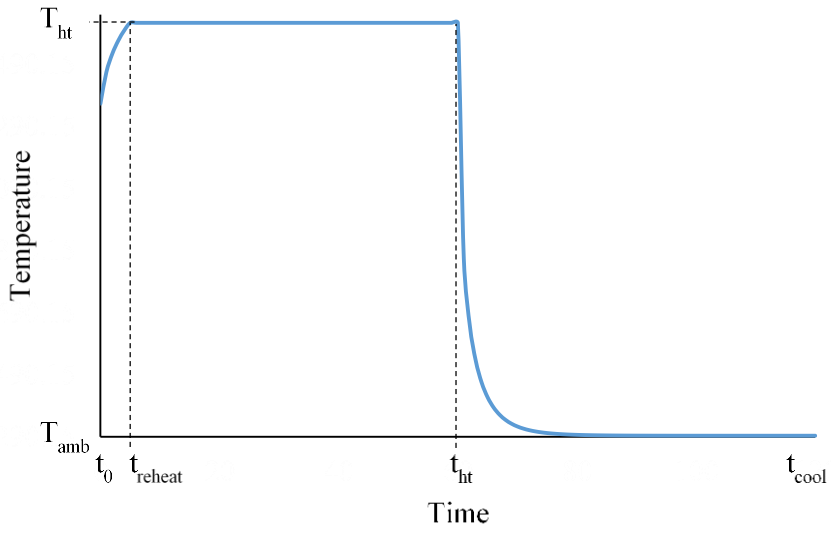

Figure 3.2 – Typical temperature profile during the heat treatment.

i. The reheating curve, starting at t_0 with the samples at the furnace temperature, assumed due to the small dimensions of the samples, which favours a fast heating towards thermal equilibrium. Since there is a temperature drop while its door is opened to introduce the samples, this curve is relative to the period t_{reheat}-t_0, until T_{ht} is re-established, about 4 minutes for T_{ht} between 1200-1350 ºC.

ii. During the remaining time until the heat treatment is finished, t_{ht}-t_{reheat}, the samples are kept approximately at T_{ht}. While in the furnace, the temperature is measured by a thermocouple placed roughly 5 cm above the samples;

iii. Finally, the samples are retrieved from the furnace, with the surfaces of interest facing upwards and the back surfaces in contact with a refractory. Also exposed to the natural convection of the surrounding air and losing heat through radiation, they cool until T_{amb} during t_{cool}-t_{ht}. The couples often fall apart when retrieved from the furnace and therefore all are intentionally cooled separately. To disassemble them takes about 1 minute.

3.4 Remarks on concentration vs depth profiles

Both the diffusivities and solubilities of the transition metal species vary accordingly to the temperature profile, although during the cooling phase the impurity source is removed. The low amount of contaminants in the silicon sample promotes a diffusion from the crucible towards an equilibrium state, according to Fick's 2nd law. However, if a certain metal cannot be dissolved any further in silicon (especially relevant during cooling), supersaturation may lead to the following reactions, depending on process conditions (e.g. temperature, cooling rate or impurity species), to overcome the inability of the host material to accommodate more atoms of this species in its lattice [65]:

i. The impurity precipitates within the bulk of the silicon wafer if the concentration exceeds the solubility limit. The diffusivity needs to be sufficient to facilitate the migration of the impurity atoms in order to form nuclei (homogeneous precipitation) or to reach foreign nuclei (heterogeneous precipitation), formed by lattice defects or other impurity precipitates;
ii. The impurities diffuse towards the surfaces of the silicon and precipitate. Likewise, the diffusivity must be sufficient to allow the atoms to travel the distance from their position until the surface;
iii. The atoms remain dissolved within the volume because of low diffusivities or short migration periods, achieved when high cooling rates are applied to the sample. Often the dissolved impurities form complexes with other impurities, e.g., in the form of donor-acceptor pairs.

Although the exact composition of the crucible has not yet been confirmed, based on the crucible specifications provided by the manufacturer (Table 3.3) and solubility data available for Ti ($<5 \times 10^{-5}$ mol/m^3 at 1330 ºC) and Fe (<0.03 mol/m^3 at 1200 ºC) in Cz silicon, one may expect this type of phenomena to occur. It has been stated by the manufacturer that the data is purely indicative as the material is still under development. Uncertainties of ±0.5 were assumed for the elements' mass fractions and density. The uncertainty in the molar mass of each element was also taken into account, according to [66].

Table 3.3 - Technical specifications of the advanced RBSN crucible conceded by Steuler Solar

Chemical composition	Typical values	Concentration (mol/m^3)
Al	10 ppmw	0.91-1.02
Fe	5 – 10 ppmw	0.21 - 0.49
Ca	5 ppmw	0.29-0.36
B	1 – 5 ppmw	0.12 - 1.32
P	1 – 5 ppmw	0.04 - 0.46
Ti	1 ppmw	0.03-0.08
α-Si_3N_4	50%	
β-Si_3N_4	46%	
SiC	1-3%	
Si-met.	<1%	
Physical Properties		
Density	2.6 kg/dm^3	
Porosity	12%	
Bending strength	185 MPa	
E-Module	150 GPa	
Thermal expansion	$3.3 \times 10^{-6}/℃$	
Heat conductivity	12 W/m K	

3.4.1 Other considerations

At quenching or moderately-fast cooling rates, iron forms electrically active defects in silicon, as a consequence of its moderate diffusion coefficient. With slow cooling rates, as in this work, precipitation becomes more likely, since the overall diffusion length can be higher. Iron can appear electrically active while dissolved on interstitial sites and as α-$FeSi_2$ precipitates, but from theoretical considerations [67], substitutional iron is not stable in this host. Usually these precipitates form via segregation of iron atoms towards foreign nuclei. Titanium is deduced to precipitate exclusively by heterogeneous nucleation.

If a Si|SiO_2 interface is formed due to heat treatment in an atmosphere with oxygen, many impurities can precipitate there preferably [68]. Transition metal silicides have enhanced lattice parameters in comparison to the silicon lattice and consequently tend to migrate to the surface of the host material [69]. Thereby, even if one takes the data available for the solubilities and diffusivities of the species diffusing from the crucible in a silicon matrix, as well as their concentrations in the starting conditions, the experimental results should present higher amounts of Fe and Ti near the silicon surface region than it would if only diffusion occurred. This is due to the supersaturation, the eventual exposure to oxygen, the free surface that acts as a crystalline defect, and the presence of other elements diffusing from the crucible, which may increase the likelihood heterogeneous precipitation.

3.5 Impurity transport estimation

As determining the exact depth at which the formation of foreign nuclei occurs remains challenging, while it can also drastically influence the distribution of the impurities, observations of Fe concentration profiles reported by Ekstrøm, also studying diffusion in the same crucible, were taken into account (Figure 4.2).

This study was primarily focused in Fe, but the opportunity of knowing more about other transition metals led to the heat treatment of more diffusion couples, during periods from 3 to 180 minutes at

temperatures below the melting point of silicon (T_{ht} between 1200 ºC and 1350 ºC). This range of temperatures allows for faster diffusion and is consequently relevant during the DS cooling stage.

It is noticeable that Fe profiles are only shown for 1200 ºC, since the analysis of Fe in samples treated at higher temperatures was disregarded, by motives stated in 5.1.

Ti could be analysed with a similar technique and was expected to reach shorter depths, according to equation (2.14) and following the crucible composition and literature diffusivities. Accordingly, it was analysed due to the likelihood of achieving applicable results.

The prediction of the concentration profiles relied instead on equation (2.14) with an average diffusivity between T_{amb} and T_{ht}, following the heating curve in Figure 3.2, with a period of 1 hour after the heat treatment. In addition, C_s for Fe was considered to be one order of magnitude below the solubility limit at T_{ht}=1200 ºC (Figure 3.3), while for Ti it was noticed that even with C_s equal to the maximum solubility at the eutectic temperature, the impurity concentration would cross the detection limit of the GD-MS at 415 µm (Figure 3.4).

Based on the Fe profiles in Figure 4.2, it was assumed by excess that the section starting 15 µm below the surface would be less prone to the occurrence of precipitates, when taking into account the composition of the crucible material and the measured concentrations near the silicon surface.

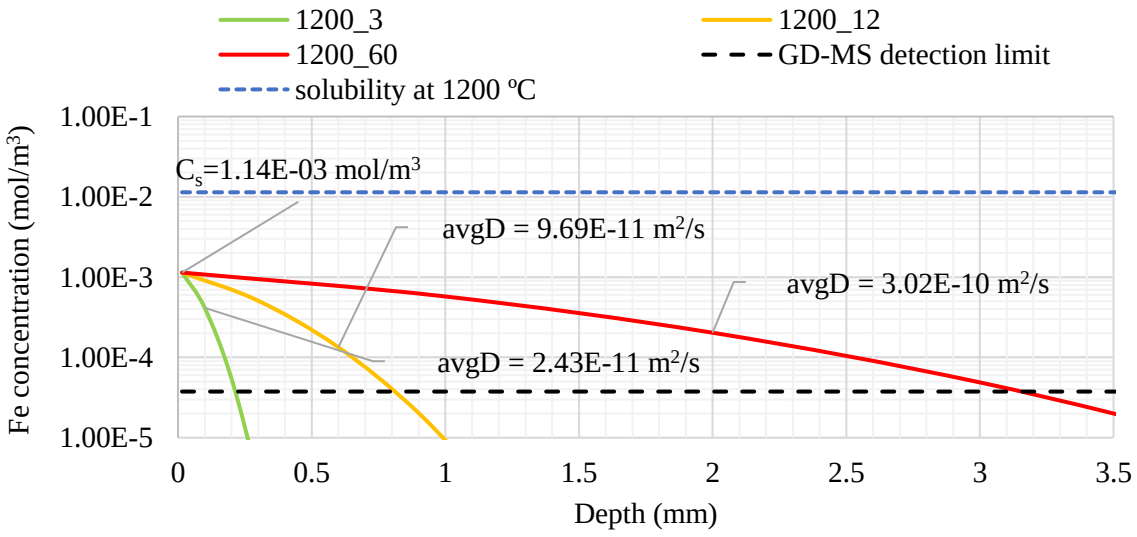

Figure 3.3 - Fe concentration profile, determined based on equation (2.14) starting at 15 µm. 1200_3, 1200_12 and 1200_60 represent a sample treated during 3, 12 and 60 minutes, respectively, up to 1200 ºC.

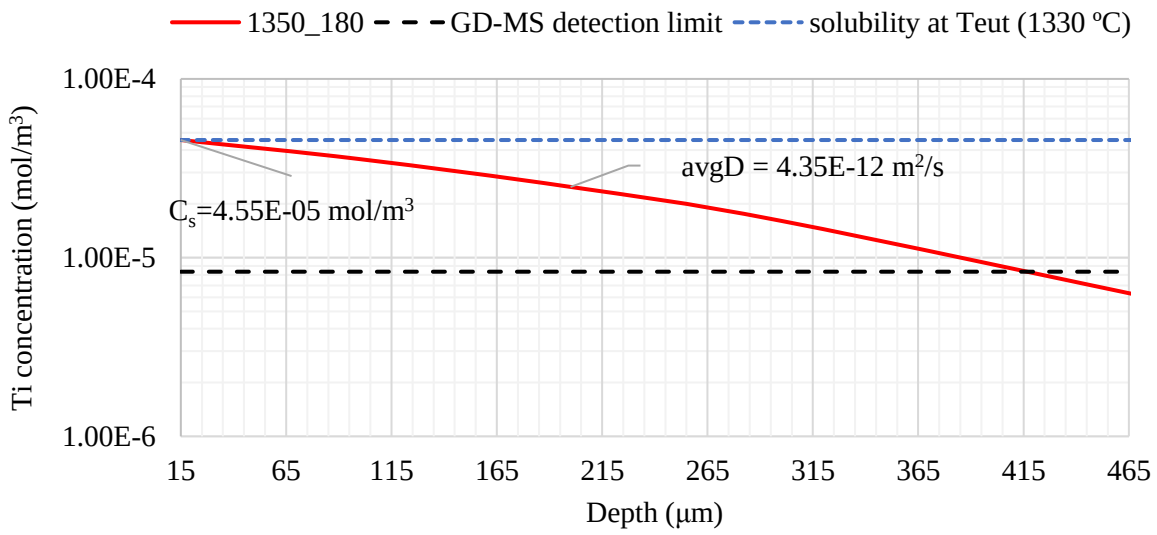

Figure 3.4 - Ti concentration profile, determined based on equation (2.14), starting at 15 µm. 1350_180 represents a sample treated during 180 minutes, respectively, up to 1350 ºC.

If one considers that the heat treatment conditions are maintained and other sources of the studied element are absent, the amount of detected impurities should be similar. Thereby, if any impurities migrate further than 15 µm and precipitate within the bulk, the depth at which the detection limit is crossed should only be expected to decrease.

The previous samples, in Figure 4.2, were 2 mm thick and the concentration profiles on the sputtered surfaces suggest that with deeper analysis one might be able to associate them, below the solubility limit, to a certain diffusivity in silicon. By the suggestion of Figure 3.3, for a 60-minute treatment up to 1200 ºC, if no bulk precipitation occurs, iron can be detected at about 3.2 mm of depth. Consequently, it seemed reasonable to increase the thickness of the silicon samples, which was extended to 3.5 mm.

3.6 Sample preparation

3.6.1 Cutting

Although changes were made throughout the different samples, this stage was common to every one of them. Starting by cutting 5 mm thick squares, from a portion of a Cz silicon ingot produced at SINTEF. Relying on a Cz ingot ensures a lower impurity amount, in comparison to directionally solidified ingots and a diffusion process free of grain boundary or dislocation influences.

Similarly, Si_3N_4 squares were cut in squares, keeping the original 8 mm thickness of the crucible wall. To perform these cutting steps a Conrad diamond blade, owned by SINTEF, was employed. As it was also used to cut other metallic pieces, it was deemed a relevant source of contamination in the following preparation steps.

3.6.2 Grinding and polishing

To remove the impurities introduced by the saw blade or previously, both materials were submitted to grinding in all surfaces, following the steps seen in Table 3.4 and Table 3.5. The thickness of the silicon wafers ended up being roughly 3.5 mm and 6 mm for the Si_3N_4 samples. This ensures a regular contact interface near the sputtering area, to achieve a diffusion as unidimensional as possible, without preferential pathways.

To achieve it, the contact between the two media has to be maximized, so that the concentration gradient is as equal as possible for all points on a given plane, perpendicular to the flow direction. This motivates the polishing of the contact surfaces of the materials, but in fact, all the surfaces were polished, with exception to the lateral faces and the backside of the silicon layer, in attempt to limit the eventual contamination from the surroundings towards the interfacial region.

The same could be done to the crucible layer, but it turns out undistinguishable whether a surface was polished or not, since the material resembles compacted powder, easily losing grains when friction is applied. Moreover, there is lack of an adequate procedure, therefore it is uncertain if the polishing fulfils the requirements.

Further notice must be acquainted when using 9 μm or lower sized diamond particle suspensions in the silicon nitride preparation. Its pores allow the adsorption of the suspension, visible due to its black colour, which could not be successfully removed with a Branson 5510 ultrasonic bath in ethanol after 40-minute-long periods.

The samples' dimensions meant that they could not be fit into a sample holder, for this reason they were held manually in every step. Different MD-Mol plates were used in the DP and OP1 steps for silicon, each with the corresponding suspension and every plate was used only for this purpose, being kept away from contamination sources. After polishing, the absence of Ti and Fe contamination prior to heat treatment was confirmed with GD-MS analysis, but only for the silicon wafers.

Table 3.4 - Silicon nitride grinding and polishing procedures

Grinding step	**PG**	**FG1**	**FG2**
Equipment	Struers Tegramin-20		
Surface	MD-Piano 120	MD-Allegro	MD-Largo
Suspension	-	DiaPro Allegro/Largo 9 μm	DiaPro Allegro/Largo 9 μm
Lubricant	Water	-	-
Rotation speed [rpm]	300	150	150
Time	As needed	5 min	10 min

Polishing step	**DP**	**OP**
Equipment	Struers Tegramin-20	
Surface	MD-Dac	MD-Chem
Suspension	DiaPro Mol 3 μm	DiaPro OP-S
Rotation speed [rpm]	150	150
Time	8 min	2 min

Table 3.5 - Silicon grinding and polishing procedures

Grinding step	PG	FG1	FG2
Equipment	Struers Labopol-21		
Surface	SiC P#320	SiC P#320	SiC P#1200
Lubricant	Water	Water	Water
Rotation speed [rpm]	500	500	500
Time	As needed	As needed	As needed

Polishing step	DP	OP 1	OP 2
Equipment	Struers Rotopol-31		
Surface	MD-Mol	MD-Mol	MD-Nap
Suspension	DP 9 µm	DP 3 µm	DP 1 µm
Lubricant	Blue	Blue	Blue
Rotation speed [rpm]	500	500	500
Time	As needed	As needed	As needed

3.6.3 Couple assembly

Some of the couples were held together with kanthal wire, a FeCrAl alloy, to study Ti (Figure 3.5 a)), while for Fe this wire is replaced by a silicon weight, from the same Cz ingot, placed on top of the samples (Figure 3.5 b)). Additionally, some silicon samples, without the Si_3N_4 crucible, were treated in order to check for undesirable contamination sources.

Figure 3.5 - Representation of the prepared diffusion couples - a) used for Ti; b) focused on avoiding Fe external sources, with a mono-Si weight replacing the kanthal wire.

4 Results

4.1 Preliminary results

4.1.1 Nabertherm N17/HR

Firstly, Ekstrøm has prepared silicon samples using a Nabertherm N17/HR furnace, enclosed in a protective argon fed box with hinged lid, as displayed in Figure 4.1. This section relies on his unpublished report.

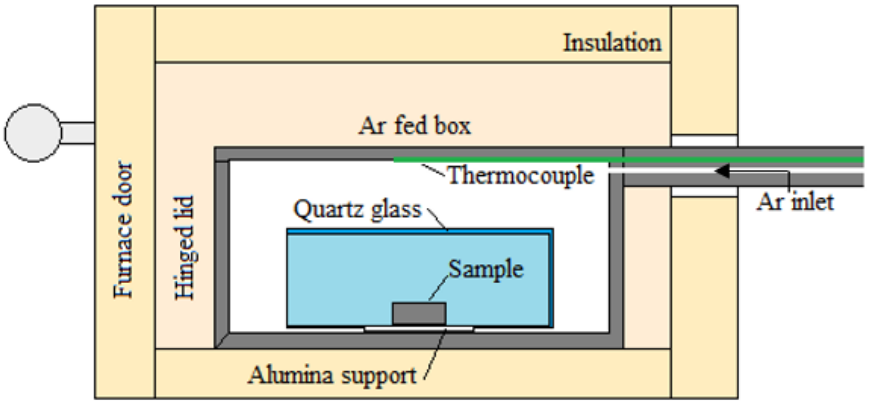

Figure 4.1 - Schematic by Ekstrøm of Nabertherm N17/HR with the sample and quartz glass crucible inside the argon fed box.

The overpressure generated within the box exits through the hinged lid that closes due to its own weight. Following the specifications, it is made with heat-resistant steel alloy 314 (AISI) and has a maximum operation temperature is 1100 °C, which can be monitored in the interior with a type K thermocouple [70].

Prior to using the quartz glass in Figure 4.1, the heat treatments were made with an alumina crucible. The iron content seen for a silicon-only sample, 1200_60_alumina in Figure 4.2, may justify the increased the concentration in the bulk, by diffusion into the back surface of the wafer, resulting in a less pronounced gradient and putting at stake the assumption of a single contamination source.

To verify this influence, another silicon sample was placed in a quartz glass, held horizontally by shards of a similar alumina crucible and treated in the same conditions, for 60 minutes and up to 1200 ºC. The GD-MS results correspond to the 1200_60_Ar scatter plot, also in Figure 4.2.

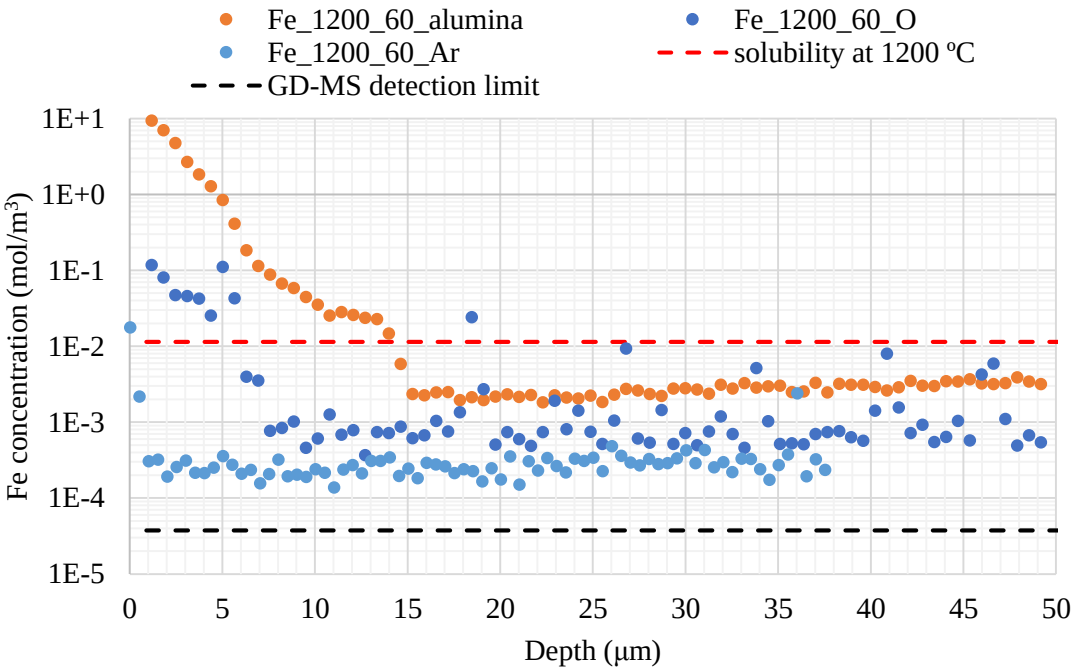

Figure 4.2 - Iron concentration profiles analysed by Ekstrøm through GD-MS.

In a more detailed fashion, the graph above comprises the following samples: 1200_60_O – silicon sample placed in a cylindrical quartz glass, held by alumina supports in air atmosphere, 1200_60_Ar – silicon sample placed in a cylindrical quartz glass, held by alumina supports in argon atmosphere; 1200_60_alumina – silicon sample placed in an alumina crucible. All were heat treated at 1200 ºC for 60 minutes and the depth values were determined by the product of the sputtering time by the sputtering rate (20 nm/s).

The analysis of the heat-treated samples indicates other sources near the polished surfaces, clear due to the observation of considerable amounts of dust inside the crucibles, originating from the steel alloy box, which could not withstand running in temperatures above its specifications.

A third sample was prepared, without feeding argon into the protective box, represented in Figure 4.2 by the scatter 1200_60_O. It shows higher iron concentration than the sample prepared in argon atmosphere, conceiving the possibility that the rate of iron transport towards the sample might increase in the presence of oxygen. The overall inferior contamination justified the choice of quartz over alumina in the following experiments.

4.1.2 Nabertherm LHT 04/18

The deterioration of the steel box led to seeking another furnace, while continuing the study of iron for 1200 ºC treatments, in a non-oxidizing atmosphere. In the same lab at NTNU, a Nabertherm LHT 04/18 could provide heat treatments in argon atmosphere up to 1800 ºC, without requiring an atmosphere-protective box. Unfortunately, previous experiments in this furnace have shown signs of air infiltration from the surrounding environment, resulting in oxidation of the treated samples.

As stated previously, oxidation can lead to precipitates in the Si|SiO_2 interface, estimated to happen at depths smaller than 0.1 µm [71]. This section, usually lost during preliminary sputtering [60], may contain a considerable portion of the total amount of impurity, since it is closest to the source, meaning that there is a chance of decreasing the number of points above the GD-MS detection limits, especially

for short duration treatments and low diffusivities. Less data can be detrimental for curve fitting with Fick's equations or for estimation of the quantity of contaminant in the silicon sample.

Therefore, a series of 60-minute oxidation tests with mono-Si was performed, changing argon inlet conditions, sample holder and maximum temperatures. None of these samples was analysed between the different preparations, as the GD-MS was unavailable.

Two samples were prepared at 1200 ºC, for 60 minutes, with the same quartz glass apparatus, with 5N purity argon. The first at a volumetric flow of 250 L/h (20 ºC, 300 mbar) and the second with 500 L/h (20 ºC, 300 mbar), attempting to decrease oxidation (Figure 4.3).

a) b)

Figure 4.3 - Silicon test samples annealed in Nabertherm LHT 04/18 up to 1200 ºC, during 60 minutes with an argon flow of a) 250 L/h (20 ºC, 300 mbar) b) 500 L/h (20ºC, 300 mbar).

It is visible that the first sample, in Figure 4.3 a), experienced different levels of oxidation or contamination, and that the second, in Figure 4.3 b), showed a less heterogeneously coloured surface. These different colours are given by the interaction of the reflective response of regions with varying composition and lattice positioning to the incident wavelengths of the ambient light spectrum.

A factor that could contribute to oxidation was identified and so an alternative to the quartz glass was proposed. As depicted in Figure 4.4, the argon inlets are placed in the sides of the chamber, while the dimensions of the quartz glass limit its placement, keeping its aperture towards the furnace door. This means not only that the direct flow of argon into the crucible is obstructed, but also that when the door is opened for sample placement, the air can get entrapped around the sample taking a longer period to be flushed out.

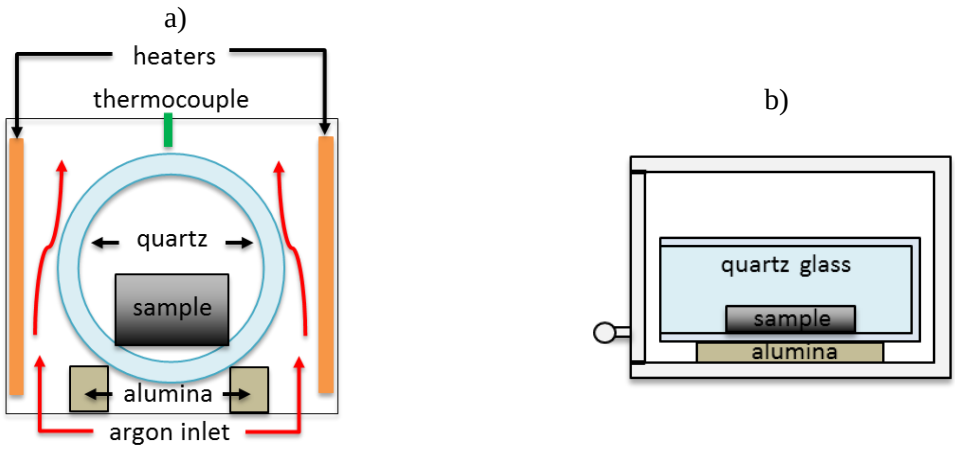

Figure 4.4 - Schematic of the apparatus with previously used quartz glass crucible: a) illustration of the argon inlets and components inside the furnace; b) side view for length comparison of the crucible and furnace interior.

The alternative consisted in replacing the quartz glass with a Heraeus HSQ 100 electrically fused quartz plate, provided by the glass blowing workshop at NTNU. Another two samples were prepared in the new apparatus (Figure 4.5 a)). The furnace was flushed with argon for 30 minutes before placing the samples, in attempt to flush out air entrapped within the pores of the refractories, keeping the volumetric rate at maximum, 500 L/h (20 ºC, 300 mbar).

The first (Figure 4.5 b)), was similarly treated at 1200 ºC, for comparison to the already mentioned samples and the second (Figure 4.5 c)), until 1350 ºC, to ensure that silicon remained below its melting point, since the type B thermocouple which was placed above the sample, registered higher values than the furnace's display. This temperature excess could not be avoided, due to the reheating occurring after the samples were introduced and the furnace's door was shut. The radiative heating process always caused a faster increase on the surfaces (white and porous, otherwise non-specified fibrous refractory bricks). Consequently, while the temperature on the furnace display was constant, at desired maximum temperature, the thermocouple would measure instead a decreasing profile from about 50 ºC above the display, to a 30 ºC excess after 1 hour or 10 ºC after 3 hours.

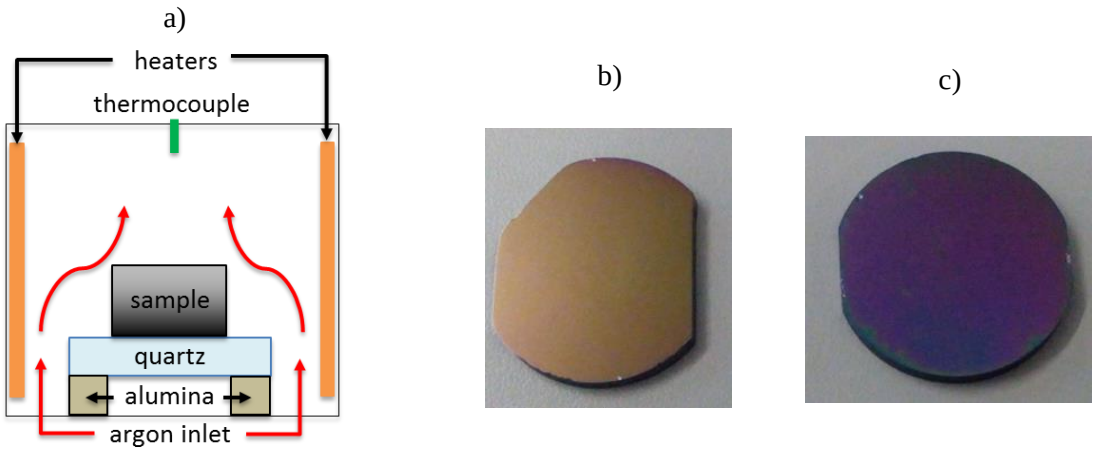

Figure 4.5 - a) Representation of the apparatus with quartz plate; Aspect of the silicon samples annealed during 60 minutes b) up to 1200 ºC c) until 1350 ºC.

At 1200 ºC, a noticeable change in colour could mean that the oxide layer thickness was altered and the sample treated at 1350 ºC might have had a thicker layer as expected. The lack of further GD-MS analysis led to the heat treatment of diffusion couples, despite of oxidation.

4.2 Diffusion couples

The data gathered for the heat treated couples is shown in Table 4.1 as well as in Figure 4.7, Figure 4.8 and Figure 4.9. Additionally, one couple assembled with kanthal wire was treated during 60 minutes up to 1200 ºC and verified in the GD-MS (Figure 4.6).

Table 4.1 - Annealing conditions of the couples, whose silicon parts were analysed by GD-MS

		t_{ht} (minutes)			
		3	12	60	180
T_{ht} (ºC)	1200	Fe	Fe	Fe	Ti
	1275	-	-	-	Ti
	1350	-	Ti	Ti	-

Until Figure 4.9, the depth was once again determined by the product of the sputtering time by the sputtering rate (20 nm/s) and the points below the detection limit present no meaning other than locating non-quantified sections.

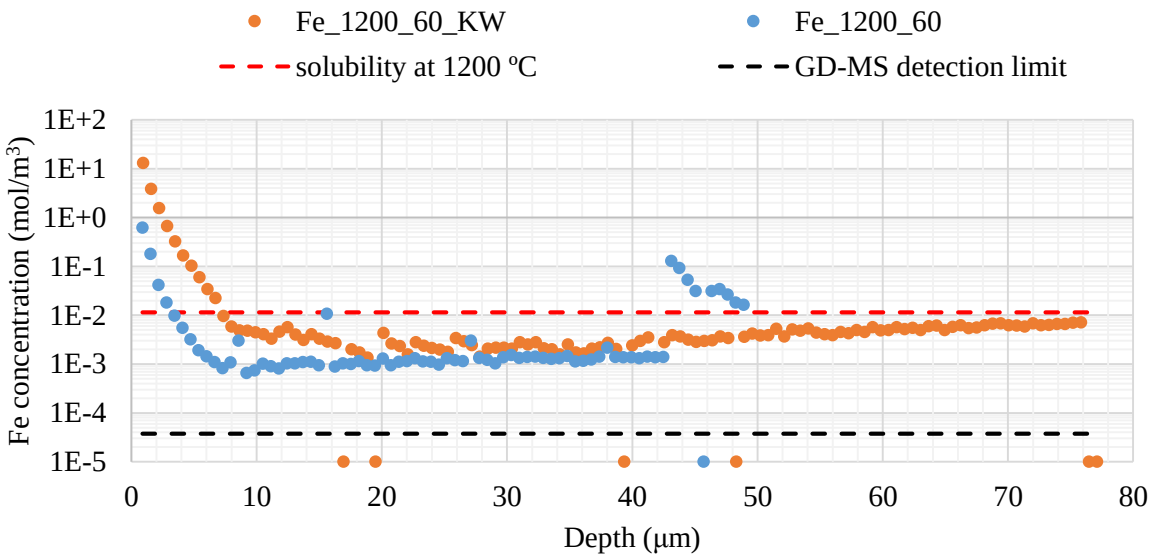

Figure 4.6 - Iron concentration profiles obtained by GD-MS, of couples treated for 60 minutes up to 1200 ºC. Contains the following samples: Fe_1200_60_KW – diffusion couple held with kanthal wire; Fe_1200_60 – diffusion couple held with silicon weight.

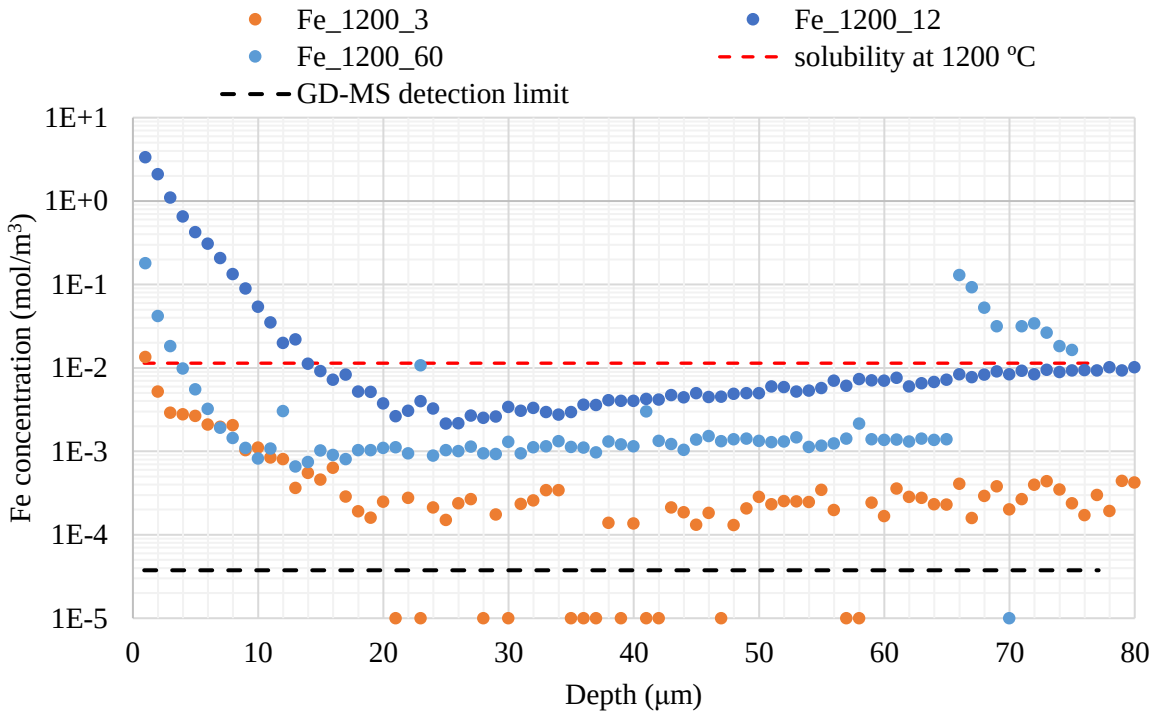

Figure 4.7 - Iron concentration profiles obtained by GD-MS of the diffusion couples held with silicon weight, heated up to 1200 ºC. The following samples are considered: Fe_1200_3 - treated for 3 minutes; Fe_1200_12 - treated for 12 minutes and Fe_1200_60 - treated for 60 minutes.

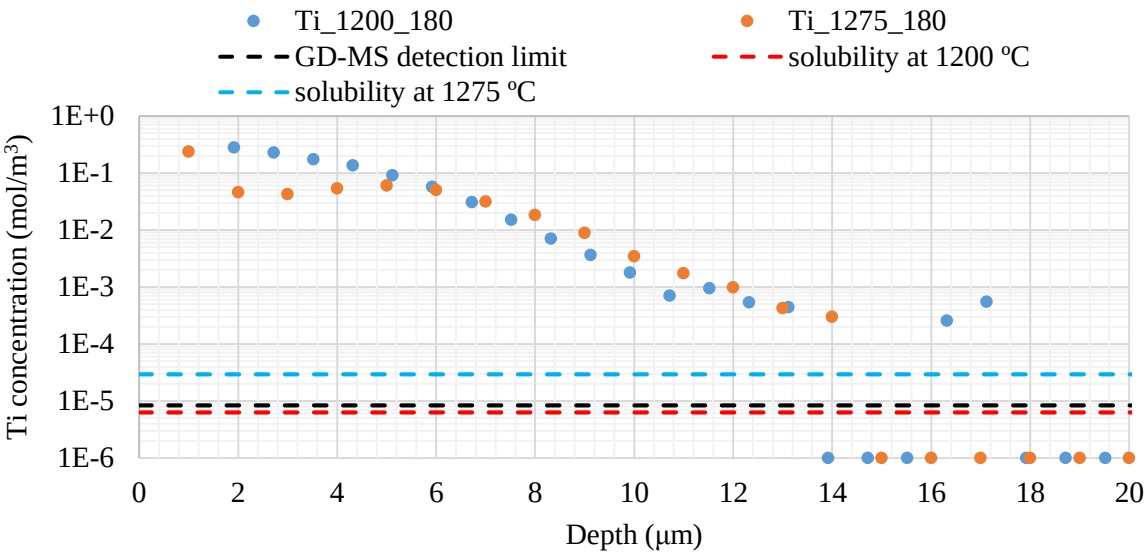

Figure 4.8 - Titanium concentration profiles obtained by GD-MS of the diffusion couple held with silicon weight: Ti_1200_180 – heated up to 1200 ºC; Ti_1275_180 - heated up to 1350 ºC. Both during 180 minutes and put together with kanthal wire.

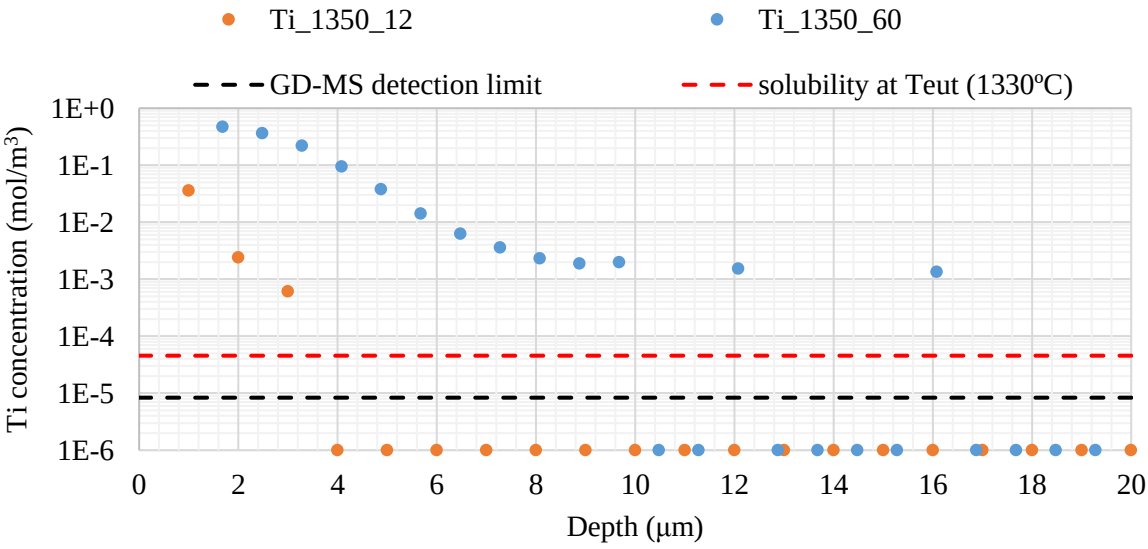

Figure 4.9 - Titanium concentration profiles obtained by GD-MS of the diffusion couple held with silicon weight: Ti_1350_12 – heated for 12 minutes; Ti_1350_60 - heated for 60 minutes. Both up to 1350 ºC and put together with kanthal wire.

4.3 Ti diffusivity in the crucible

A method which considers the presented depth profiles of Ti in order to achieve an estimate for the diffusion coefficient in the Si_3N_4 crucible has been employed, applying a MATLAB script (Appendix B), as explained in the following chapter, according to a set of assumptions and three different scenarios. The first low end scenario, considers the average titanium concentration in silicon, based on the GD-MS measurements and assumes non-detected regions as zeros. The second uses the detected value nearest to the interface to describe the missing data near the surface, being conservative regarding the decreasing profile suggested by Fick's 2^{nd} law. Finally, the third resources to curve fitting of the GD-MS profiles with the particular solution of this law for an inexhaustible source. It is vital to keep in mind that this should only be regarded if proven that there were no other Ti sources than the crucible itself, that the eventual cracks in the crucible did not affect the rate of diffusion and when the Ti content of the crucible is confirmed.

Table 4.2 - Estimates of the diffusion coefficients at the annealing temperature for each sample, considering different amounts of Ti in the crucible and the three scenarios

Scenario	Ti content in the crucible (mol/m^3)	T_{ht} (°C)	t_{ht} (min)	D (m^2/s)
1	0.027	1200	180	9.79×10^{-14}
		1275	180	2.62×10^{-14}
		1350	60	4.62×10^{-13}
		1350	12	7.21×10^{-15}
	0.054	1200	180	2.22×10^{-14}
		1275	180	7.18×10^{-15}
		1350	60	1.06×10^{-13}
		1350	12	4.37×10^{-15}
	0.082	1200	180	9.94×10^{-15}
		1275	180	3.57×10^{-15}
		1350	60	4.82×10^{-14}
		1350	12	2.82×10^{-15}
2	0.027	1200	180	2.72×10^{-13}
		1275	180	9.18×10^{-14}
		1350	60	1.90×10^{-12}
		1350	12	2.11×10^{-14}
	0.054	1200	180	5.48×10^{-14}
		1275	180	2.24×10^{-14}
		1350	60	3.49×10^{-13}
		1350	12	9.02×10^{-15}
	0.082	1200	180	2.33×10^{-14}
		1275	180	1.04×10^{-14}
		1350	60	1.46×10^{-13}
		1350	12	5.69×10^{-15}
3	0.027	1200	180	3.87×10^{-13}
		1275	180	5.50×10^{-13}
		1350	60	4.19×10^{-12}
		1350	12	1.37×10^{-13}
	0.054	1200	180	7.37×10^{-14}
		1275	180	1.09×10^{-13}
		1350	60	6.50×10^{-13}
		1350	12	4.38×10^{-14}
	0.082	1200	180	3.08×10^{-14}
		1275	180	4.63×10^{-14}
		1350	60	2.58×10^{-13}
		1350	12	2.46×10^{-14}

From the results of every scenario, it is visible how relying only on the three known points, in the sample treated during 12 minutes, can drastically affect the resulting diffusivity. As the sample treated up to 1350 ºC during 60 minutes indicates, if there are no external sources of Ti, the diffusivity should be much higher, meaning that in fact, the concentration for the non-quantified points near the surface of the 12 minute-annealed sample must be superior to what each scenario proposes. Since there are so few points, the unknown values near the surface contribute to a much higher uncertainty, relatively to the other samples. Therefore, it has been excluded for the following exponential regression (Figure 4.10, Figure 4.11 and Figure 4.12), to estimate D_0 and H_M of equation (2.15), according to the annealing temperatures and calculated diffusivities:

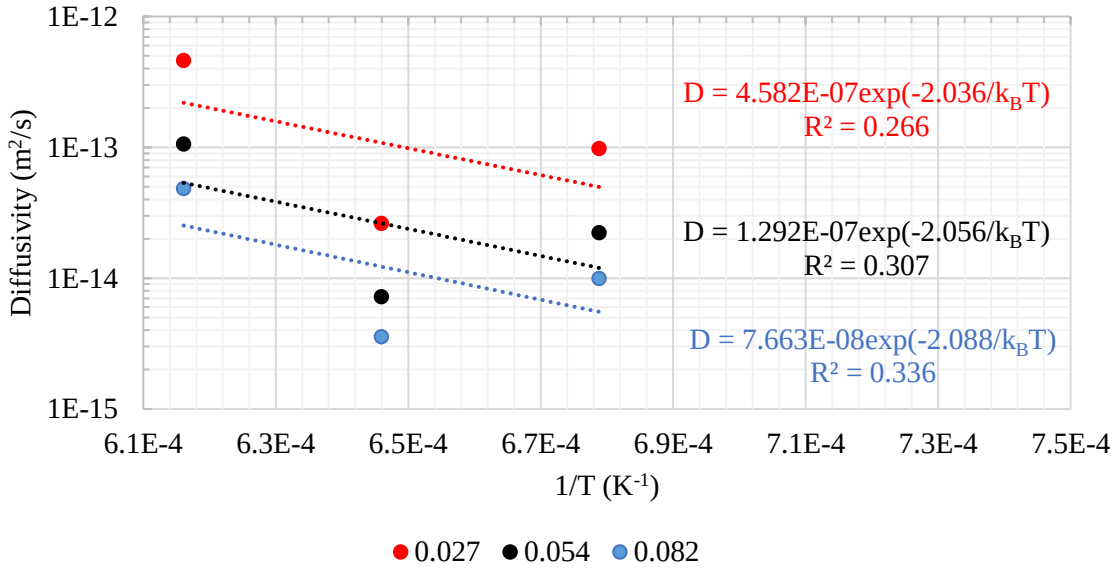

Figure 4.10 - Arrhenius fit of scenario 1, for three different Ti compositions in the crucible: low estimate (0.027 mol/m^3), proposed by manufacturer (0.054 mol/m^3) and high estimate (0.082 mol/m^3).

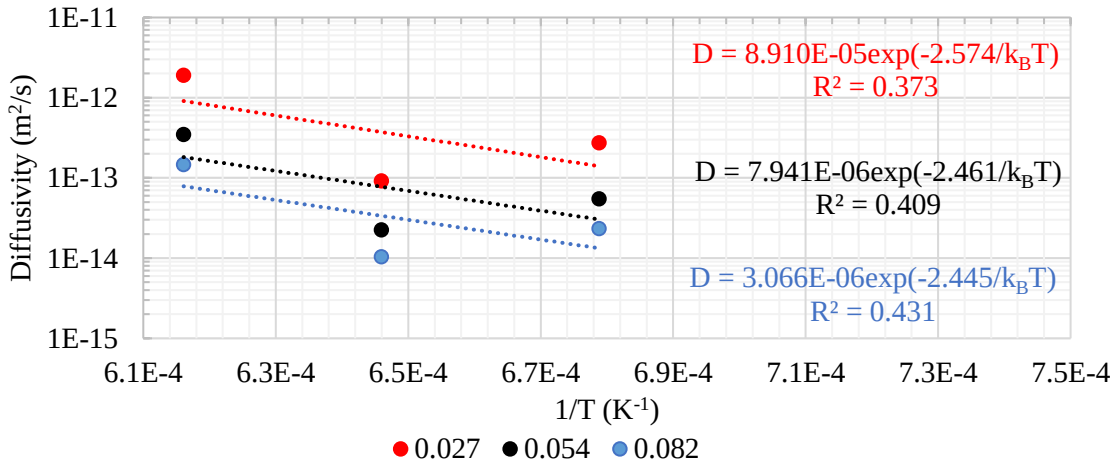

Figure 4.11 - Arrhenius fit of scenario 2, for three different Ti compositions in the crucible: low estimate (0.027 mol/m^3), proposed by manufacturer (0.054 mol/m^3) and high estimate (0.082 mol/m^3).

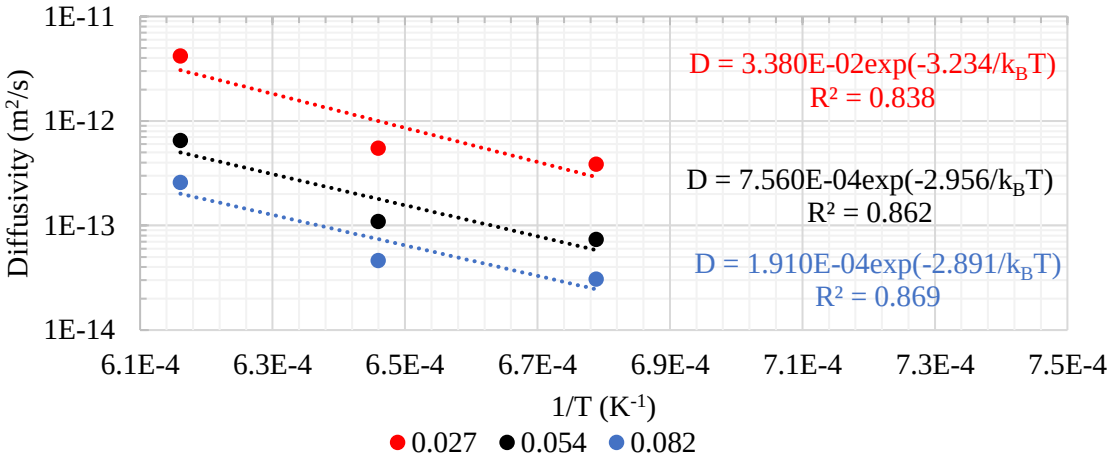

Figure 4.12 - Arrhenius fit of scenario 3, for three different Ti compositions in the crucible: low estimate (0.027 mol/m^3), proposed by manufacturer (0.054 mol/m^3) and high estimate (0.082 mol/m^3).

5 Discussion

5.1 Analysis of the Fe profiles

The diffusion couples heated for 60 minutes show a similar trend, with the one which had kanthal wire presenting a higher Fe content near the interface. This suggests that the impurity amount in the wire has increased the concentration gradient, bringing more Fe atoms into the mono-Si wafer, or that it was present in its vicinity, migrating into the posteriorly sputtered region and accumulating at the surface aided by the occurrence of supersaturation. Non-quantified points can signal the existence of nucleation sites and the increasing slope, after 20 μm, seems to relate to a traveling trend towards the surface, during the cooling stage, according to how far a solute atom is from it at the beginning.

There also appears to be a not so steep increasing slope, at sample Fe_1200_60, followed by a section where precipitation occurs, which might explain the difference in slope, as atoms have an increased probability of diffusing towards it when cooling starts, and they are located nearby at that time.

According to the predictions in Figure 3.3, the penetration depths are far longer than what was analysed, so even if there is a region that matches a profile described by equation (2.14), this has more to do with the solubility limit in silicon. This precludes the determination of the diffusivity in the crucible without a good description of all the present Fe sources, a balance of the Fe content in the silicon sample (prior and after the treatment) or a direct study of the crucible material.

This challenge remains in the samples annealed for shorter periods, with a similar increasing slope. On a first glance, the couple that went through 3 minutes of annealing displays less iron concentration than every other sample, as predicted, by considering that there is a direct relationship between the amount of diffused impurity and the elapsed time. The peak temperature however, was just reached before removing the couple from the heated environment, meaning that diffusion mostly occurred at inferior temperatures, where the solubility is lower than represented maximum, at 1200 ºC.

The couple heated for 12 minutes shows higher iron content, which prompts the possibility of contamination. As every sample was assembled and handled in a similar fashion, it cannot be excluded that it also happened at some extent with all the samples. Given the rather quick diffusivity of Fe in silicon, as suggested by the cited authors, the wafer dimensions and Figure 3.3, less iron is required to produce a concentration gradient capable of affecting the measurements, the closest it stands near the sputtered area. Most likely the source of Fe was present prior to heat treatment, since this allows its diffusion into the samples at a much faster rate than while cooling, phase on which the trend in the supersaturated silicon should occur in the opposite sense.

The composition of the refractories inside the furnace was not specified by the manufacturer. If this was the source, the contamination should me more noticeable in longer treatments due to longer exposure, however this does not explain why Fe_1200_12 presents more iron than Fe_1200_60. Dust particles present on the refractory brick and table where the couples stood before annealing, or the tweezers used to insert them in the furnace, capable of scratching the polished silicon surface, may be the main contributors. Particularly in the first case, since it is deposited at a region closer to the studied surface (up to 3.5 mm) while the second hypothesis signifies a length of at least about 1 cm, as tweezer contact was made on the lateral surfaces. When considering the preparation of the crucible samples, on which contamination was not verified, the saw cutting may possibly introduce iron in the crucible into a region deeper than the grinded portion of 2 mm, or part of it could have persisted in the pores of the material, after all the grinding and polishing steps.

5.2 Analysis of the Ti profiles

All the samples analysed for Ti were sputtered up to a depth of 89 µm without any point above the detection capabilities. By the approach in section 3.5, the impurity amount could cross the detection limit at about 62 µm for a sample heated up to 1350 ºC, during 12 minutes (Figure 5.1):

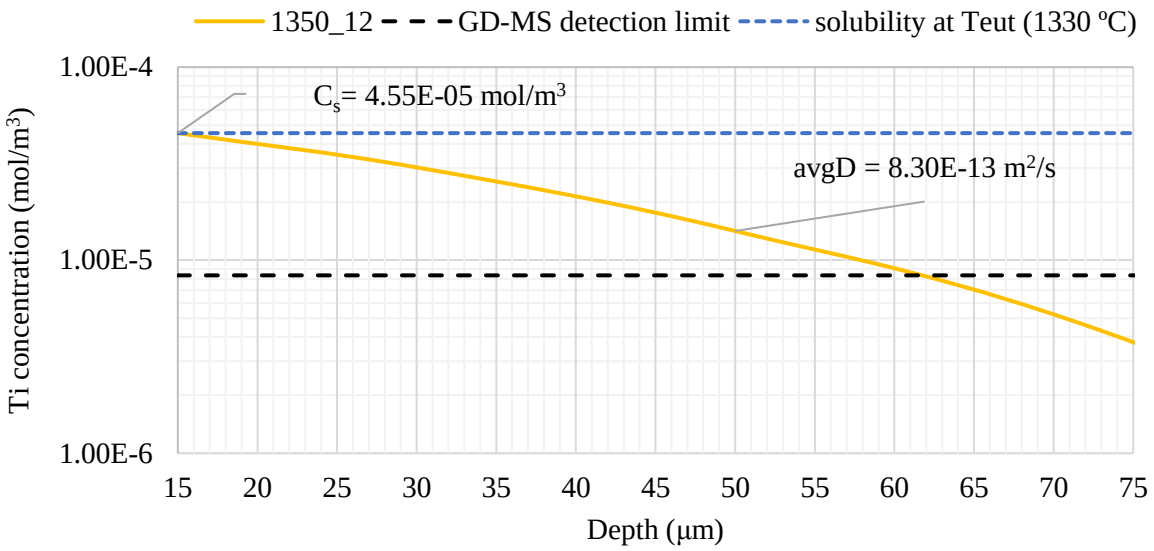

Figure 5.1 - Ti concentration profile, determined based on equation (2.14**)**, starting at 15 µm, for a sample treated during 12 minutes, up to 1350 ºC.

Most likely, if the sputtering went on to the following sections, there would be no more to regions above the detection limit. This is due to the proneness for Ti oxidation and silicate formation at these high temperatures, in addition to a solubility limit at the highest temperature that is near the detection capability. Also, the employed cooling rate is slow and there is a high amount of other elements near the surface that could form nucleation centres.

Considering that longer heating periods, as well as higher temperatures, typically resulted in superior amounts of impurity near the surface (Figure 4.8 and Figure 4.9) and that similarly, all data after a certain point is below the detection limit, the same assumption was taken for the other Ti samples.

This can provide a low-end estimate of the diffusivity in the crucible, based on the fact that it dictates how much of the impurity reaches the silicon wafer, if the diffusivity in the ceramic is lower than in mono-Si. However, one cannot certainly judge whether other Ti sources were present, which could be clarified through a reproducibility analysis with more samples.

Comparing Ti_1200_180 with Ti_1275_180, there is more impurity at 1200 ºC, but the profiles are similar and the higher temperature may permit atoms to diffuse from longer distances, towards the silicon surface by the contribution of supersaturation. Thereby, more Ti can potentially be found in the non-quantified depth, from 0 to 1.68 µm, of the sample annealed up to 1275 ºC, relatively to the other mention.

Also worth referring to, every detected amount of Ti was measured above the solubility limit for the annealing temperature, so the solubility above eutectic temperature is not clarified by the results and the concentration profiles do not match equation (2.14). Thus, it suggests that an inexhaustible source could eventually be assumed for some section below the detection limit, where a matching slope may occur.

5.2.1 Diffusion couple cracks

Both components of several couples secured with kanthal wire have visibly cracked. For silicon, this meant flaking at its edges and back surface (this sample was not submitted to analysis), so it should not influence the sputtered region to a great extent. Additionally, the Si_3N_4 crucible cracked frequently in the surface facing the silicon wafer. This may be due to mechanical stress when tightening the wire, followed by a thermal expansion of the wire during heat treatment as the couples held in place with a silicon weight do not show cracks, at least at the macroscopic level.

The existence of cracks during the annealing period is relevant, as the impurities may diffuse faster through them and, therefore, the estimate is a combination of the diffusion in every available pathway, which might not describe a situation where no cracks have been formed. Moreover, if one considers glow-discharge sputtering to obtain the depth profiles in the crucible, the working plasma may reach deeper sections, putting at stake the flatness of the surface and thereby the spatial character of the results.

5.2.2 Scenarios

Seeking to achieve the stated diffusivity estimate in the crucible, a different approach was developed. It relies on describing the silicon sample as a vector, in which the depth interval between elements matches the one presented in the measurements. The available concentration data is placed in the corresponding depth and the missing elements, including non-detected points, are set as zeros (scenario 1), which is necessarily less than the amount present in the samples.

Furthermore, the depth spacing between elements signals missing data points near the interface. According to the concentration gradient, the average concentration in these points should be above the subsequent. Therefore, scenario 2 was also considered, where the first registered concentration value was attributed to them (as shown in Figure 5.6), as this should provide a closer description, probably still lower than what was effectively present in the samples.

Alternatively, one could figure out the missing points by fitting the GD-MS measurements to a diffusivity and constant surface concentration (equation (2.14)). This was done with MATLAB's curve fitting tool and showed in Figure 5.2, Figure 5.3, Figure 5.4 and Figure 5.5. Due to the previously stated phenomena occurring in addition to diffusion, this translates into smaller diffusion coefficients, among 10^{-16} – 10^{-14} m^2/s, in comparison to what the literature suggests for Ti diffusion in silicon (10^{-13}-10^{-12} m^2/s). Simultaneously, the surface concentrations of 0.46 – 1.2 mol/m^3, are much higher than what has been specified by the manufacturer for the titanium content of the crucible (0.027-0.082 mol/m^3).

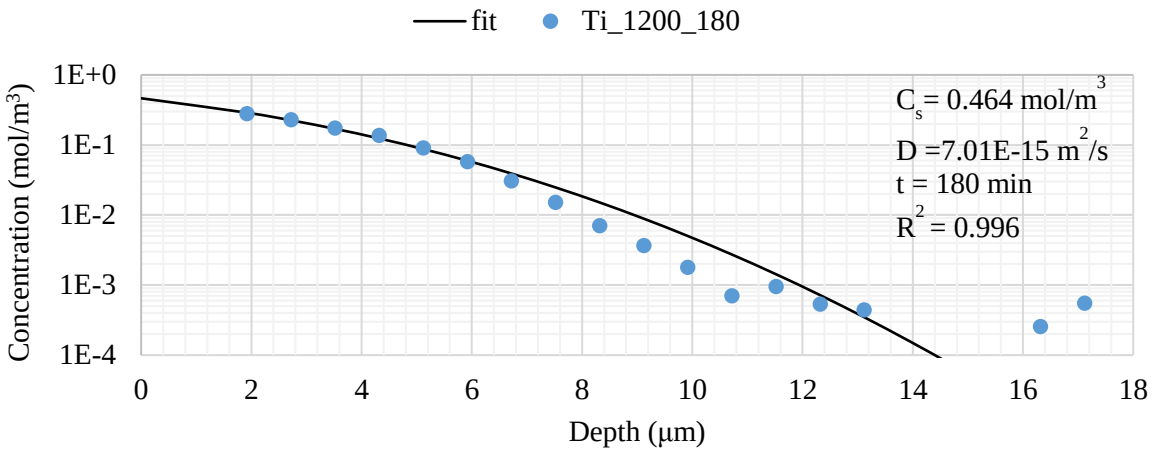

Figure 5.2 - Curve fitting results of equation (2.14**)** for the GD-MS profile of the sample heated up to 1200 ºC during 180 minutes. The curve fit refers to every data point.

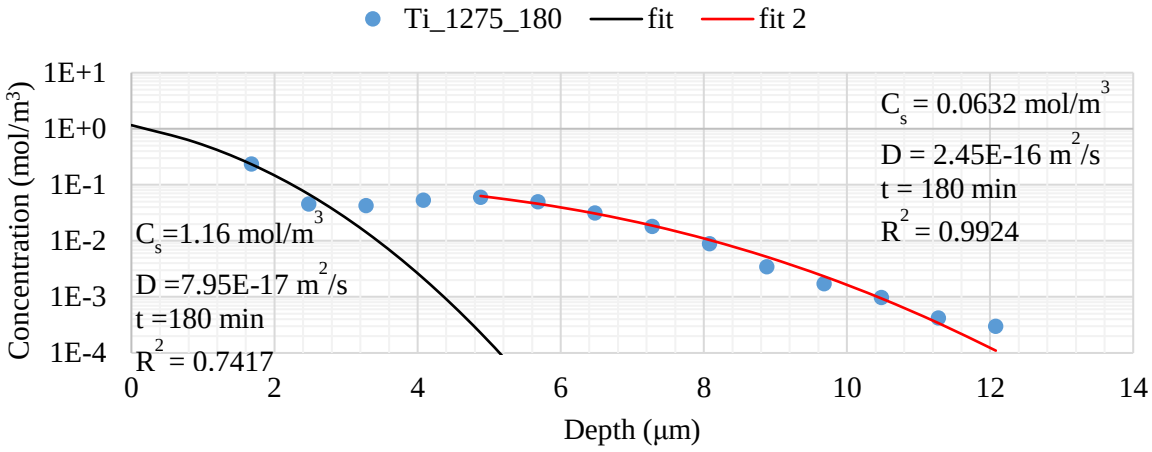

Figure 5.3 - Curve fitting results of equation (2.14**)** for the GD-MS profile of the sample heated up to 1275 ºC during 180 minutes. Fit refers to every data point, but for fit 2 the profile starts at the first considered concentration value, taken as the surface.

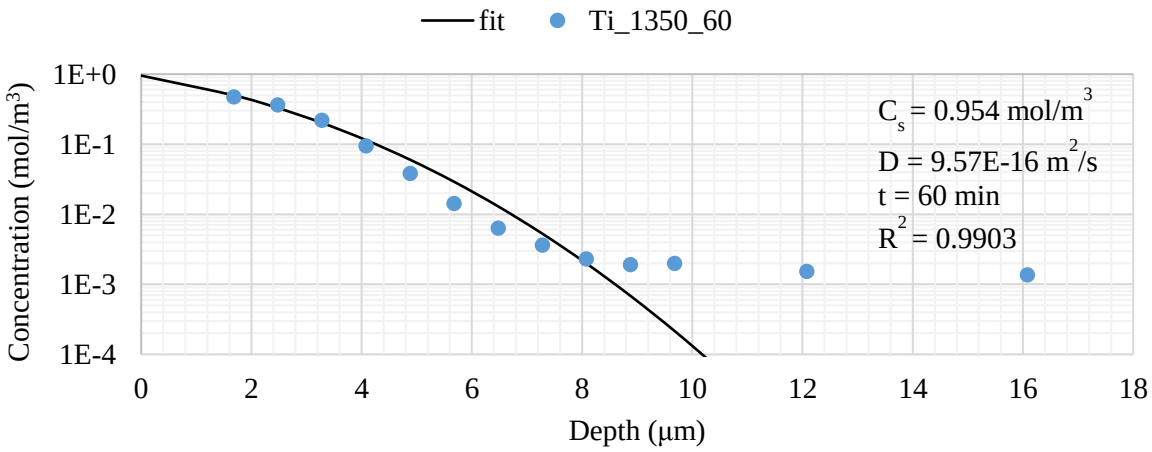

Figure 5.4 - Curve fitting results of equation (2.14**)** for the GD-MS profile of the sample heated up to 1350 ºC during 60 minutes. The curve fit refers to every data point.

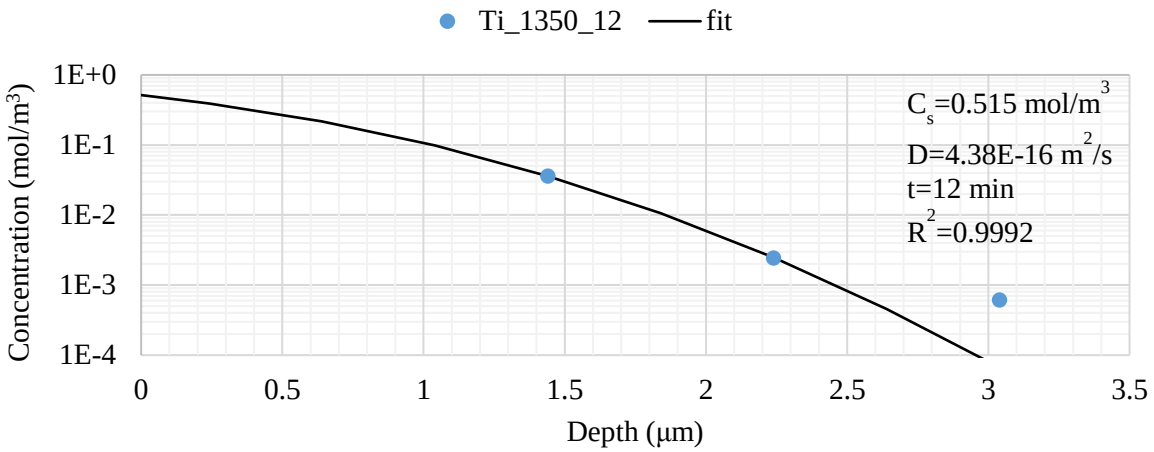

Figure 5.5 - Curve fitting results of equation (2.14**)** for the GD-MS profile of the sample heated up to 1350 ºC during 12 minutes. The curve fit refers to every data point.

Nonetheless, these profiles point out that this type of trend cannot be always predicted using the same parameters. Take for example Figure 5.3, where concentration increases, between two regions where the opposite happens. Given that the majority of the impurity atoms lie near the surface, a poor prediction can significantly affect the estimate for the diffusion coefficient in the crucible, potentially in orders of magnitude. Thus, this scenario (3) lacks more results for comparison, to know whether it is a reasonable approach for the diffusivity estimates of Ti in the Si_3N_4 crucible. The non-quantified concentration points near the interface were determined according to the parameters in Figure 5.2, Figure 5.3, Figure 5.4 and Figure 5.5, relatively to the black fit curve and equation (2.14).

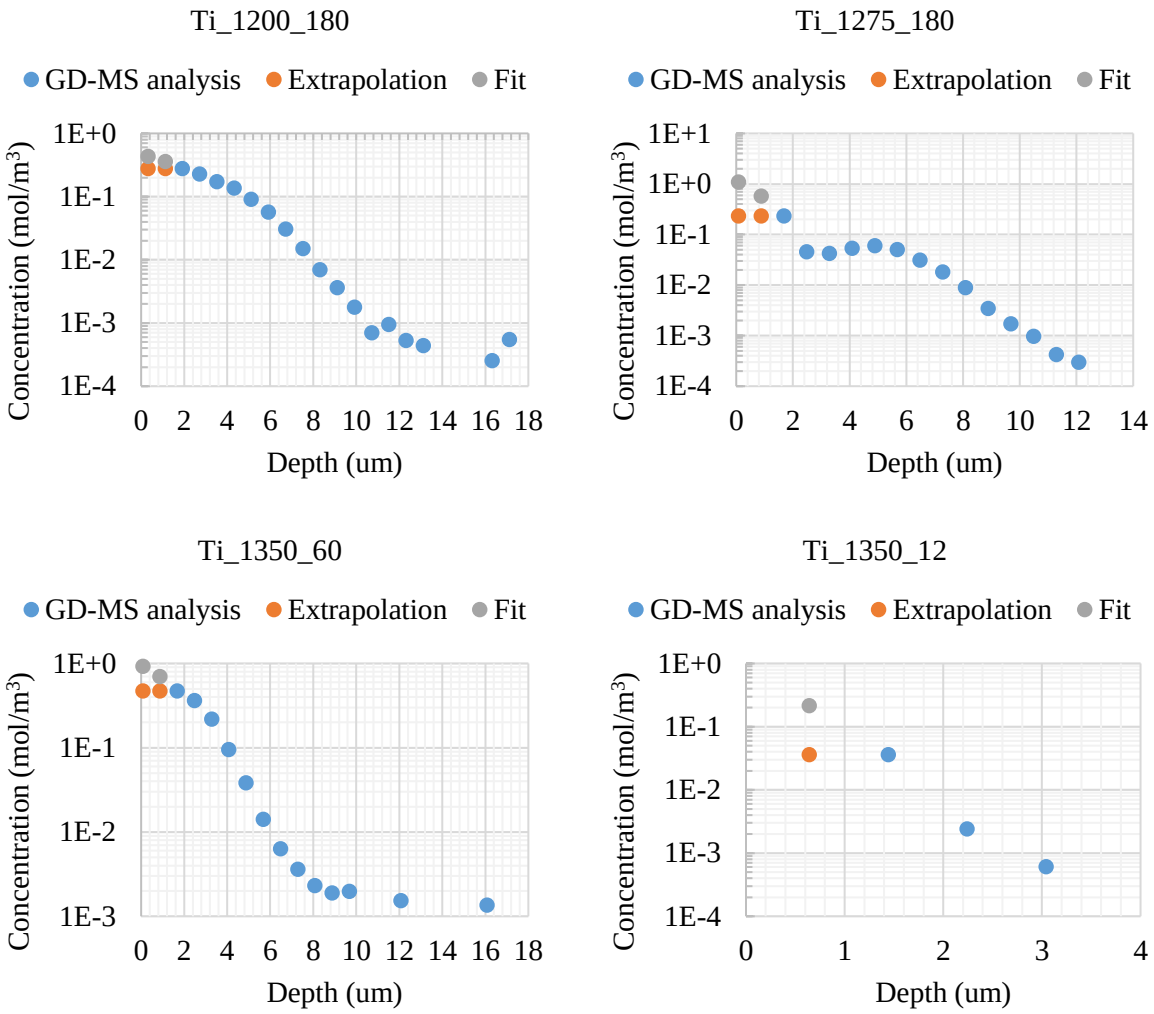

Figure 5.6 - Ti concentration profiles for scenario 1 (GD-MS analysis), scenario 2 (GD-MS analysis with extrapolation) and scenario 3 (GD-MS analysis with fit).

5.2.3 Impurity amounts

Afterwards, the average concentration among the vectors was determined, which means that, for a continuous profile, the gap between two points corresponds to the average of their concentrations, with the first and last elements relating in the same manner. For this to be true, however, the sputtered area from the sample surface must be seen as constant, a fair stipulation since the GD-MS analysis follows a verified method for monocrystalline silicon, where one of the objectives is to keep a flat sputtered section.

The product of the average concentration by the thickness of the silicon sample, $t_{Si} = 3.5\ mm$, is then approximated to n, the total impurity amount in the sample portion of the same thickness, delimited by the sputtered cross section, in mol/m^2.

$$n \sim t_{Si} \times \frac{\sum_{i=1}^{N} C(i)}{N} \tag{5.1}$$

where $i = 1$ refers to first element of the concentration vector C, and N to the last one before t_{Si}. The respective results are presented in Table 5.1:

Table 5.1 - Calculated amount of Ti in the mono-Si samples for each scenario

T_{ht} (ºC)	t_{ht} (min)	n (mol/m^2) Scenario 1	Scenario 2	Scenario 3
1200	180	0.823	1.270	1.457
1275	180	0.443	0.821	1.792
1350	60	0.981	1.741	2.288
1350	12	0.031	0.060	0.204

5.2.4 Correction for the constant temperature assumption

With this in mind, an explicit finite difference method for equation (2.12) was developed in MATLAB, to estimate the diffusivity in the crucible that provided similar n values. As the temperature was not always constant, but instead followed a profile similar to Figure 3.2, finding a constant value for diffusivity at the heat treatment temperature requires a correction to the $t_f=t_{ht}+t_{cool}$ period.

The literature data regarding the diffusivity of Ti in silicon was taken for this correction, although it should be expressed, preferably, by the limiting process at each time step, i.e. the smallest diffusion coefficient. This is due to it being the major contributor for the final amount of contaminant, by its effect on the concentration gradient and the rate of mass transfer in the system. Even then, this approach is ambitious, thanks to the role played by the diffusion coefficient in the concentration values at each time step.

$$t_{f,T=const} = t_f \times \frac{\overline{D_{Si}}}{D_{Si,T_{ht}}} \tag{5.2}$$

$t_{f,T=const}$ expresses the period of the heat treatment at the highest registered temperature, which should yield the same contamination as the treatment with reheating and cooling stages. It is determined by the product of the original duration by the ratio of the mean diffusivity predicted in silicon, $\overline{D_{Si}}$ (relying on the values at each time step) and the diffusivity in silicon at the highest temperature $D_{Si,T_{ht}}$.

The influence of this consideration has been verified with the MATLAB script in Appendix C**,** using the Arrhenius equations in Figure 4.12. The impurity amounts in silicon after treatment were determined according to the varying and constant temperature profiles:

Table 5.2 - Relative change of the estimates for Ti amount in silicon, for the varying profile in comparison with the constant temperature assumption

Scenario	Ti content in the crucible (mol/m^3)	T_{ht} (ºC)	t_{ht} (min)	$\frac{n - n_{T=const}}{n_{T=const}}$ (%)
1	0.027	1200	180	-0.062%
		1275	180	-0.064%
		1350	60	-0.239%
		1350	12	-1.526%
	0.054	1200	180	-0.070%
		1275	180	-0.073%
		1350	60	-0.277%
		1350	12	-1.939%
	0.082	1200	180	-0.079%
		1275	180	-0.081%
		1350	60	-0.318%
		1350	12	-2.354%
2	0.027	1200	180	-0.127%
		1275	180	-0.126%
		1350	60	-0.454%
		1350	12	-2.787%
	0.054	1200	180	-0.123%
		1275	180	-0.124%
		1350	60	-0.462%
		1350	12	-2.998%
	0.082	1200	180	-0.126%
		1275	180	-0.127%
		1350	60	-0.482%
		1350	12	-3.286%
3	0.027	1200	180	-0.181%
		1275	180	-0.175%
		1350	60	-0.609%
		1350	12	-3.680%
	0.054	1200	180	-0.173%
		1275	180	-0.171%
		1350	60	-0.626%
		1350	12	-3.917%
	0.082	1200	180	-0.173%
		1275	180	-0.172%
		1350	60	-0.640%
		1350	12	-4.151%

There is concordance between heat treatment duration and the relative change in the resulting amount of Ti in the silicon sample. Longer periods are associated to larger fractions of the temperature profile at the maximum value, therefore the description using $t_{f,T=const}$ and $D_{Si,T_{ht}}$ is closer to the result for a

varying temperature profile, with its corresponding diffusivity. Remembering that the couple heated for 12 minutes was disregarded in the estimates, these differences in impurity amount are severely lower than those imposed by the coefficients resulting from the Arrhenius fits (Figure 4.12). Therefore, if we were able to avoid the constant temperature assumption, accounting instead the variations in temperature, these diffusion coefficient estimates would remain within their order of magnitude.

5.2.5 Iterative method results

A 2D matrix was defined to describe the Ti concentration in the crucible and the silicon wafer along their thickness in each dt time step. The depth spacing, dx, was determined through a function of von Neumann's stability condition, where a k factor of 2.5 was used, keeping the sum of the uncertainties of each point at the end of the calculation below $\pm 1 \times 10^{-15}$ mol/m^3, ensuring that it is much lower than the concentration values.

$$dx = \sqrt[2]{k\, D_{max}\, dt} \tag{5.3}$$

D_{max} corresponds to the highest value of diffusivity among both materials. The dt increment was set to $\frac{1}{100}$ minutes, according to the available computing capacity. This means that dx is not equal to the depth spacing between each data point, $dx_{\mathrm{GD-MS}}$, in Figure 5.6. Table 5.3 presents these values, together with the dt increment relative to $dx_{\mathrm{GD-MS}}$, designated by $dt_{\mathrm{GD-MS}}$, resulting from equation (5.3).

Table 5.3 - dx values for $dt = \frac{1}{100}$ minutes, according to the heat treatment temperature, applicable to every sample

T_{ht} (ºC)	dx (µm)	$dx_{\mathrm{GD-MS}}$ (µm)	D_{max} (m^2/s)	$\frac{1}{dt_{\mathrm{GD-MS}}}$ (minutes^{-1})
1200	2.309	0.800	3.55×10^{-12}	833.090
1275	3.157		6.65×10^{-12}	1557.744
1350	4.195		1.17×10^{-11}	2749.049

Higher dt values were employed to check at what extent the estimated diffusivities may differ from the hypothetical values determined for the depth between each GD-MS measurement. These suggest a decay similar to a power function of the estimated diffusivities, with the trend pointing towards values in the same order of magnitude (scenario 1 is shown in Figure 5.7, Figure 5.8 and Figure 5.9, whereas scenarios 2 and 3 are in Appendix E).

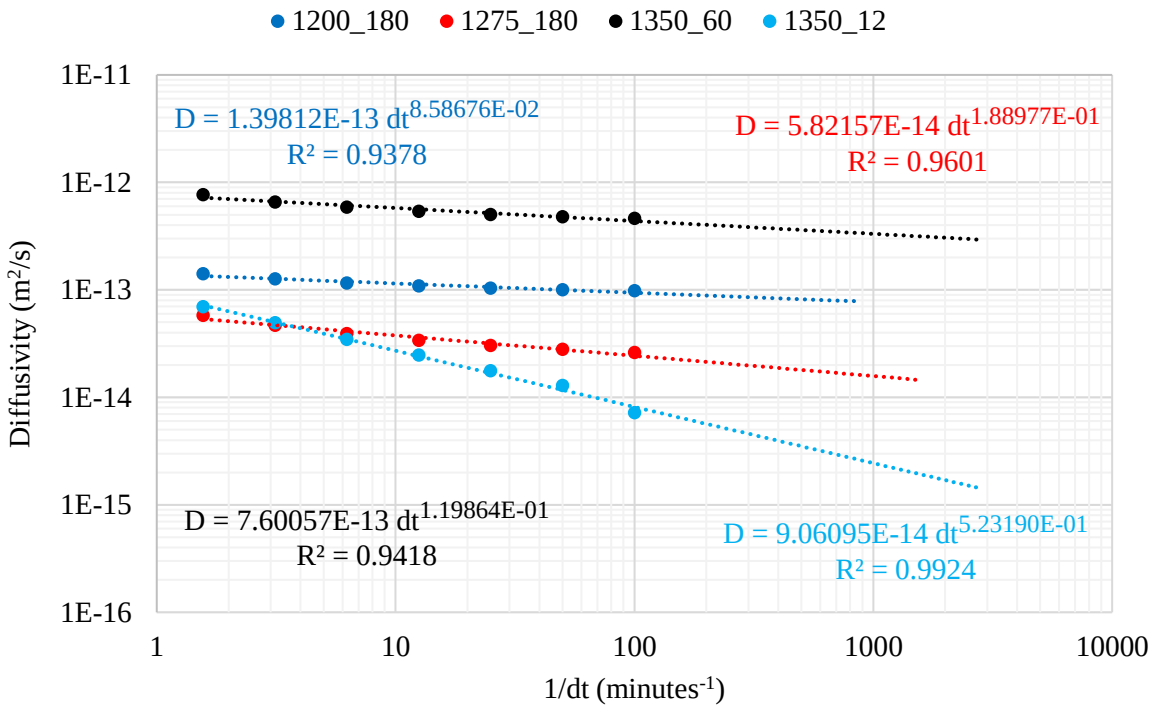

Figure 5.7 - Extrapolation of the diffusivity estimates at the GD-MS depth increment, for scenario 1 and a Ti content in the crucible of 0.027 mol/m^3, by curve fitting a power function.

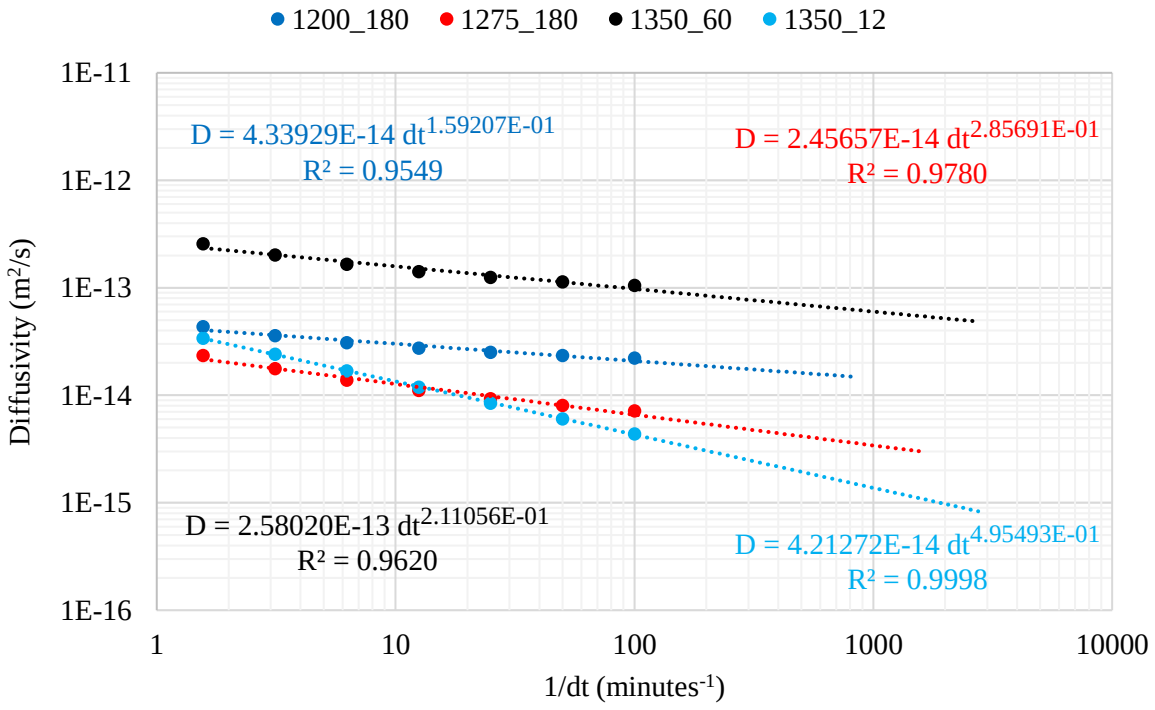

Figure 5.8 - Extrapolation of the diffusivity estimates at the GD-MS depth increment, for scenario 1 and a Ti content in the crucible of 0.054 mol/m^3, by curve fitting a power function.

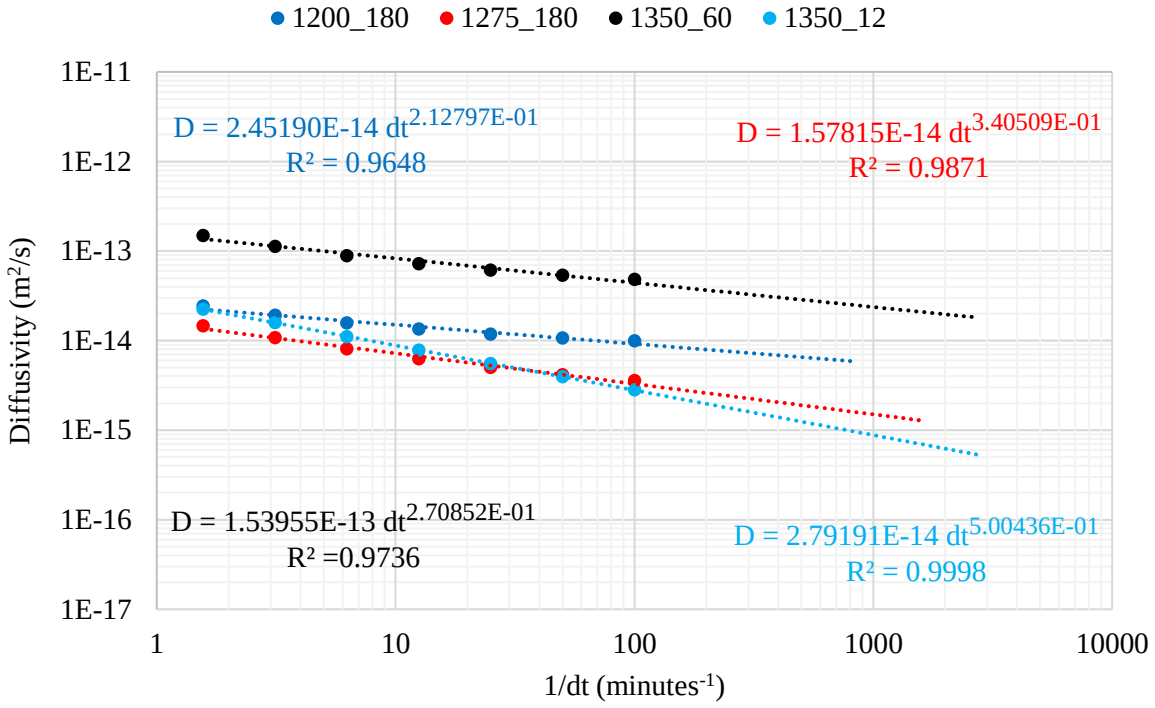

Figure 5.9 - Extrapolation of the diffusivity estimates at the GD-MS depth increment, for scenario 1 and a Ti content in the crucible of 0.082 mol/m^3, by curve fitting a power function.

Since the sample 1350_12 was disregarded, the major expected deviation does not contribute to the Ti diffusion coefficients presented in 4.3. Likewise, Appendix E comprises diffusivity estimates, similar to Figure 4.12, according to the extrapolations. Although these values could not be confirmed by the numerical method, they are slightly lower, so one might be interested in regarding them for a safer low-end approach on the diffusivity of Ti in the crucible.

The initial conditions state that the mono-Si did not contain any titanium atom, however it is only known that the amount was low enough not to be detected by GD-MS of a non-treated sample. In the Si_3N_4 crucible the concentration was considered homogeneous and defined based on three Ti compositions, regarding what has been specified by the manufacturer. A low estimate (0.027 mol/m^3 ~ 0.5 ppmw) and a high estimate (0.082 mol/m^3 ~ 1.5 ppmw) were chosen to include the interval of uncertainty, from Table 3.3, as well as the value in the technical datasheet (1 ppmw ~ 0.054 mol/m^3). Since the requirement is that the amount of Ti is below 1 ppmw, the 0.027 mol/m^3 composition illustrates how the diffusivity computation may vary due to having less impurity available.

By varying the diffusivity in the crucible for a heat treatment at constant temperature, the resulting amount of titanium that would reach the silicon sample, n_{test}, was calculated. Comparison to the previous n values, led to new diffusivity values which were tested until the following tolerance condition was met:

$$n_{test} = n \pm 10^{-10}\ \frac{mol}{m^2} \tag{5.4}$$

These diffusivity values were achieved for each sample, as shown in Table 4.2 and evaluated as explained in 4.3, to provide D_0 and H_M parameters, in Figure 4.10, Figure 4.11 and Figure 4.12.

Given the current challenges and the defined scenarios, the aim is to determine values above which the effective diffusion coefficients are more likely to be found. With this in mind, the profiles from Figure

7.2 were tested, to check what literature should be considered to obtain the lowest diffusion coefficients in the crucible. This happens for the maximum values, at each temperature, of the suggested diffusivities, as follows:

Table 5.4 - Maximum diffusivities of Ti in silicon, from 20 to 1350 ºC, according to Figure 7.2

$D_0[cm^2\ s^{-1}]$	$Q[eV]$	Temperature range [ºC]	Reference
1.2×10^{-1}	2.05	20-825	[72] [73]
1.5×10^{-3}	1.64	825-950	[74] [75, 76, 77]
1.45×10^{-2}	1.64	950-1350	[77]

5.2.6 Comparison with published data

In [78], a Ti layer of thickness 270 nm was deposited on a Si_3N_4/Si substrate, which Si_3N_4 layer was 120 nm thick. The main aim was to study Si diffusion and reaction across the interface, according to different annealing times and temperatures.

The presented results are for temperatures above 600 ºC, where the formation of Ti silicides is evident. The diffusion of Ti through the Si_3N_4 film is hard to describe, due to the simultaneous reaction and interdiffusion mechanisms, on which silicon migrates across the Si_3N_4 coating at a faster rate than Ti, causing silicide formation above the thin film. Both the diffusion of Si and the formation of titanium nitrides (TiN_x) were promoted by raising the temperature.

The small resolution of the auger electron spectroscopy (AES) depth profiles makes it difficult to judge how far the Ti species has reached. It also seems that it made its way across the silicon nitride thin layer in longer annealing times (8h at 650ºC). Additionally, its reaction with other present species can reduce the penetration depth, so taking the approach suggested in [55], to evaluate diffusivity according to:

$$D \sim \frac{x^2}{t} \tag{5.5}$$

only allows a low-end estimate for the 650-700 ºC range. In the expression, x is computed by multiplying the sputtering time in the presented figures by the sputtering rate (30 nm/min) and t corresponds to the annealing time.

Table 5.5 - Diffusivity values determined from Figure 5.10, through equation (5.5**)**

Temperature (ºC)	Annealing time (h)	Sputtering time (min)	Diffusivity (m^2/s)
650	8	10	3.125×10^{-24}
650	1	20-12.5=7.5	1.406×10^{-23}
700	1	25-12.5=12.5	3.906×10^{-23}

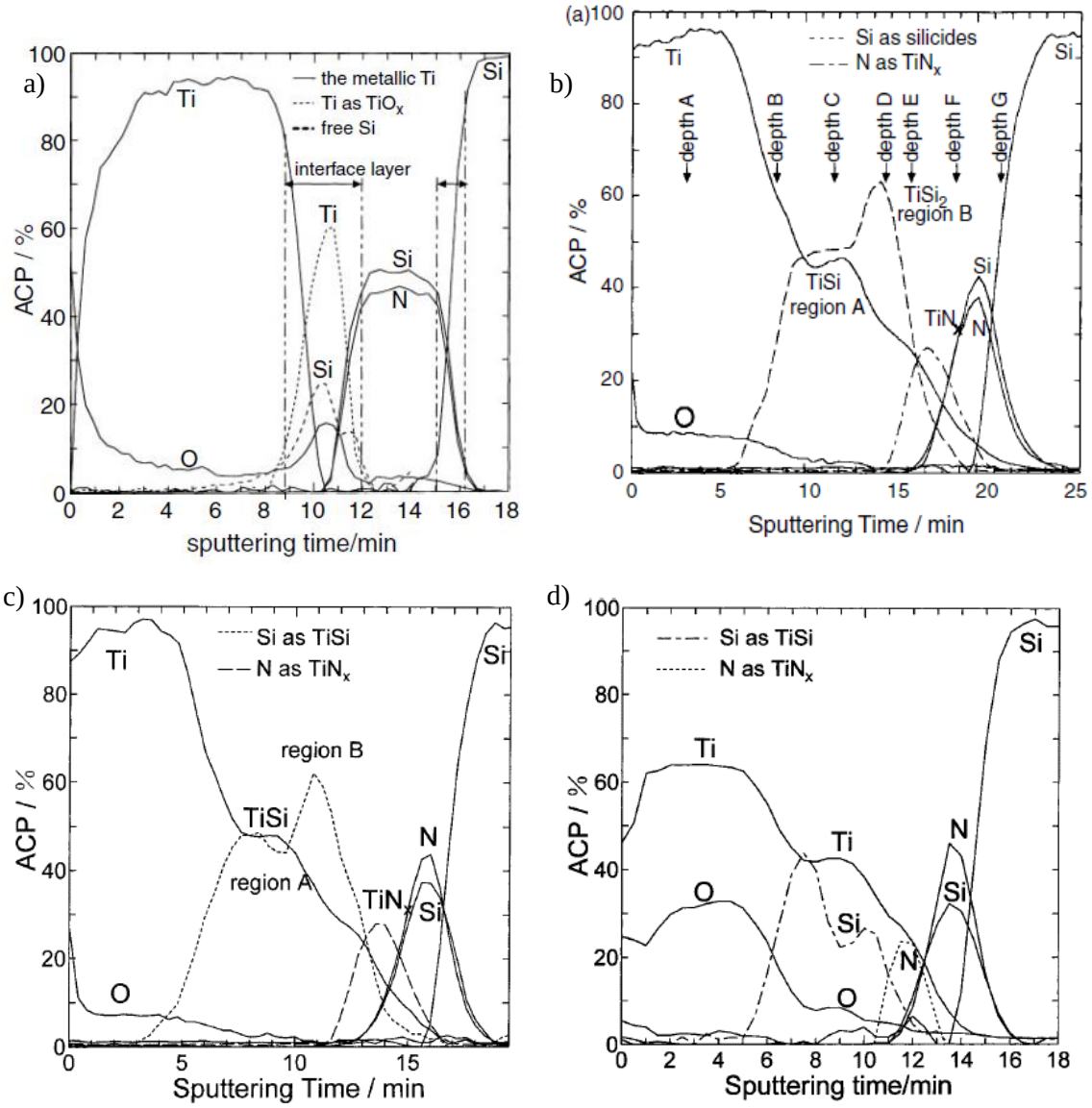

Figure 5.10 - The depth profile spectrum of a) a deposited sample; b) a sample annealed at 700 ºC for 1 h in a high vacuum; c) a sample annealed at 650 ºC for 1 h in a high vacuum; d) a sample annealed at 650 ºC for 8 h in a high vacuum; ACP stands for atomic concentration percent [78].

If one takes the expression that is closest to these calculated diffusivities, from scenario 3, for a Ti concentration in the crucible of 0.082 mol/m^3, the diffusion coefficients differ more than three orders of magnitude. Although the migration enthalpy is located among scenarios 2 and 3, the comparison is restrained since it is difficult to judge the penetration depths by means of the sputtering times in Figure 5.10, adding to the different preparation conditions and materials.

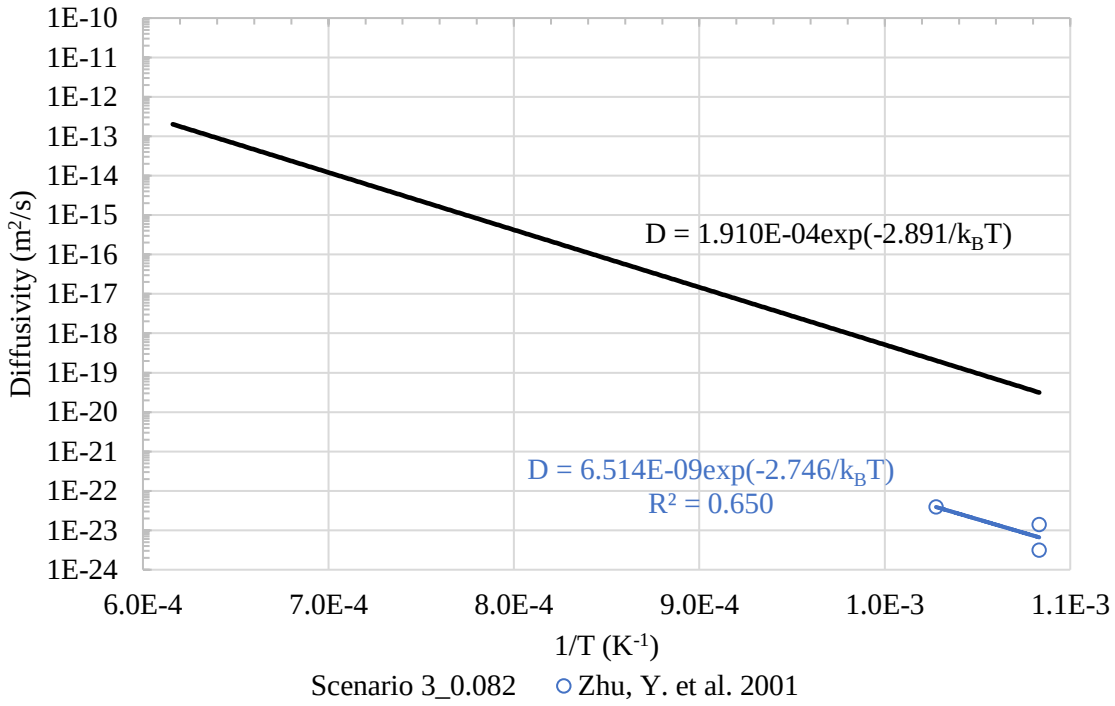

Figure 5.11 - Comparison of diffusivity estimates from this work (scenario 3 with the high estimate of Ti in the crucible) and Zhu, Y. et al. 2001 [78].

Such a discrepancy resembles the comparison done in [20] for the diffusion of aluminium, through a numerical estimate relying on measured Al concentrations in DS ingots, cast using a NBSN crucible. There was a difference of 1 to 3 orders of magnitude, relatively to values extrapolated from the analysis of [79], done for the crucible operation temperature of 1420 °C. That work concerns amorphous, chemical vapour deposited silicon nitride films for the range of 450-530 ºC, which led to diffusion coefficients among 10^{-17}-10^{-15} cm^2/s [20].

Following the reasoning in [20], both the stated crucible and the presented in this study are considerably porous and mainly constituted by α and β polycrystalline silicon nitride, as opposed to the cited amorphous films. This suggests a higher concentration of grain boundaries and porosity, likely to provide paths where diffusion may be increased by orders of magnitude.

5.3 Reheating and cooling

The heating curve of this particular furnace has been evaluated and is depicted in Figure 5.12**:**

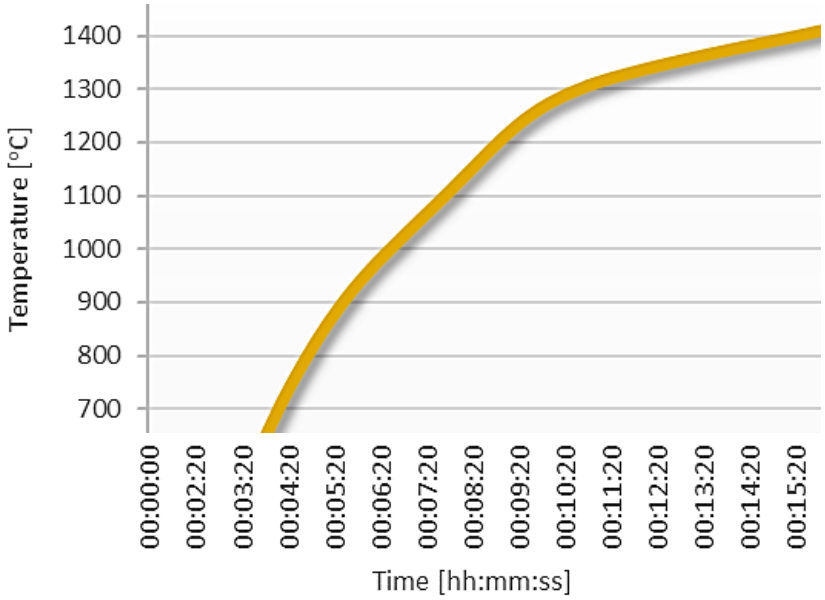

Figure 5.12 - Nabertherm LHT 04/18 rapid heating profile, adapted from [80].

Sample introduction forced heat loss and consequently, a reheating was necessary. The temperature drop has been registered, as well as the elapsed time until the annealing conditions were reset. Both agree with the heating curve and, thereby, more points from the profile relative to each reheating phase were taken, to achieve logarithmic approximations of this thermal behaviour (Figure 5.13).

The cooling process has not been registered directly, but relies in the observation of the first tests with silicon samples. Their temperature after 20 minutes of cooling was about 30 ºC. To describe this phase, for the other samples, a lumped capacity method which illustrated a similar process was employed:

$$\left[(h_c + h_{cv})(T_{Si} - T_{amb}) - \varepsilon\sigma\left(T_{Si}^4 - T_{amb}^4\right)\right]A_s = \rho V c \frac{dT_{Si}}{dt} \tag{5.6}$$

As the impurity source was no longer in contact with the studied sample shortly after leaving the furnace, it only refers to the silicon sample. The solution considers radiative, convective and conductive heat transfer to the surroundings at 20 ºC. Heat conduction occurred through contact with a refractory brick, while its back surface remained close to room temperature.

As suggested in [81], the Biot number was calculated to check if the temperature along the sample thickness could be considered uniform and the error associated with this method was small (Bi<0.1):

$$Bi = \frac{h_{cv}\, t_{Si}}{2\, k_{Si}} \tag{5.7}$$

The heat transfer coefficient considers a laminar flow, predicted for the instant at which the temperature difference between the air and the sample is maximum, i.e. when it is at the annealing temperature with equations (5.8) to (5.14). Given the relatively high conductivity of silicon ($k_{Si} = 22$ W/m K at 1350 ºC [82]), the large ratio between the surface area A_s (0.025×0.03 m^2) and its perimeter P_s ($2 \times (0.025 + 0.03)$ m) and the physical properties of air [81], $Bi < 0.1$ is satisfied for the convection process.

$$L_c = \frac{A_s}{P_s} \tag{5.8}$$

$$T_f = \frac{T_{Si} + T_{amb}}{2} \tag{5.9}$$

$$\beta = \frac{1}{T_f} \tag{5.10}$$

$$Gr = \frac{L_c^3 \, g \, \beta \, (T_{Si} - T_{amb})}{\nu^2} \tag{5.11}$$

$$Ra = Gr \, Pr \tag{5.12}$$

$$Nu = 0.54 \, Ra^{1/4} \; (10^4 \leq Ra \leq 10^7) \tag{5.13}$$

$$h_{cv} = \frac{Nu \, k_{air}}{L_c} \tag{5.14}$$

Where L_c is the characteristic length for this problem [m], T_f is the air film temperature [K], β is the thermal expansion coefficient, assuming air as an ideal gas [K^{-1}]. ν stands for the kinematic viscosity of air at film temperature [m^2/s] and g is the gravitational acceleration (9.807 m/s^2). Pr, Ra and Nu are Prandtl's, Rayleigh's and Nusselt's numbers for air, k_{air} is its thermal conductivity at film temperature [W/m K] and h_{cv} the convection heat transfer coefficient [W/m^2].

The insulating refractory (k_{refr}~1.01 W/m K taken from [83], $L_{refr} = 0.064$ m) should favour the constant temperature consideration, as heat loss is not limited to the top surface and the radiation is responsible for the majority of the cooling when the temperature difference between the sample and the exterior is at its maximum. A total emissivity of ε~0.7 is suggested in [84], however this translates in a cooling rate much faster than what was noticed. Thereby, $\varepsilon = 0.6$ was applied, while keeping in mind that the oxide film thickness is irregular, knowing that the contamination and doping density of silicon can drastically influence this parameter and that part of the radiation was lost through the windows to the exterior at temperatures in the range of -5 to 15 ºC.

$$h_c = \frac{k_{refr}}{L_{refr}} \tag{5.15}$$

Equation (5.16) was solved with $h_{cv,t}$ calculated according to each estimated sample temperature, $T_{Si,t+\Delta t}$, determined for $\Delta t = \frac{1}{60}$ minutes or dt (5.2.5), when smaller than this value. Both ρ_t and c_t, the density (kg/m^3) of silicon and its heat capacity (J/kg K) were corrected for each temperature according to [85].

$$T_{Si,t+\Delta t} = T_{Si,t} - \left[\left(h_c + h_{cv,t}\right)\left(T_{Si,t} - T_{amb}\right) - \varepsilon\sigma\left(T_{Si,t}^4 - T_{amb}^4\right)\right]\frac{A_s}{\rho_t V c_t}\Delta t \tag{5.16}$$

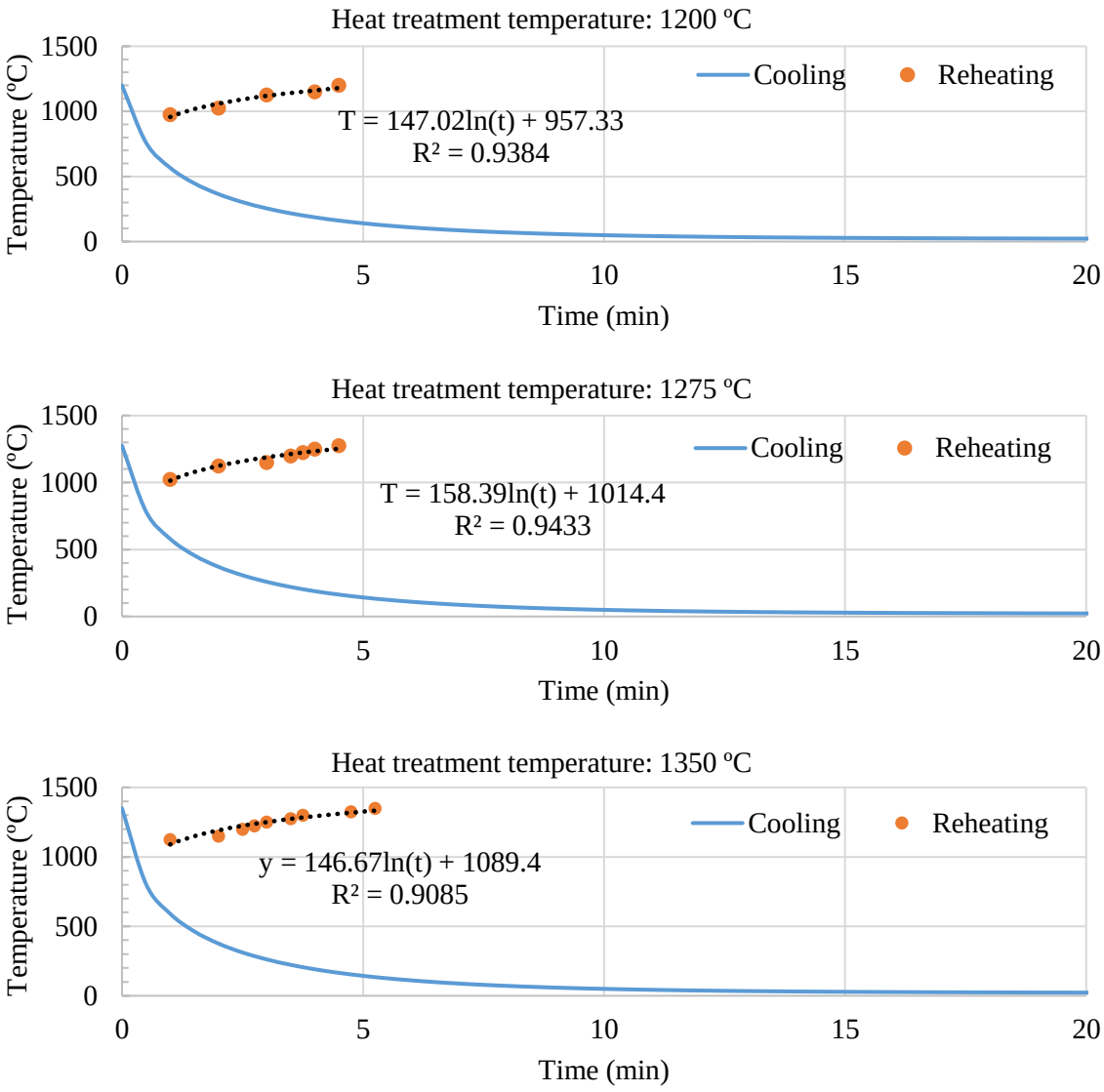

Figure 5.13 - Reheating and cooling curves for the different heat treatment temperatures.

As illustrated by Figure 4.10, Figure 4.11 and Figure 4.12, a drop in 150 ºC means a 10 times lower diffusivity. This means that, even if the presented reheating and cooling profiles deviate at some extent from the real temperature of the samples, the majority of the impurities reach the silicon sample at the maximum temperature, so that the Ti diffusivity estimates still suggest diffusion coefficients of the same order of magnitude.

5.4 Validation of the unidimensional diffusion approach

Another MATLAB script was prepared in order to treat the diffusion problem in 2D (Appendix D). This way one may evaluate whether the measurements were affected by diffusion on a different plane. As depicted in Figure 5.14, the crucible was cut with a smaller cross section than the silicon sample. A matrix was developed to represent the spatial distribution of Fe and Ti in the couple, according to relevant heat treatment conditions. This dictates that diffusion can occur across this width, if considering that no impurity source is in contact with silicon at the outer edges. The width was designated as radius due to being relatable to the sputtered region, as it seeks to demonstrate if the non-unidimensional diffusion could affect the GD-MS results. Points where no couple component is present, are associated

to the surrounding atmosphere inside the furnace and regarded as a medium where no impurity transport occurs.

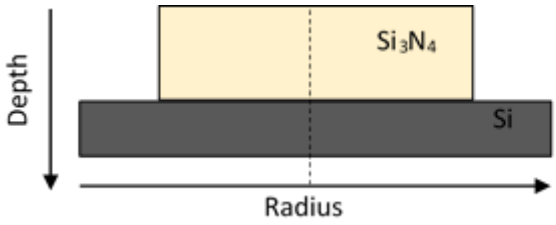

Figure 5.14 - Schematic of the diffusion couple considered in the script. The depth and radius axis have zeros set in the interface and the dashed centre line, respectively.

The widest section of the mono-Si wafer (3 mm) and the shortest section of the crucible sample (2 mm) were selected, as these increase the region where silicon is not in contact with the impurity source, thence magnifying the concentration gradient and the overall impurity flux along the radius axis. The symmetry of the presented system, led to its description only from the centre point of the couple, out towards the edge of the silicon sample (at 1.5 mm).

The effect of supersaturation and reactions in silicon should cause the impurity to accumulate near the Si_3N_4|Si interface, as the crucible composition exceeds the solubility limit at the annealing temperature. Consequently, more Ti and Fe atoms would remain near the sputtered region, instead of spreading across the radius, enhancing the unidimensional assumption for the GD-MS data points.

In agreement with the worst-case scenario for the Ti couples, based on the diffusion coefficient in silicon, the impurity should be able to migrate longer distances in the silicon lattice for the longest annealing period (180 min) at 1275 ºC. The higher the diffusion in silicon, the more will there be tendency for impurity diffusion parallel to the couple's interface. That leads again to the consideration of the literature values in Table 5.4.

Additionally, more diffusivity in the crucible intensifies the concentration gradient between the outer edge of the silicon sample. As result, there is an increased flow of titanium atoms towards it, accentuating the discrepancy between the concentration vs depth profiles for the centre point and at a 7.5 mm radius, in the second graph of Figure 5.15. This depicts the results when applying a demanding scenario to the section that should include the sputtered region, taking the diffusivity in silicon multiplied by a factor of 5 as the diffusion coefficient for Ti in the crucible itself.

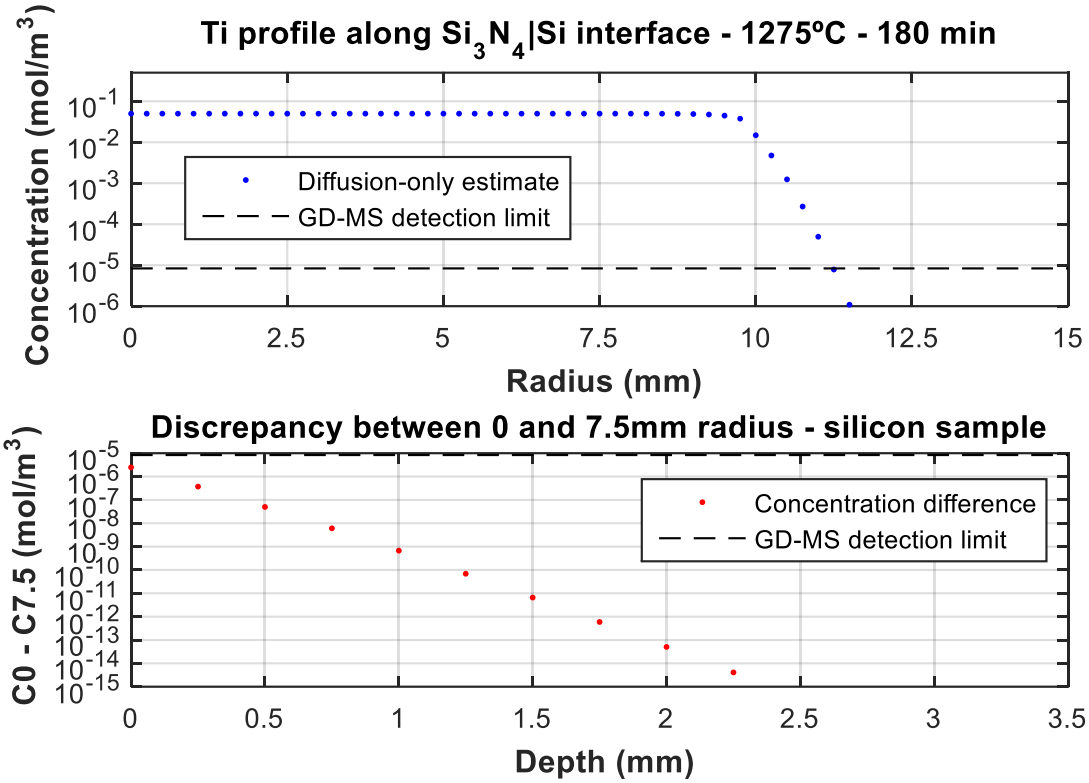

Figure 5.15 - Unidimensional analysis for Ti diffusion in the couple, for the most demanding scenario.

The magnitude of the discrepancy values indicates that the GD-MS analysis for Ti in the heat-treated samples can describe a unidimensional diffusion problem, when other occurring mechanisms are excluded, as the difference is below the detection limit, meaning that the influence in the results would go unnoticed. As the estimates for the diffusivity of Ti in the Si_3N_4 crucible are significantly lower than in this computation, it seems fair that diffusion can be considered as only occurring perpendicularly to the sputtered depth.

For Fe, the diffusion coefficient in the crucible has not been determined, but the annealing conditions expected to enhance the diffusion length of the Fe atoms, for the presented couples, are 1200 ºC during 60 minutes (Figure 3.3). Hence, the diffusion coefficient in silicon was applied to the crucible as well, which should be smaller in fact. As for titanium, the maximum diffusion coefficients of iron in silicon, suggested by the literature at each temperature were considered (Figure 7.1).

Considering that both the discrepancy and the width unaffected by impurity flow along the radius axis should decrease for smaller diffusivities in the materials, Figure 5.16 checks whether this hypothesis can relate the analysed couples to a case of unidimensional diffusion.

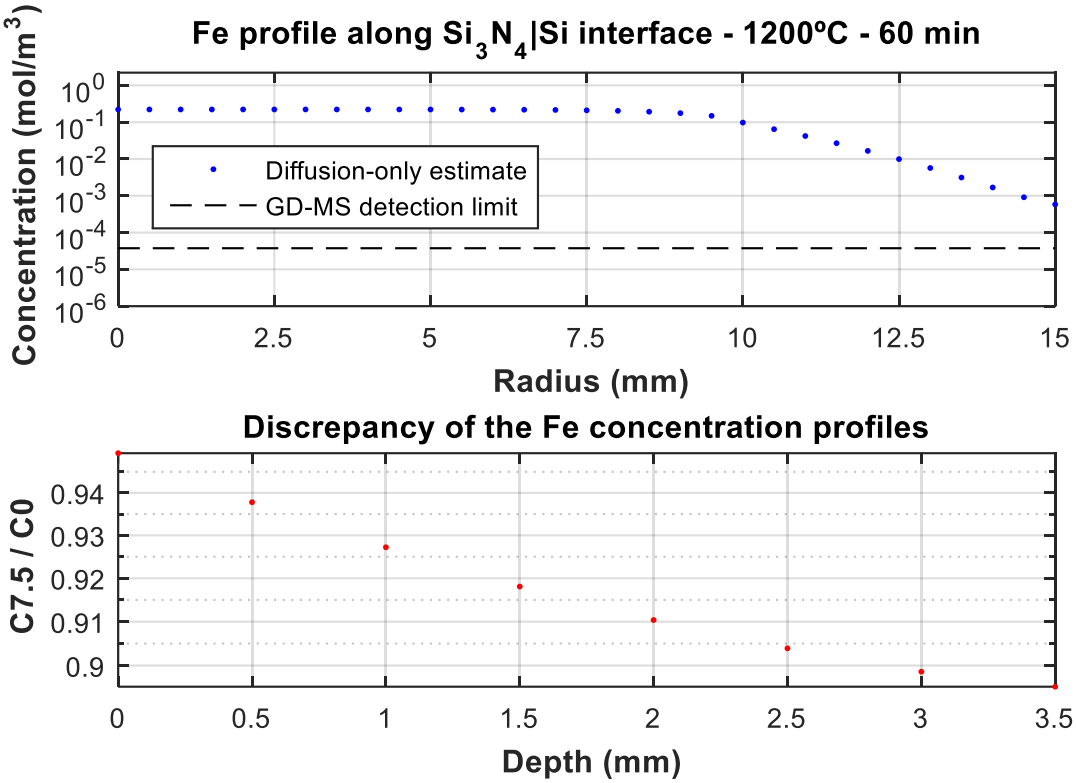

Figure 5.16 - Unidimensional analysis for Fe diffusion in the couple, for the most demanding scenario.

The discrepancy was accentuated in comparison to the previous solution and is shown, in the second graph, as a ratio instead. It seems that the concentration values at a 7.5 mm radius differ from the ones respective to the centre point at least 5%, so that the GD-MS data could be referring to a surface where the process is not unidimensional. Moreover, even the centre point, with a radius equal to 0 mm, seems to be affected by the diffusion of iron atoms towards the outer edge of the silicon wafer, not covered by the crucible material. This was checked by increasing the radius where Si_3N_4 is in contact with the mono-Si, from 10 mm to 20 mm (where diffusion does not happen across the radius), so that the previous centre point is now at 10 mm (Figure 5.17).

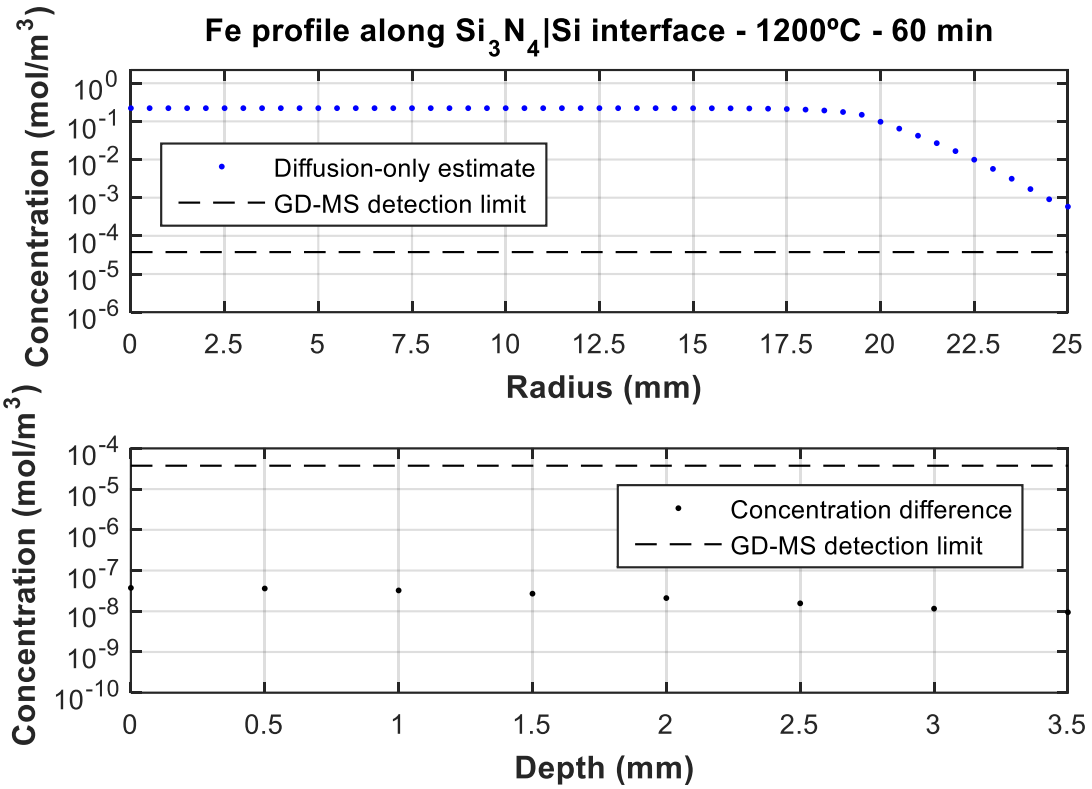

Figure 5.17 - Comparison of the Fe concentration profiles in the silicon sample, for a wider interface (20 mm of half-width or radius) where diffusion is unidimensional, relatively to the effectively employed couples (10 mm of half-width or radius).

The concentration difference, a subtraction of the values at 0 mm by the ones at 10 mm, is lower than the detection limit and, for that reason, not noticeable in the GD-MS data. With this established, the consequence of not having a unidimensional diffusion, for the previous couple, with 10 mm of crucible radius, was questioned. Necessarily, the difference decreases towards the centre and thus the integrating effect for a circular area with 7.5 mm radius, attenuates the discrepancy, as displayed in Figure 5.18. It shows a comparison of the Fe concentration profiles in the silicon sample, for the effectively employed couples (10 mm of half-width or radius), at the centre point (0 mm radius) relatively to the average concentration for a circular surface of 7.5 mm radius, with the same centre point, where the sputtered region is included.

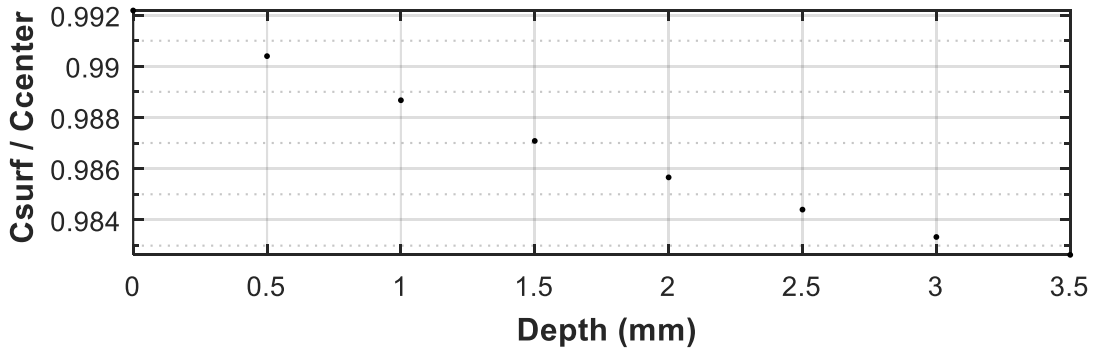

Figure 5.18 - Comparison of the Fe concentration profiles in the silicon sample for the effectively employed couples, relatively to the average concentration for a circular surface of 7.5 mm radius.

To clarify the meaning of this profile one should take notice that the 2D diffusion problem was solved with 0.5 mm between each point, across the radius axis. Their respective concentration values were averaged, according to the surface area they occupy in the stated circle of 7.5 mm radius, along the depth of the silicon wafer. Only data from 0 to 7 mm was taken, so the depicted discrepancy is a low-end estimate, but can illustrate better than the previous figure, that the impact in GD-MS concentration data is small. At worst, about 1% decrease should be altering the values within the analysed depth, causing even less impact for shorter annealing periods, temperatures lower than 1200 ºC and slower diffusivities of Fe in the Si_3N_4 crucible.

6 Conclusion and further work

The incorporation of impurities, from SiO_2 and Si_3N_4 crucibles, by DS mc-Si ingots was addressed, in addition to mitigation measures. Due to the usual application of a Si_3N_4 coating, the growth processes at different scales and the lack of in-depth description of the crucible materials, the direct comparison between reports is often hindered. Nonetheless, the purity of the crucible raw material and flow conditions of the silicon melt and furnace atmosphere were proposed as main contributors to the impurity distribution in the as grown-ingots.

This work also aimed to characterise solute diffusion in a commercial Si_3N_4 slip-cast crucible, to describe its behaviour as a contamination source for multicrystalline silicon. Inspired by the works of Skarstad [30] and Ekstrøm a solid-state method was developed, by heat-treating couples with Cz silicon, in order to investigate the transport process of iron and titanium in the ceramic material.

The results suggest that the experimental procedure still requires modifications for studying iron successfully, due to signs undesirable contamination sources, while a numerical method was created to estimate titanium diffusivity from the GD-MS concentration vs depth profiles of the silicon samples.

A first low end scenario considered the average titanium concentration in silicon, based on the GD-MS measurements and non-detected regions as zeros. A second, used the value nearest to the interface to describe missing values in between with the same concentration, being conservative regarding the increasing profile suggested by Fick's 2nd law. The third, resulted from calculating concentration values in the same depths, resourcing to curve fits of the GD-MS profiles with the particular solution of this law for an inexhaustible source.

Regarding scenario 1, the lowest diffusivity estimates were among 10^{-15} and 10^{-13} m^2/s at temperatures between 1200 and 1350 ºC, meaning that the diffusion of Ti in the Si_3N_4 crucible in the experimental conditions was most likely exceeded by these values, since the impurity was not accounted for in the non-quantified section near the interface. With less certainty, the second scenario still attempted to provide diffusivities below what effectively occurred in the experiments, yielding values in the orders between 10^{-14} to 10^{-12} m^2/s for the stated interval. Such values are closer to scenario 3, with the least confidence for a low-end estimate, but more ambitious towards the effective diffusivity of Ti in the crucible, which led to the orders of 10^{-14} to 10^{-12} m^2/s. from 1200 to 1350 ºC.

The presented values only point out the order of magnitude, as gathering further proof with a reproducibility analysis is essential. The results showed that the amount of titanium in the crucible can influence the estimates significantly, as 0.5 ppmw is enough to yield estimates diverging by a factor 10. Consequently, owning a quantitative analysis of Ti below the ppmw range, instead of relying on technical specifications would be valuable.

One should note that the extrapolated values in Table 7.5 were not computed through the numerical method, expressing only how the estimates may deviate if the simulated amount of contamination in silicon was calculated, as it was for the GD-MS profiles.

Registration of the temperatures during the cooling stage would add more credibility to the estimates, but quenching is an option to consider, since limiting the diffusion towards the interface in the cooling stage may yield better curve fitting if an approach like scenario 3 is utilized. This scenario also calls for longer heat treatments when slow diffusers are studied (more than 1 hour for titanium), in order to have enough data for representative fits and a more accurate representation through a constant temperature profile.

For posterior work, especially with iron diffusivity, it is advisable to seal the couples inside evacuated or argon filled quartz ampoules to avoid contamination from the exterior. Tight fitting of the ampoule may suffice to keep the couple in contact. Otherwise, the sealed environment avoids the presence of oxygen, so a wire may be employed without combusting and compromising the contact at the interface. It must not contain the studied impurity (at most in the ppbw range), be ductile enough to enable wrapping without excessive tensile strength (which can lead to cracks) and withstand the high temperatures without breaking.

Even if it becomes possible to analyse impurity amounts in the crucible directly, avoiding non-characterised impurity sources still comes as a priority. Having the same detection capabilities as for a silicon matrix, would ease the understanding of its composition and the solute diffusivity. In that case, it would also be relevant to study the crucible prior to heat treatment, to confirm the technical guidelines regarding its composition and the absence of added impurities prior to the couples' assembly.

References

[1] The Quartz Corp, "Polysilicon Production," 28 April 2014. [Online]. Available: http://www.thequartzcorp.com/en/blog/2014/04/28/polysilicon-production/61. [Accessed 20 September 2016].

[2] G. Fisher, M. R. Seacrist and R. W. Standley, "Silicon Crystal Growth and Wafer Technologies," *Proceedings of the IEEE May 13th, 2012,* vol. 100, pp. 1454-1474, 2012.

[3] National Renewable Energy Laboratory (NREL), "Best research-cell efficiencies," 2017. [Online]. Available: https://www.nrel.gov/pv/assets/images/efficiency-chart.png. [Accessed 15 June 2017].

[4] Fraunhofer Institute for Solar Energy Systems, "Photovoltaics Report," 6 June 2016. [Online]. Available: https://www.ise.fraunhofer.de/de/downloads/pdf-files/aktuelles/photovoltaics-report-in-englischer-sprache.pdf. [Accessed 3 October 2016].

[5] K. Nakajima and N. Usami, Eds., Crystal growth of Si for solar cells, vol. 14, Berlin Heidelberg: Springer, 2009, pp. 1-39.

[6] K. E. Ekstrøm, Structure Control of Multicrystalline Silicon, Trondheim: PhD Thesis, 2016.

[7] S. Woo and M. Bertoni, "An insight into dislocation density reduction in multicrystalline silicon," *Solar Energy Materials & Solar Cells,* vol. 155, p. 88–100, 2016.

[8] C. W. Lan, W. C. Lan, T. F. Lee, A. Yu, Y. M. Yang, W. C. Hsu, B. Hsu and A. Yang, "Grain control in directional solidification of photovoltaic silicon," *Journal of Crystal Growth,* vol. 360, pp. 68-75, 2012.

[9] C. W. Lan, A. Lan, C. F. Yang, H. P. Hsu, M. Yang, A. Yu, B. Hsu, W. C. Hsu and A. Yang, "The emergence of high-performance multi-crystalline silicon in Photovoltaics," *Journal of Crystal Growth,* vol. 468, p. 17–23, 2017.

[10] A. Ciftja and G. Stokkan, "Growth of High Performance Multicrystalline Silicon: A Literature Review," SINTEF Materials and Chemistry, Trondheim, 2014.

[11] M. P. Bellmann, E. A. Meese and L. Arnberg, “Impurity segregation in directional solidified multi-crystalline silicon,” *Journal of Crystal Growth,* vol. 312, p. 3091–3095, 2010.

[12] W. Kwapil , A. Zuschlag, I. Reis , I. Schwirtlich , S. Meyer, R. Zierer, R. Krain, F. M. Kießling , M. Schumann, C. Schmid and S. Riepe, “Influence of crucible and coating on the contamination of directionally solidified silicon: first results of the german research network "SolarWinS",” in *27th European Photovoltaic Solar Energy Conference and Exhibition,* Frankfurt, 2012.

[13] G. Coletti, *Impurities in silicon and their impact on solar cell performance,* PhD thesis, 2011, pp. 3-63.

[14] T. U. Nærland, L. Arnberg and A. Holt, “Origin of the Low Carrier Lifetime Edge Zone in Multicrystalline PV Silicon,” *Progress in Photovoltaics: Research and Applications,* vol. 17, pp. 289-296, 2009.

[15] R. Kvande, L. Arnberg and C. Martin, “Influence of crucible and coating quality on the properties of multicrystalline silicon for solar cells,” *Journal of Crystal Growth,* vol. 311, p. 765–768, 2009.

[16] P. Li, S. Ren, D. Jiang, K. Wang and J. Li, “Distributions of substitutional and interstitial impurities in silicon ingot with different grain morphologies,” *Materials Science in Semiconductor Processing,* vol. 67, pp. 1-7, 2017.

[17] R. Kvande, L. J. Geerlings, G. Coletti, M. Di Sabatino, E. J. Øvrelid and C. C. Swanson, “Distribution of iron in multicrystalline silicon ingots,” *Journal of Applied Physics ,* vol. 104, p. 064905, 2008.

[18] D. Macdonald, A. Cuevas, A. Kinomura, Y. Nakano and L. J. Geerlings, “Transition-metal profiles in a multicrystalline silicon ingot,” *Journal of Applied Physics,* vol. 97, p. 033523, 2005.

[19] B. Gao , S. Nakano and K. Kakimoto, “Effect of crucible cover material on impurities of multicrystalline silicon in a unidirectional solidification furnace,” *Journal of Crystal Growth,* vol. 318, p. 255–258, 2011.

[20] V. Schneider, C. Reimann, J. Friedrich and G. Müller, "Nitride bonded silicon nitride as a reusable crucible material for directional solidification of silicon," *Crystal Research and Technology,* vol. 51 (1), pp. 74-86, 2016.

[21] S. Richter , J. Bauer and O. Breitenste, "Growth of carbon and nitrogen containing precipitates in crystalline solar silicon and their influence on solar cells," *Physica Status Solidi Rapid Research Letters,* Vols. 11, No. 2, p. 1600354, 2017.

[22] H. Kitagawa, "Diffusion and Electrical Properties of 3d Transition-Metal Impurities in Silicon," *Solid State Phenomena,* vol. 71, pp. 51-72, 2000.

[23] W. Shockley and W. T. Read Jr., "Statistics of the Recombinations of Holes and Electrons," *Physical Review,* vol. 87 Iss. 5, pp. 835-842, September 1952.

[24] Wikiwand, "p-n junction," 2007. [Online]. Available: https://upload.wikimedia.org/wikipedia/commons/d/d6/Pn-junction-equilibrium.png. [Accessed 22 February 2017].

[25] J. L. Gray, "The Physics of the Solar Cell," in *Handbook of Photovoltaic Science and Engineering*, A. Luque and S. Hegedus, Eds., West Sussex, John Wiley & Sons Ltd, 2003, pp. 83-87.

[26] C. Honsberg and S. Bowden, "PVCDROM," 2017. [Online]. Available: http://www.pveducation.org/pvcdrom. [Accessed 21 February 2017].

[27] G. Coletti, P. C. P. Bronsveld, G. Hahn, W. Warta, D. Macdonald, B. Ceccaroli, K. Wambach, N. Le Quang and J. M. Fernandez, "Impact of metal contamination in silicon solar cells," *Advanced Functional Materials,* vol. 21, p. 879–890, 2011.

[28] G. Coletti, R. Kvande, V. D. Mihailetchi, L. J. Geerlings, L. Arnberg and E. J. Øvrelid, "Effect of iron in silicon feedstock on p- and n-type multicrystalline silicon solar cells," *Journal of Applied Physics,* vol. 104, p. 104913, 2008.

[29] P. Rudolph, Handbook of Crystal Growth, Bulk Crystal Growth: Basic Techniques, 2nd ed., Vols. II, Part A, Elsevier B.V., 2015, pp. 48-49, 358, 373-406.

[30] H. V. Skarstad, Behaviour of the slip-cast crucible as a contamination source during silicon directional solidification, Trondheim: MSc thesis, 2016, p. 5.

[31] SOLAR CERA Co., Ltd., “Fused silica crucible,” 2016. [Online]. Available: http://www.fusedsilicacrucible.com/images/photo/Solar%20Cera%20Crucible.jpg. [Accessed 6 September 2016].

[32] V. Pupazan, R. Negrila , O. Bunoiu, I. Nicoara and D. Vizman, “Effects of crucible coating on the quality of multicrystalline silicon grown by a Bridgman technique,” *Journal of Crystal Growth,* vol. 401, p. 720–726, 2014.

[33] R. Roligheten, G. Rian and S. Julsrud , “Reusable crucibles and method of manufacturing them”. International Patent WO 2007/148986 A1, 27 December 2007.

[34] A. S. Abyzov, R. Androsch, G. V. Baidakov, V. M. Fokin, S. Gutzov, I. S. Gutzow, G. P. Johari, N. Jordanov, A. Karamanov and V. K. Leko, Glass: Selected Properties and Crystallization, J. W. P. Schmelzer, Ed., Walter de Gruyter & Co, 2014, pp. 137-148.

[35] Science education resource center at Carleton College, “Teaching Phase Equilibria,” 31 March 2007. [Online]. Available: http://d32ogoqmya1dw8.cloudfront.net/files/research_education/equilibria/silicaminerals.pdf. [Accessed 8 September 2016].

[36] H. Matsuo , R. B. Ganesh, S. Nakano, L. Liu, K. Arafune, Y. Oshita, M. Yamaguchi and K. Kakimoto, “Effect of crucible rotation on oxygen concentration during unidirectional solidification process of multicrystalline silicon for solar cells,” *Journal of Crystal Growth,* vol. 311, pp. 1123-1128, 2009.

[37] S. Nakano, B. Gao and K. Kakimoto, “Relationship between oxygen impurity distribution in multicrystalline solar cell silicon and the use of top and side heaters during manufacture,” *Journal of Crystal Growth,* vol. 375, pp. 62-66, 2013.

[38] K. Ellingsen, D. Lindholm and M. M'Hamdi, “The effect of heating power on impurity formation and transport during the holding phase in a Bridgman furnace for directional solidification of multi-crystalline silicon,” *Journal of Crystal Growth,* vol. 444, pp. 39-45, 2016.

[39] S. Nakano, L. J. Liu, X. J. Chen, H. Matsuo and K. Kakimoto, “Effect of crucible rotation on oxygen concentration in the polycrystalline silicon grown by the unidirectional solidification method,” *Journal of Crystal Growth,* vol. 311, pp. 1051-1055, 2009.

[40] L. Liu, W. Ma, X. Qi, Z. Li and Y. Zhang, “Global simulation of coupled oxygen and carbon transport in an industrial directional solidification furnace for crystalline silicon ingots: Effect of crucible cover coating,” *International Journal of Heat and Mass Transfer,* vol. 108, p. 2355–2364, 2017.

[41] X. Qi, L. Liu and W. Ma, “Effects of furnace pressure on oxygen and carbon coupled transport in an industrial directional solidification furnace for crystalline silicon ingots,” *Journal of Crystal Growth,* vol. 468, pp. 933-938, 2017.

[42] P. Li , S. Ren, D. Jiang , J. Li, L. Zhang and Y. Tan, “Effect of alternating magnetic field on the removal of metal impurities in silicon ingot by directional solidification,” *Journal of Crystal Growth,* vol. 437, pp. 14-19, 2016.

[43] T. Saito, A. Shimura and S. Ichikawa, “A reusable mold in directional solidification for silicon solar cells,” *Solar Energy Materials ,* vol. 9, pp. 337-345, 1983.

[44] P. Prakash, P. K. Singh, S. N. Singh, R. Kishore and B. K. Das, “Use of silicon oxynitride as a graphite mold releasing coating for the growth of shaped multicrystalline silicon crystals,” *Journal of Crystal Growth,* vol. 144, pp. 41-47, 1994.

[45] E. Olsen, A. Solheim and H. Sørheim, “Mould parts of silicon nitride and method for producing such mould parts”. International Patent WO 2004/016835 A1, 26 February 2004.

[46] C. P. Khattak and F. Schmid, “Reusable crucible for silicon ingot growth”. US Patent US 2004/0211496 A1, 28 October 2004.

[47] S. Julsrud and T. L. Naas, “Method and crucible for direct solidification of semiconductor grade multi-crystalline silicon ingots”. International Patent WO 2007/148987 A1, 27 December 2007.

[48] L. L. Zhao, T. Z. Ly and Q. S. Zhu, “Si3N4/fused quartz composite crucible with enhanced thermal conductivity for multicrystalline silicon ingot growth,” *Journal of Crystal Growth,* vol. 415, pp. 51-56, 2015.

[49] Encyclopædia Britannica, “Advanced ceramics - Encyclopædia Britannica Online,” Encyclopædia Britannica Inc., 2016. [Online]. Available:

https://global.britannica.com/technology/advanced-ceramics. [Accessed 10 September 2016].

[50] M. P. Bellmann, E. A. Meese, M. Syvertsen, A. Solheim, H. Sørheim and L. Arnberg, "Silica versus silicon nitride crucible: influence of thermophysical properties on the solidification of multi-crystalline silicon by Bridgman technique," *Journal of Crystal Growth,* vol. 318, pp. 265-268, 2011.

[51] Z. Li, L. Liu, Y. Zhang and G. Zhou, "Influence of Crucible Thermal Conductivity on Crystal Growth in an Industrial Directional Solidification Process for Silicon Ingots," *International Journal of Photoenergy,* vol. 2016, 2016.

[52] C. Modanese, M. Di Sabatino, M. Syvertsen and L. Arnberg, "Chemical bulk properties of multicrystalline silicon ingots for solar cells cast in silicon nitride crucibles," *Journal of Crystal Growth,* vol. 354, pp. 27-33, 2012.

[53] I. Brynjulfsen, A. Bakken, M. Tangstad and L. Arnberg, "Influence of oxidation on the wetting behavior of liquid silicon on Si3N4-coated substrates," *Journal of Crystal Growth,* vol. 312, pp. 2404-2410, 2010.

[54] J. Crank, The mathematics of diffusion, 2nd ed., London: Oxford University Press, 1975, pp. 1-7,11-16, 375-376.

[55] J. Pelleg, Diffusion in Ceramics, vol. 211, Switzerland: Springer, 2016, pp. 3-6, 9-10, 413-444.

[56] H. Mehrer, Diffusion in solids: fundamentals, methods, materials, diffusion-controlled processes, vol. 155, Germany: Springer, 2007, pp. 2-3, 27-31.

[57] W. D. Callister Jr. and D. G. Rethwisch, Materials science and engineering: an introduction, 8th ed., United States of America: John Wiley & Sons, Inc., 2009, pp. 126-134,283.

[58] H.-W. Guo, *Diffusion and precipitation models for silicon gettering and ultra shallow junction formation,* PhD thesis, 2008, pp. 14-15.

[59] F. L. King, J. Teng and R. E. Steiner, "Glow Discharge Mass Spectrometry: Trace Element Determinations in Solid Samples," *Journal of Mass Spectometry,* vol. 30, pp. 106-1075, 1995.

[60] A. A. Ganeev, A. R. Gubal, K. N. Uskov and S. V. Potapov, “Analytical glow discharge mass spectrometry,” *Russian Chemical Bulletin, International Edition,* Vols. 61-4, no. A. A. Ganeev, A. R. Gubal, K. N. Uskov, and S. V. Potapov, pp. 752-767, 2012.

[61] Thermo Fisher Scientific, “Finnigan™ ELEMENT GD Glow Discharge Mass Spectrometer,” 2005. [Online]. Available: http://www.thermo.com.cn/resources/200802/productpdf_25212.pdf. [Accessed 27 May 2017].

[62] M. Di Sabatino, “Detection limits for glow discharge mass spectrometry (GDMS) analyses of impurities in solar cell silicon,” *Measurement,* vol. 50, pp. 135-140, 2014.

[63] A. Bogaerts and R. Gijbels, “New developments and applications in GDMS,” *Fresenius Journal of Analytical Chemistry,* vol. 364 (5), pp. 367-375, 1999.

[64] R. Morrell, Gmelin Handbook of inorganic and organometallic chemistry: Si Silicon: Silicon nitride : mechanical and thermal properties; diffusion., 8 ed., vol. B5b1, W. Kurtz and F. Schröder, Eds., Berlin: Springer, 1996, pp. 403-412.

[65] K. Graff, Metal lmpurities in Silicon-Device Fabrication, vol. 24, R. Hull, R. M. Osgood, Jr., H. Sakaki and A. Zunger, Eds., New York: Springer-Verlag Berlin Heidelberg, 2000, pp. 5-18.

[66] Commission on Isotopic Abundances and Atomic Weights, “Standard Atomic Weights,” 2017. [Online]. Available: http://www.ciaaw.org/atomic-weights.htm. [Accessed 13 May 2017].

[67] F. Beeler, O. K. Andersen and M. Scheffler, “Physical Review Letters,” vol. 55, p. 1498, 1985.

[68] B. O. Kolbesen, W. Bergholz and H. Wendt, “Impact of Defects on the Technology of Highly Integrated Circuits,” *Material Sciences Forum,* Vols. 38-41, pp. 1-12, 1989.

[69] M. Seibt and K. Graff, “Tem Study of Metal Impurity Precipitates in the Surface Regions of Silicon Wafers,” *Materials Research Society Symposium Proceedings,* vol. 104, p. 215, 1988.

[70] Nabertherm, “Thermal Process Technology II - Annealing, Hardening, Brazing, Forging, Nitriding,” 2017. [Online]. Available:

http://www.nabertherm.com/produkte/thermprozesstechnik/thermalprocesstechnology2_english.pdf. [Accessed 3 May 2017].

[71] Brigham Young University, "Oxide Growth Thickness Calculator," 2016. [Online]. Available: http://www.cleanroom.byu.edu/OxideThickCalc.phtml. [Accessed 22 September 2016].

[72] V. P. Boldyrev, I. I. Pokrovskii, S. G. Romanovskaya, A. V. Tkach and I. E. Shimanovich, *Soviet physics: Semiconductors (English Transl.)* , vol. 11, p. 709, 1977.

[73] K. Graff and H. Pieper, *Proceedings of the Electrochemical Society,* Vols. 81-5 , p. 331, 1981.

[74] A. Rohatgi, J. R. Davis, R. H. Hopkins and P. G. McMullin, *Solid-State Electronics,* vol. 26, p. 1039, 1983.

[75] E. R. Weber, "Transition Metals in Silicon," *Applied Physics A,* vol. 30 , p. 1, 1983.

[76] K. Graff, *Proceedings of the Electrochemical Society* , Vols. 86-4, p. 751, 1986.

[77] W. Schröter, M. Seibt and D. Gilles, "High-Temperature Properties of Transition Elements in Silicon," in *Electronic Structure and Properties of Semiconductors*, vol. 4, W. Schröter, Ed., Weinheim, Materials Science and Technology: Wiley VCH, 1991, pp. 539, 607.

[78] Y. Zhu, L. Wang, W. Yao and L. Cao, "Interface diffusion and reaction between Ti layer and Si3N4/Si substrate," *Surface and Interface Analysis,* vol. 32, p. 296–300, 2001.

[79] H. Ogata, K. Kanayama, M. Ohtani, K. Fujiwara and H. Abe, "Diffusion of aluminum into silicon nitride films," *Thin Solid Films,* vol. 48, pp. 333-338, 1978.

[80] T. C. Eikevik, "Nabertherm LHT 04/18," NTNU, 10 October 2016. [Online]. Available: https://www.ntnu.no/wiki/pages/viewpage.action?pageId=89170115. [Accessed 12 February 2017].

[81] T. L. Bergman, A. S. Lavine, F. P. Incropera and D. P. Dewitt, Fundamentals of Heat and Mass Transfer, USA: John Wiley & Sons, 2011, pp. 280-294.

[82] C. J. Glassbrenner and G. A. Slack, "Thermal Conductivity of Silicon and Germanium from 3°K to the Melting Point," *Physical Review Letters,* vol. 134, p. A1058 , 1964.

[83] E. Ruh and J. S. McDowell, “Thermal Conductivity of Refractory Brick,” *Journal of' The American Ceramic Society,* Vols. 45-4, pp. 189-195, 1962.

[84] N. M. Ravindra, B. Sopori, O. H. Gokce, S. X. Cheng, A. Shenoy, L. Jin, S. Abedraboo, W. Chen and Y. Zhang, “Emissivity Measurements and Modeling of Silicon-Related Materials: An Overview,” *International Journal of Thermophysics,* Vols. 22-5, pp. 1593-1611, 2001.

[85] R. K. Endo, Y. Fujihara and M. Susa, “Calculation of density and heat capacity of silicon by molecular dynamics simulation,” *High Temperatures-High Pressures,* vol. 35/36 (5), pp. 505-511, 2003.

[86] N. A. Stolwijk and H. Bracht, “Diffusion in silicon,” in *Landolt-Börnstein - New Series - III/33 A: Diffusion in Semiconductors*, D. L. Beke, Ed., Berlin, Springer-Verlag, 1998, pp. (2-22)-(2-29).

[87] H. Nakashima, T. Isobe, Y. Yamamoto and K. Hashimoto, *Japanese Journal of Applied Physics* , vol. 27, p. 1542, 1988.

[88] T. Isobe, H. Nakashima and K. Hashimoto, *Japanese Journal of Applied Physics* , vol. 28, p. 1282, 1989.

[89] H. Nakashima and K. Hashimoto, *Materials Science Forum,* Vols. 83-87, p. 227, 1992.

[90] J. D. Struthers, “Solubility and Diffusivity of Gold, Iron, and Copper in Silicon,” *Journal of Applied Physics,* vol. 27, p. 1560, 1956.

[91] L. C. Kimerling, J. L. Benton and J. J. Rubin, *Institute of Physics Conference Series,* vol. 59, p. 217, 1981.

[92] W. H. Shepherd and J. A. Turner, *J. Phys. Chem. Solids,* vol. 23, p. 1697, 1962.

[93] G. W. Ludwig and H. H. Woodbury, in *Proceedings of the International Conference on Semiconductor Physics*, Prague, 1960.

[94] E. R. Weber and N. Wiehl, *Materials Research Society Symposium Proceedings,* vol. 14, p. 19, 1983.

[95] M. Aoki, A. Hara and A. Ohsawa, “Fundamental properties of intrinsic gettering of iron in a silicon wafer,” *Journal of Applied Physics,* vol. 72, p. 895, 1992.

[96] Y. Ishikawa, I. Kobayashi and I. Nakamichi, *Japanese Journal of Applied Physics*, vol. 28, p. 1272, 1989.

[97] Y. H. Lee, R. L. Kleinhenz and J. W. Corbett, *Applied Physics Letters*, vol. 31, p. 142, 1977.

[98] J. J. R. Davis, A. Rohatgi, R. H. Hopkins, P. D. Blais, P. Rai-Choudhury, J. R. McCormick and H. C. Mollenkopf, *IEEE Transactions on Electron Devices*, Vols. ED-27, p. 677, 1980.

[99] F. A. Trumbore, "Impurities in silicon solar cells," *Bell System Technical Journal*, vol. 39, p. 205, 1960.

[100] S. Fischler, *Journal of Applied Physics*, vol. 33 , p. 1615 , 1962.

[101] E. Schibli and A. G. Milnes, *Materials Science and Engineering*, vol. 2, p. 173, 1967.

[102] J. S. K. Williams, Metastable Materials Formation by Ion Implantation, S. T. Picreaux and W. J. Choyke, Eds., New York: Elsevier Science Publishing, 1982, p. 109.

[103] T. Carlberg, *Journal of The Eletrochemical Society*, vol. 133, p. 1940, 1986.

[104] K. Graff, Semiconductor Silicon 1986, Vols. 86-4, H. R. Huff, T. Abe and B. Kolbesen, Eds., Pennington, NJ: The Electrochemical Society, 1986, p. 751.

[105] R. C. Newman, *Materials Research Society Symposium Proceedings*, p. 25, 1988.

[106] C. W. White, S. R. Wilson, B. R. Appleton and J. F. W. Young, *Journal of Applied Physics*, vol. 51 , p. 738, 1980.

[107] M. K. Bakhadyrkanov, B. I. Boltaks and G. S. Kulikov, *Soviet Physics, Solid State* , vol. 14 , p. 1441, 1972.

[108] S. Hocine and D. Mathiot, "Titanium diffusion in silicon," *Applied Physics Letters*, vol. 53, p. 1269, 1988.

[109] M. C. Chen, A. G. Milnes and A. Rohatgi, *Journal of The Electrochemical Society*, vol. 129, p. 1294, 1979.

[110] T. W. Clyne and W. Kurz, "Solute redistribution during solidification with rapid solid state diffusion," *Metallurgical Transactions A*, vol. 12(6), pp. 965-971, 1981.

7 Appendixes

Appendix A

Diffusivity in silicon

Since a portion p-type Cz silicon was used, data was selected with preference towards mono-Si, supported by multiple analysis techniques and multiple authors.

The diffusion data for iron in silicon specified in Table 7.1 and plotted in Figure 7.1 was considered from room temperature, about 20 ºC, up to 1200 ºC. For titanium in silicon, the temperature range was extended up to 1350 ºC, as presented in Table 7.2 and Figure 7.2.

The red profiles in Figure 7.1 and Figure 7.2, represent the mean value of the diffusion coefficients, determined based on equation (2.15), according to the temperature ranges stated in Table 7.1 and Table 7.2, respectively. These approximations were applied in 3.5, justified by the poor fitting by the exponential function in equation (2.15), which presents a considerable deviation from the published values at high temperatures.

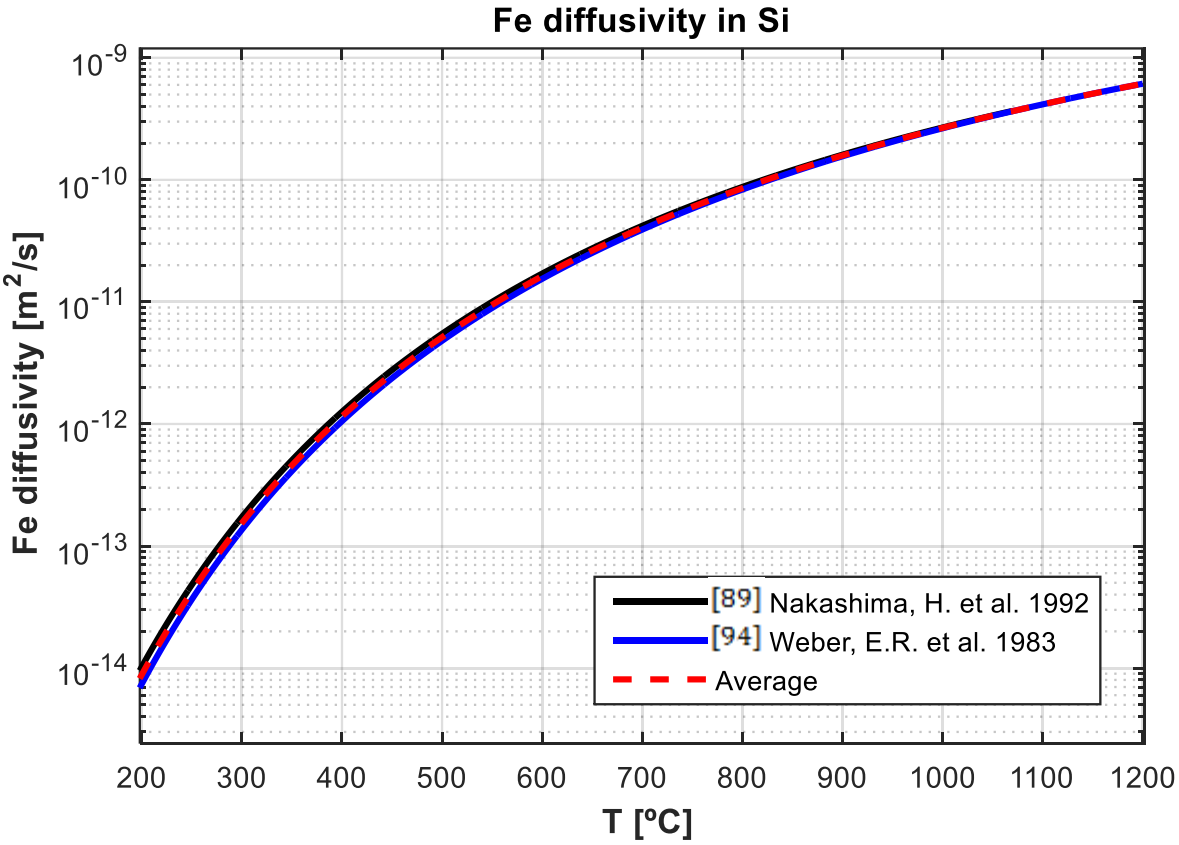

Figure 7.1 - Diffusion data for iron in silicon. The red profile represents the mean value of the profiles described in Table 7.1.

Table 7.1 - Iron diffusivity in silicon [86]

$D_0[cm^2\ s^{-1}]$	$Q[eV]$	Temperature range (Range applied to) [°C]	Methods and remarks	Reference
1.1×10^{-3}	0.66	0-1070 (20-1070)	FZ crystals. DLTS, Hall effect. [87] FZ crystals. DLTS. [88]	[89]
1.3×10^{-3}	0.68	20-1250 (20-1200)	overall fit to: high-temperature radiotracer diffusion [90], low-temperature DLTS [91], resistivity [92] and EPR measurements [93]	[94, 75]

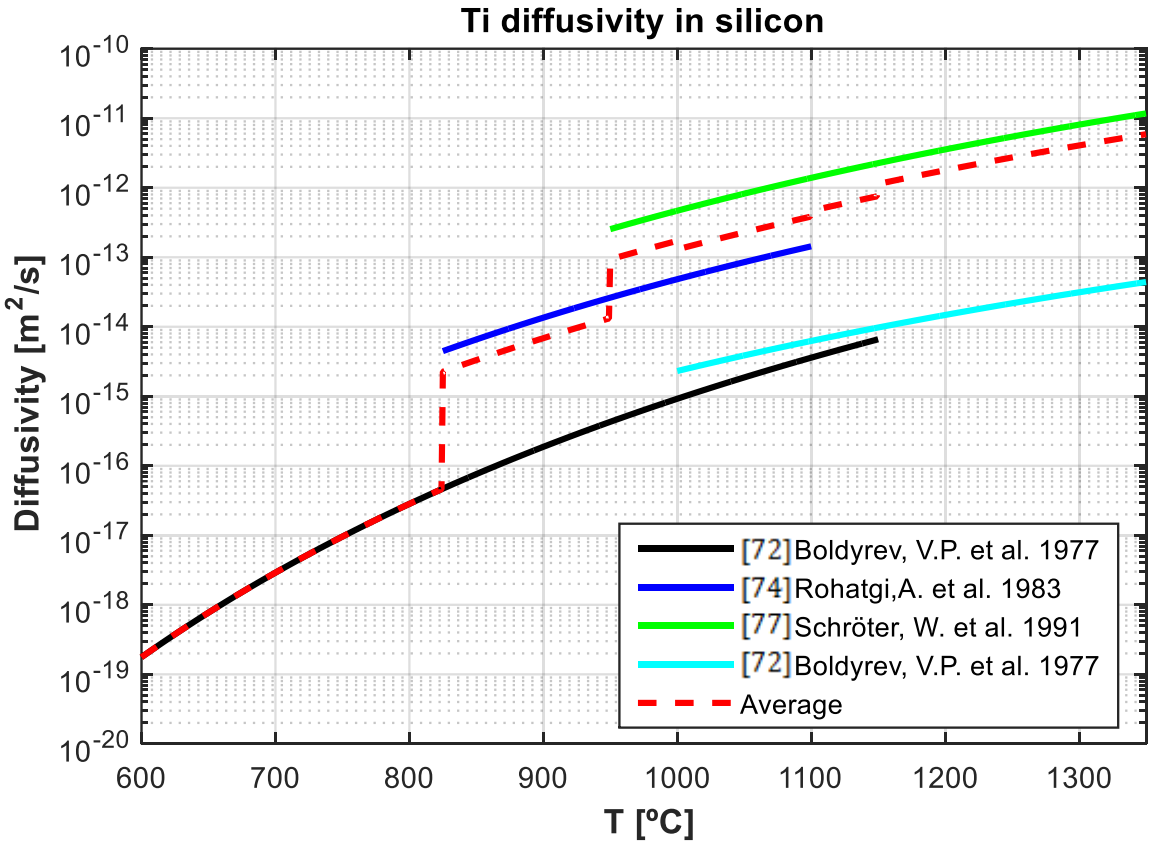

Figure 7.2 - Diffusion data for titanium in silicon. The red profile represents the mean value of the profiles described in Table 7.2.

Table 7.2 - Titanium diffusivity in silicon [86]

$D_0[cm^2\ s^{-1}]$	$Q[eV]$	Temperature range (Range applied to) [ºC]	Methods and Remarks	Reference
1.2×10^{-1}	2.05	600-1150 (20-1150)	DLTS. FZ crystals. DLTS and thermally stimulated capacitance measurements.	[72] [73]
1.5×10^{-3}	1.64	825-1100 (825-1100)	Recalculated from given data. Cz crystals. DLTS. Data reviews.	[74] [75, 76, 77]
1.45×10^{-2}	1.64	950-1200 (950-1350)	Cz and FZ crystals. DLTS and C-V measurement, chemical sectioning.	[77]
2×10^{-5}	1.5	1000-1250 (1000-1350)	Radiotracer ^{44}Ti, mechanical sectioning. Cz and FZ crystals. DLTS.	[72] [73]

Solubility in silicon

Solubility data was collected for the same elements in silicon samples, following various analysis techniques and was considered for the previous temperature ranges. The aspects regarding iron solubility are shown in Table 7.3 and plotted in Figure 7.3, while Table 7.4 and Figure 7.4 are relative to titanium. The red profiles in Figure 7.3 and Figure 7.4 represent the mean solubility coefficients, determined for the temperatures stated in the tables, resourcing to equation (2.16). These approximations were also applied in 3.5.

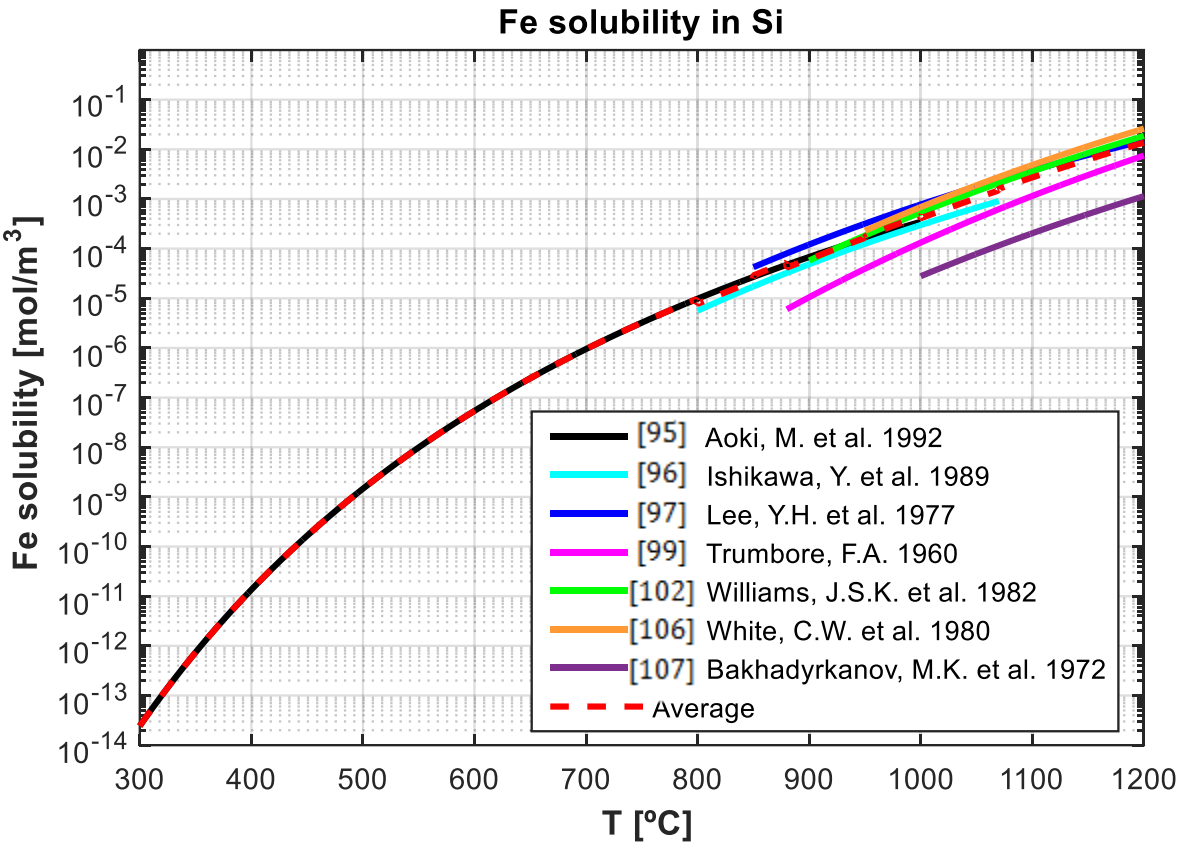

Figure 7.3 - Solubility of iron in silicon. The red profile represents the mean value of the profiles described in Table 7.3.

Table 7.3 - Solubility of iron in silicon

$S_0[at\ cm^{-3}]$	$Q[eV]$	Temperature range (Range applied to) [ºC]	Reference
4.30×10^{22}	2.1	670-1000 (20-1000)	[95]
3.30×10^{23}	2.34	800-1070 (800-1070)	[96]
1.35×10^{24}	2.39	850-1250 (850-1200)	[97, 98]
6.40×10^{26}	3.26	880-1310 (880-1200)	[90, 99, 100, 101]
7.40×10^{25}	2.87	900-1200 (900-1200)	[75, 94, 102, 103, 104, 105]
1.80×10^{26}	2.94	950-1200 (950-1200)	[106]
1.26×10^{25}	3	1000-1300 (1000-1200)	[107]

As an exception, the authors of [77] described Ti solubility instead based on:

$$S\ [at\ cm^{-3}] = 5 \times 10^{22} \exp(T\ S_M\ k_B - \frac{Q_M}{k_B\ T}) \quad (7.1)$$

where S_M is the pre-factor of the Arrhenius plot of the solubility of metal atoms M in silicon, expressed as $5 \times 10^{22} \exp\left(\frac{S_M}{k_B}\right)$ $[at\ cm^{-3}]$ and Q_M represents this plot's slope. Noticeably, the eutectic temperature for Ti in silicon is 1330 ºC [77], meaning that for higher values the Arrhenius equation no longer applies.

To aid the study of Ti contamination for temperatures up to 1350 ºC, it was assumed that the solubility would remain constant after 1330 ºC, since it is a small temperature increment and literature suggests that the solubility should decrease for other 3d transition metals in silicon [77].

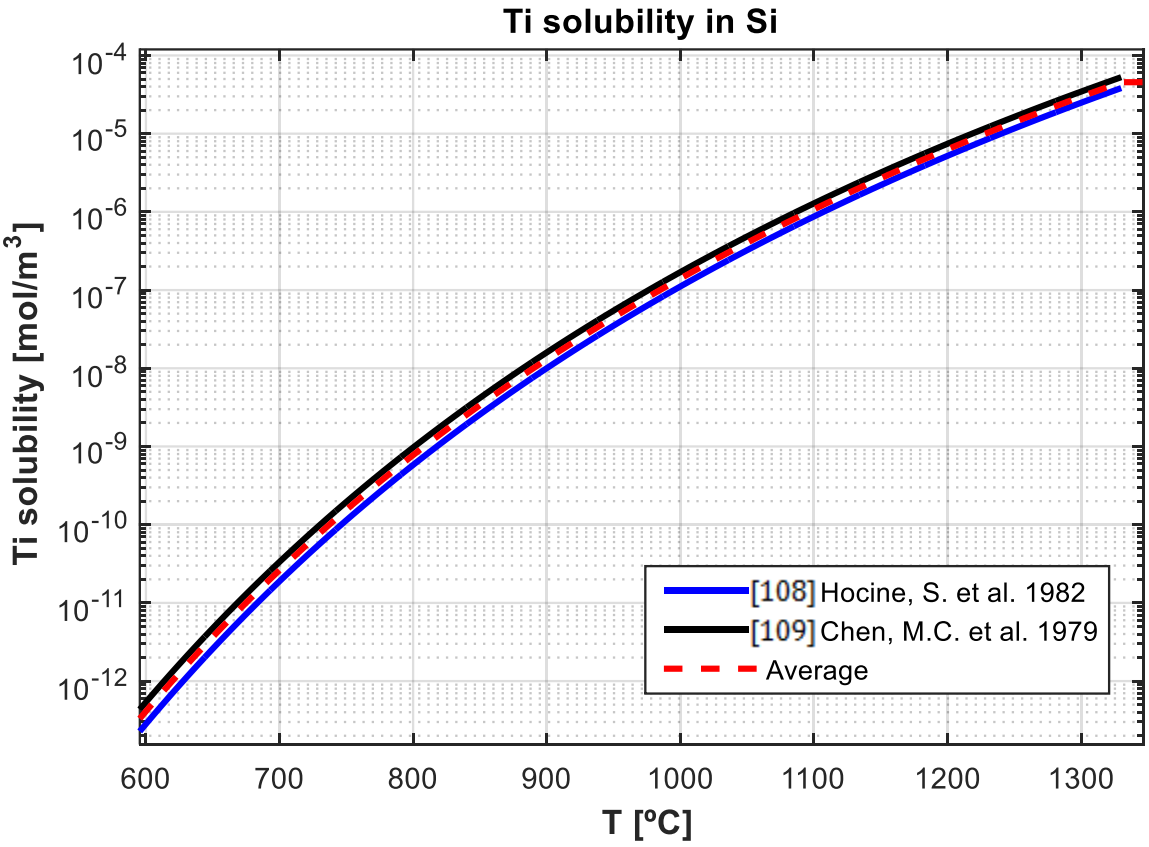

Figure 7.4 - Solubility of titanium in silicon. The red profile represents the mean value of the profiles described in Table 7.4.

Table 7.4 - Solubility of titanium in silicon [77]

$S_M[k_B]$	$Q_M[eV]$	Temperature range (Range applied to) [ºC]	Reference
4.2	3.05	950-1330 (20-1330)	[108]
3.9	3	1000-1250 (20-1330)	[109]

Appendix B

MATLAB script for the determination of diffusivity of Ti in the Si_3N_4 crucible:

```
% Main function
clc; close all; clear all;

% This method works for the assumption of heat treatment at constant
temperature (1)
Tconst=1;

% Thickness of the crucible sample (micrometers)
x1=6*1000;
% Thickness of the mono-Si sample (micrometers)
x2=3.5*1000;
% Ambient temperature (K)
Tamb=20+273.15;
% Time step (minutes)
dt=1/100;

% Scenario: GD-MS data and zeros (Scenario=1), with near surface
adjustment (Scenario=2) or based on curve fitting (Scenario=3)

for Scenario=1:3

    % Cc: Concentration of impurity in the crucible: lower estimate
(0), manufacturer value (1), higher estimate (2)
    for Cc=0:2

        % Solves the problem for the 4 samples
        for sample=1:4
            if sample==1 % Ti_1200_180
                %Duration of the heat treatment (minutes)
                tht=180;
                %Heat treatment temperature (K)
                Tht=1200+273.15;
            elseif sample==2 % Ti_1275_180
                tht=180;
                Tht=1275+273.15;
            elseif sample==3 % Ti_1350_60
                tht=60;
                Tht=1350+273.15;
            elseif sample==4  % Ti_1350_12
                tht=12;
                Tht=1350+273.15;
            end

            tf=tht+60; % Adds cooling period (60 minutes)
            t=0:dt:tf; % Creates a vector for time (minutes)

            % Function that loads the estimated amount of Ti (mol/m^2)
from excel file
            [n]=ndata(tht,Tht,Scenario);

            % Function that calculates the temperature profile (K)
            [T]=Tprofile(t,dt,Tht,Tamb,tht);
```

```
            % Function that computes the diffusivity in silicon along
the temperature profile (m^2/s)
            [D,~,~]=Ti(T,t,Tamb,Cc,Scenario);

            % Mean diffusivity in silicon during heat treatment
            meanD=mean(D);
            % Maximum diffusivity in silicon during heat treatment
            maxD=max(D);
            % Adjusts the time vector for a constant temperature(Tht)
and diffusivity(maxD)
            t=0:dt:tf*meanD/maxD;

            % Resets the temperature vector for the constant
temperature assumption (Tht)
            T=zeros(1,length(t));
            T(:)=Tht;

            % Function which sets the concentration of impurity in
the crucible and the diffusivity in silicon for the current temperature
profile
            [D,~,Ccrucible]=Ti(T,t,Tamb,Cc,Scenario);

            % Determines the diffusivity in the crucible which leads
to the similar amount of impurity in silicon after heat-treatment, for
each sample
            if sample==1 % Ti_1200_180
                [R1]=Iterationprocess(t,dt,n,Ccrucible,D,x1,x2,tht,
Tht,Tconst);
                D1=R1(4);
            elseif sample==2 % Ti_1275_180
                [R2]=Iterationprocess(t,dt,n,Ccrucible,D,x1,x2,tht,
Tht,Tconst);
                D2=R2(4);
            elseif sample==3 % Ti_1350_60
                [R3]=Iterationprocess(t,dt,n,Ccrucible,D,x1,x2,tht,
Tht,Tconst);
                D3=R3(4);
            elseif sample==4 % Ti_1350_12
                [R4]=Iterationprocess(t,dt,n,Ccrucible,D,x1,x2,tht,
Tht,Tconst);
                D4=R4(4);
            end
        end

        if Cc==0
            RC0=[Scenario,R1;Scenario,R2;Scenario,R3;Scenario,R4];
        elseif Cc==1
            RC1=[Scenario,R1;Scenario,R2;Scenario,R3;Scenario,R4];
        elseif Cc==2
            RC2=[Scenario,R1;Scenario,R2;Scenario,R3;Scenario,R4];
        end
    end %Gathers results for the different Ti contents in the crucible

    if Scenario==1
        RS1=[RC0;RC1;RC2];
```

```
    elseif Scenario==2
        RS2=[RC0;RC1;RC2];
    elseif Scenario==3
        RS3=[RC0;RC1;RC2];
    end

end %Gathers results for the different Scenarios

Results=[RS1;RS2;RS3]; % Groups results from the iterative method
```

Auxiliary functions

1 function [n]=ndata(tht,Tht,Scenario)

% Loads estimated amount of Ti (mol/m^2), for the experimental results, read from excel file named 'DcTi'. According to the annealing temperature and chosen scenario

```
if Scenario==1
    if Tht==1200+273.15
        n=xlsread('DcTi','1200_180','F2');
    elseif Tht==1275+273.15
        n=xlsread('DcTi','1275_180','F2');
    elseif Tht==1350+273.15
        if tht==12
            n=xlsread('DcTi','1350_12','F2');
        else
            n=xlsread('DcTi','1350_60','F2');
        end
    end
elseif Scenario==2
    if Tht==1200+273.15
        n=xlsread('DcTi','1200_180','F3');
    elseif Tht==1275+273.15
        n=xlsread('DcTi','1275_180','F3');
    elseif Tht==1350+273.15
        if tht==12
            n=xlsread('DcTi','1350_12','F3');
        else
            n=xlsread('DcTi','1350_60','F3');
        end
    end
elseif Scenario==3
        if Tht==1200+273.15
            n=xlsread('DcTi','1200_180','F4');
        elseif Tht==1275+273.15
            n=xlsread('DcTi3','1275_180','F4');
        elseif Tht==1350+273.15
            if tht==12
                n=xlsread('DcTi','1350_12','F4');
            else
                n=xlsread('DcTi','1350_60','F4');
            end
        end
end
```

```
2     function [T]=Tprofile(t,dt,Tht,Tamb,tht)
% Computation of the temperature profile according to the annealing
temperature and period

T=zeros(1,length(t)); %introduces temperature vector

for i=1:length(t)
    if t(i)<=4.25 %reheating stage
        if Tht==1350+273.15 %for annealing temperature of 1350 °C
            T(i)=146.67*log(t(i)+1)+1362.6;
        end
        if t(i)<=3.5
            if Tht==1275+273.15 %for annealing temperature of 1275
°C
                T(i)=158.39*log(t(i)+1)+1287.5;
            elseif Tht==1200+273.15 %for annealing temperature of
1200 °C
                T(i)=147.02*log(t(i)+1)+1230.5;
            end
        elseif t(i)>4.25 && t(i)<=tht % Maximum temperature
            T(i)=Tht;
        else
            if Tht==1275+273.15 || Tht==1200+273.15 %Temperature
stabilizes earlier for these annealing conditions
                T(i)=Tht;
            end
        end
    end
end

% Separate function which calculates temperatures during the cooling
stage
T=Cooling(t,dt,Tamb,tht,T);
```

2.1 function [T]=Cooling(t,dt,Tamb,tht,T)

```
% Determines the temperature of silicon during the cooling stage

v=(3.5/1000)*0.03*0.025; %volume of silicon sample – thermal expansion considered negligible (m^3)
A=0.03*0.025; %surface area of silicon sample - thermal expansion considered negligible (m^2)
L=A/0.11; %characteristic length for horizontal plane (m)
g=9.807; %gravitational acceleration at sea level (m/s^2)
trefr=0.064; %refractory thickness (m)
sigma=5.67e-8; %Stefan-Boltzmann constant (W/(m^2*K^4))
MSi=28.0855*10^-3; %silicon atomic mass (kg/mol)
e=0.6; %total emissivity of silicon sample
krefr=1.01; %thermal conductivity of the refractory W/(m*K)

vair=[11.44,15.89,20.92,26.41,32.39,38.79,45.57,52.69,60.21,68.1,76.
37,84.93,93.8,102.9,112.2,121.9]*10^-6; %kinematic viscosity of air used for interpolation (m^2/s)
Prair=[0.72,0.707,0.7,0.69,0.686,0.684,0.683,0.685,0.69,0.695,0.702,
0.709,0.716,0.72,0.723,0.726];  %Prandtl nr of air used for interpolation
kair=[22.3,26.3,30,33.8,37.3,40.7,43.9,46.9,49.7,52.4,54.9,57.3,
59.6,62,64.3,66.7]*10^-3;  %thermal conductivity of air used for interpolation (W/m*K)
Tair=[250,300,350,400,450,500,550,600,650,700,750,800,850,900,950,10
00]; % Respective temperatures of vair, Prair and kair

dt2=1/60; % alternative time step 1 second (minutes)

% attributes the smallest time step to the iterative process
if dt<dt2
    dt2=dt;
end

% Preallocation of the sample temperature during cooling
Tc=zeros(1,round(dt/dt2)+1);

% Iterative process for the Lumped Capacitance Method
for j=find(t>tht,1):length(T)
    Tc(1)=T(j-1);
    for i=1:round(dt/dt2)

        rho=(2.33-0.0000219*Tc(i))*1000;
        %silicon density (kg/m^3)

        c=(23.5+(0.00305)*Tc(i)-(0.000000293)*(Tc(i))^2)/MSi;
        % silicon specific heat (J/(Kg*K))

        Tf=(Tc(i)+Tamb)/2; % film temperature (K)
        beta=1/Tf; %thermal expansion coefficient, assuming air as an ideal gas (K^-1)

        p=find(Tair>Tf,1);
        visc=vair(p)-((Tair(p)-Tf)*(vair(p)-vair(p-1))/(Tair(p)-
Tair(p-1))); %kinematic viscosity of air (m^2/s)
```

```
        Pr=Prair(p)-((Tair(p)-Tf)*(Prair(p)-Prair(p-1))/(Tair(p)-
Tair(p-1))); %Prandtl number of air
        k=kair(p)-((Tair(p)-Tf)*(kair(p)-kair(p-1))/(Tair(p)-Tair(p-
1))); %thermal conductivity of air (W/m*K) at 293.15 K
        Gr=L^3*g*beta*(Tc(i)-Tamb)/visc^2; %Grasshoff nr
        Ra=Gr*Pr; %Rayleigh nr
        Nu=0.54*Ra^0.25;  %Nusselt nr for 10^4<=Ra<=10^7 (laminar
flow)
        hcv=Nu*k/L; %convection heat transfer coefficient (W/(m^2*K))
        dT=-A*((hcv+krefr/trefr)*(Tc(i)-Tamb)+e*sigma*(Tc(i)^4-
Tamb^4))/(rho*c*v); % temperature variation (K)
        Tc(i+1)=Tc(i)+dT*dt2*60; % new temperature value (K)

        if Tc(i+1)>Tamb
            T(j)=Tc(i+1);
        else
            T(j)=Tamb;
        end %Avoids eventual cooling below ambient temperature and
attributes resulting values to the temperature profile
    end
end
```

```
3     function [D,Dc,Ccrucible]=Ti(T,t,Tamb,Cc,Scenario)

% Stipulates diffusivities of Ti in the couple according to the
temperature profile, as well as the impurity content in the crucible
for the chosen estimate

kb=0.000086173324;% Boltzmann's constant (eV/K)

% Preallocation of vectors
D1=zeros(1,length(T));
D2=zeros(1,length(T));
D3=zeros(1,length(T));
D4=zeros(1,length(T));
D=zeros(1,length(t));
Dc=zeros(1,length(t));

%Sets the concentration in the crucible (mol/m^3)
if Cc==0
    Ccrucible=0.027; %lower estimate
elseif Cc==1
    Ccrucible=0.0543171704932417; %manufacturer value
elseif Cc==2
    Ccrucible=0.082; %higher estimate
end

% Diffusivity data in silicon according to the authors (m^2/s)
for i=1:length(t)
    if T(i)>=Tamb && T(i)<=1150+273.15
% Boldyrev, V.P. et al., 1977 and Graff, K. et al., 1981
        D0=1.2*(10^-3)*(10^-4); %m^2/s
        Q=2.05; %eV
        D1(i)=D0*exp(-Q/(T(i)*kb));
    end
    if T(i)>=825+273.15 && T(i)<=1100+273.15
% Rohatgi,A. et al., 1983
        D0=1.5*(10^-3)*(10^-4); %m^2/s
        Q=1.64; %eV
        D2(i)=D0*exp(-Q/(T(i)*kb));
    end
    if T(i)>=950+273.15 && T(i)<=1350+273.15
% Schröter, W. et al., 1991
        D0=1.45*(10^-2)*(10^-4); %m^2/s
        Q=1.64; %eV
        D3(i)=D0*exp(-Q/(T(i)*kb));
    end
    if T(i)>=1000+273.15 && T(i)<=1350+273.15
% Boldyrev, V.P. et al., 1977 and Graff, K. et al., 1981
        D0=2*(10^-5)*(10^-4); %m^2/s
        Q=1.5; %eV
        D4(i)=D0*exp(-Q/(T(i)*kb));
    end
end

% Maximum diffusivity in silicon from literature (m^2/s)
for i=1:length(t)
  if T(i)>=Tamb && T(i)<825+273.15
```

```
  D(i)=D1(i);
  end
  if T(i)>=825+273.15 && T(i)<950+273.15
  D(i)=D2(i);
  end
  if T(i)>=950+273.15  && T(i)<=1350+273.15
  D(i)=D3(i);
  end
end

% Diffusivity in the crucible (m^2/s) - results from the Iterative
Method for k=2.5 and dt=1/100 (min)
if Scenario==1
for i=1:length(t)
         if Cc==0
         %Dc(i)=4.58226E-07*exp(-2.3621E+04/T(i)); % dt=1/100 minutes
         Dc(i)=2.60495E-08*exp(-1.98391E+04/T(i));      %      dx=0.8
micrometers
         elseif Cc==1
         %Dc(i)=1.29186E-07*exp(-2.3855E+04/T(i)); % dt=1/100 minutes
         Dc(i)=1.21873E-09*exp(-1.77024E+04/T(i));      %      dx=0.8
micrometers
         elseif Cc==2
         %Dc(i)=7.66305E-08*exp(-2.42261E+04/T(i));% dt=1/100 minutes
         Dc(i)=2.75122E-10*exp(-1.68273E+04/T(i));      %      dx=0.8
micrometers
         end
end
elseif Scenario==2
for i=1:length(t)
         if Cc==0
         %Dc(i)=8.9102E-05*exp(-2.98656E+04/T(i)); % dt=1/100 minutes
         Dc(i)=2.39327E-05*exp(-2.82148E+04/T(i));      %      dx=0.8
micrometers
         elseif Cc==1
         %Dc(i)=7.94144E-06*exp(-2.85554E+04/T(i));% dt=1/100 minutes
         Dc(i)=4.69121E-07*exp(-2.49094E+04/T(i));      %      dx=0.8
micrometers
         elseif Cc==2
         %Dc(i)=3.06555E-06*exp(-2.83708E+04/T(i));% dt=1/100 minutes
         Dc(i)=6.65993E-08*exp(-2.34214E+04/T(i));      %      dx=0.8
micrometers
         end
end
else
for i=1:length(t)
         if Cc==0
         %Dc(i)=3.37979E-02*exp(-3.75323E+04/T(i));% dt=1/100 minutes
         Dc(i)=2.10926E-02*exp(-3.70219E+04/T(i));      %      dx=0.8
micrometers
         elseif Cc==1
         %Dc(i)=7.56036E-04*exp(-3.43064E+04/T(i));% dt=1/100 minutes
         Dc(i)=1.27784E-04*exp(-3.20649E+04/T(i));      %      dx=0.8
micrometers
         elseif Cc==2
         %Dc(i)= 1.91039E-04*exp(-3.35493E+04/T(i));%dt=1/100 minutes
```

```
        Dc(i)=1.34535E-05*exp(-3.01715E+04/T(i));      %      dx=0.8
micrometers
        end
end
end
```

```
4    function[Results]=Iterationprocess(t,dt,n,Cc,D,x1,x2,tht,Tht,
Tconst)
% Iterative process for the diffusivity of Ti in the crucible

% Minimum value for the initial diffusivity in the crucible, set by
defect
Dmin=1e-20;
% Maximum value for the initial diffusivity in the crucible, set by
excess
Dmax=1e-10;

% Tolerance which dictates when the process should be interrupted
tolerance = 1e-10;

% Preallocation of the resulting estimate for the amount of impurity
in silicon
ntest=0;

% Preallocation of the diffusivity vector being tested
Dtest=zeros(1,length(t));

while abs(ntest-n)>tolerance
    Dprev=Dtest; % Saves the previously tested diffusivity value

    Dtest(:)=(Dmin+Dmax)/2; % Sets the average of the minimum and
maximum diffusivities as a constant diffusivity in the crucible

    if Dprev==Dtest
        tolerance=tolerance*10; % Increases tolerance if no solution
is found for the previous value
    end

    % Determination of the maximum value of the diffusivities, to
calculate an adequate depth increment
    DM=max(max(D),max(Dtest));
    % Defines the depth increment (micrometers) based on von Neumann's
stability condition
    dx=sqrt(DM*2.5*dt*60)*10^6;
    x=-x1:dx:x2; % Creates the depth vector (micrometers)
    xi=find(x>=0, 1 ); % Locates the position of the interface in the
vector
    x=x-x(xi); % Moves the interface to depth=0 (crucible/silicon
thickness increases/decreases, respectively)

    % Solves the diffusion problem according to the previously set
parameters with explicit finite difference method
    [C,E]=Diffusion(x,dx,t,tht,dt,Cc,D,Dtest,Tconst);

    % Sums uncertainty at each time step (Er), estimates the amount
of impurity in silicon (ntest), checks the concentration balance,
resulting from the method (nbal)
    [Er,ntest,nbal]=Resultparameters(E,C,x,t,tht,Tconst);

    if ntest-n>0
        Dmax=Dtest(1);
    elseif ntest-n<0
```

```
        Dmin=Dtest(1);
    end
end % If the experimental estimate for the amount of impurity in
silicon, is lower/higher than the one resulting from the iteration,
means that the diffusivity should be lower/higher than the tested
value, respectively.

% Presents a results vector with the heat treatment temperature Tht
(°C) and duration (minutes), the assumed Ti concentration in the
crucible, the resulting estimate for the diffusivity in the crucible,
the difference between the experimental and the resulting estimate for
the Ti amount in silicon, the uncertainty at the end of the calculation
and the net balance between the first and last column of the
concentration in the system, respectively.
Results=[Tht-273.15,tht,Cc,Dtest(1),n-ntest,Er(length(t)),nbal];
```

4.1 function [C,E]=**Diffusion**(x,dx,t,tht,dt,Cs,D,Dc,Tconst)

```
% Solution of the diffusion problem according to Fick's 2nd Law, by
an explicit finite difference method

% Preallocation of matrixes
C=zeros(length(x),length(t));
J=zeros(length(x),length(t));
E=zeros(length(x),length(t));
JE=zeros(length(x),length(t));

% Sets the initial concentration
C(x<0,1)=Cs;

if Tconst==1
    for j=1:length(t)-1
        for i=1:length(x)
        %boundary condition at the crucible back surface
        if i==1
            J(i,j)=Dc(j)*(C(i+1,j)-C(i,j))/(dx/(10^6))^2;
            JE(i,j)=sqrt((Dc(j)*E(i,j)/(dx/(10^6))^2)^2+(Dc(j)*E(i+
1,j)/(dx/(10^6))^2)^2);
        %boundary condition at the silicon back surface
        elseif i==length(x)
            J(i,j)=D(j)*(C(i-1,j)-C(i,j))/(dx/(10^6))^2;
            JE(i,j)=sqrt((D(j)*E(i,j)/(dx/(10^6))^2)^2+(D(j)*E(i-
1,j)/(dx/(10^6))^2)^2);
        %crucible|mono-Si interface
        elseif x(i)==0
            J(i,j)=(D(j)*(C(i+1,j)-C(i,j))+Dc(j)*(C(i-1,j)-
C(i,j)))/(dx/(10^6))^2;
            JE(i,j)=sqrt((D(j)*E(i,j)/(dx/(10^6))^2)^2+(D(j)*E(i+1,
j)/(dx/(10^6))^2)^2+(Dc(j)*E(i,j)/(dx/(10^6))^2)^2+(Dc(j)*E(i-
1,j)/(dx/(10^6))^2)^2);
        %crucible bulk
        elseif x(i)<0
            J(i,j)=Dc(j)*(C(i+1,j)-2*C(i,j)+C(i-1,j))/(dx/
(10^6))^2;
            JE(i,j)=sqrt((Dc(j)*E(i+1,j)/(dx/(10^6)^2))^2+(Dc(j)*2*
E(i,j)/(dx/(10^6))^2)^2+(Dc(j)*E(i-1,j)/(dx/(10^6)^2))^2);
        %silicon bulk
        elseif x(i)>0
            J(i,j)=D(j)*(C(i+1,j)-2*C(i,j)+C(i-1,j))/(dx/ (10^6))^2;
            JE(i,j)=sqrt((D(j)*E(i+1,j)/(dx/(10^6))^2)^2+(D(j)*2*E(
i,j)/(dx/(10^6))^2)^2+(D(j)*E(i-1,j)/(dx/(10^6))^2)^2);
        end

        C(i,j+1)=C(i,j)+J(i,j)*dt*60;
        E(i,j+1)=sqrt((C(i,j+1)-C(i,j)-J(i,j)*dt*60)^2+(JE(i,j)
*dt*60)^2);
        % current truncation error + propagation of previous error
        end
    end

else
    for j=1:find(t==(tht+1+dt))-1;
```

```
        for i=1:length(x)
        %boundary condition at the crucible back surface
        if i==1
            J(i,j)=Dc(j)*(C(i+1,j)-C(i,j))/(dx/(10^6))^2;
            JE(i,j)=sqrt((Dc(j)*E(i,j)/(dx/(10^6))^2)^2+(Dc(j)*E(i+
1,j)/(dx/(10^6))^2)^2);
        %boundary condition at the silicon back surface
        elseif i==length(x)
            J(i,j)=D(j)*(C(i-1,j)-C(i,j))/(dx/(10^6))^2;
            JE(i,j)=sqrt((D(j)*E(i,j)/(dx/(10^6))^2)^2+(D(j)*E(i-
1,j)/(dx/(10^6))^2)^2);
        %crucible|mono-Si interface
        elseif x(i)==0
            J(i,j)=(D(j)*(C(i+1,j)-C(i,j))+Dc(j)*(C(i-1,j)-
C(i,j)))/(dx/(10^6))^2;
            JE(i,j)=sqrt((D(j)*E(i,j)/(dx/(10^6))^2)^2+(D(j)*E(i+1,
j)/(dx/(10^6))^2)^2+(Dc(j)*E(i,j)/(dx/(10^6))^2)^2+(Dc(j)*E(i-
1,j)/(dx/(10^6))^2)^2);
        %crucible bulk
        elseif x(i)<0
            J(i,j)=Dc(j)*(C(i+1,j)-2*C(i,j)+C(i-1,j))/(dx/
(10^6))^2;
            JE(i,j)=sqrt((Dc(j)*E(i+1,j)/(dx/(10^6)^2))^2+(Dc(j)*2*
E(i,j)/(dx/(10^6))^2)^2+(Dc(j)*E(i-1,j)/(dx/(10^6)^2))^2);
        %silicon bulk
        elseif x(i)>0
            J(i,j)=D(j)*(C(i+1,j)-2*C(i,j)+C(i-1,j))/(dx/ (10^6))^2;
            JE(i,j)=sqrt((D(j)*E(i+1,j)/(dx/(10^6))^2)^2+(D(j)*2*E(
i,j)/(dx/(10^6))^2)^2+(D(j)*E(i-1,j)/(dx/(10^6))^2)^2);
        end

        C(i,j+1)=C(i,j)+J(i,j)*dt*60;
        E(i,j+1)=sqrt((C(i,j+1)-C(i,j)-J(i,j)*dt*60)^2+(JE(i,j)
*dt*60)^2);
        % current truncation error + propagation of previous error
        end
    end

        C(x<0,t==(tht+1+dt))=0;

    for j=find(t==(tht+1+dt)):length(t)-1
        for i=1:length(x)
            %boundary condition at the crucible back surface
            if i==1
                JE(i,j)=sqrt((Dc(j)*E(i,j)/(dx/(10^6))^2)^2+(Dc(j)*
E(i+1,j)/(dx/(10^6))^2)^2);
            %crucible bulk
            elseif x(i)<0
                JE(i,j)=sqrt((Dc(j)*E(i+1,j)/(dx/(10^6))^2)^2+(Dc(j
)*2*E(i,j)/(dx/(10^6))^2)^2+(Dc(j)*E(i-1,j)/(dx/(10^6))^2)^2);
            %boundary condition at the silicon back surface
            elseif i==length(x)
                J(i,j)=D(j)*(-C(i,j)+C(i-1,j))/(dx/(10^6))^2;
                JE(i,j)=sqrt((D(j)*E(i,j)/(dx/(10^6))^2)^2+(D(j)*E(
i-1,j)/(dx/(10^6))^2)^2);
            %crucible|mono-Si interface
```

```
            elseif x(i)==0
                J(i,j)=D(j)*(C(i+1,j)-C(i,j))/(dx/(10^6))^2;
                JE(i,j)=sqrt((D(j)*E(i,j)/(dx/(10^6))^2)^2+(D(j)*E(
i+1,j)/(dx/(10^6))^2)^2);
            %silicon bulk
            elseif x(i)>0
                J(i,j)=D(j)*(C(i+1,j)-2*C(i,j)+C(i-1,j))/(dx/
(10^6))^2;
                JE(i,j)=sqrt((D(j)*E(i+1,j)/(dx/(10^6))^2)^2+(D(j)*
2*E(i,j)/(dx/(10^6))^2)^2+(D(j)*E(i-1,j)/(dx/(10^6))^2)^2);
            end

        C(i,j+1)=C(i,j)+J(i,j)*dt*60;
        E(i,j+1)=sqrt((C(i,j+1)-C(i,j)-J(i,j)*dt*60)^2+(JE(i,j)
*dt*60)^2);
        % current truncation error + propagation of previous error
        end
    end
end
```

4.2 function [Er,n,nbal]=**Resultparameters**(E,C,x,t,tht,Tconst)

```
%Auxiliary function which calculates the total amount of impurity in
silicon according to the solution of the diffusion problem and other
useful parameters

% Sums uncertainty in every position for each time step
Er=sum(E);

% Calculates the balance of impurity concentrations in the system
between the final and starting time steps
if Tconst==1
nbal=sum(C(:,1))-sum(C(:,length(t)));   % Considering that the
assumption of a constant temperature always leads to shorter periods
than the heat treatment in the lab
else
nbal=sum(C(:,1))-sum(C(1:(find(x==0)-1),t==tht+1))-
sum(C(:,length(t))); % Considering the separation of crucible from the
silicon wafer, 1 min after heat treatment
end

% Average concentration in the silicon sample, assuming a constant
sputtering section
avgnsi=mean(C(find(x==0):length(x),length(t)));

% Estimate of the amount of impurity in silicon [mol/m^2]
n=avgnsi*3500;
```

Appendix C

MATLAB script for comparison of the Ti amounts in silicon after treatment at the varying and constant temperature profiles - auxiliary functions presented in Appendix B:

```
clc;close all; clear all;

% Thickness of the crucible sample (micrometers)
x1=6*1000;
% Thickness of the mono-Si sample (micrometers)
x2=3.5*1000;
% Ambient temperature (K)
Tamb=20+273.15;
% Time step (minutes)
dt=1/100;

% Scenario: GD-MS data and zeros (Scenario=1), with near surface adjustment (Scenario=2) or based on curve fitting (Scenario=3)
for Scenario=1:3

% Cc: Concentration of impurity in the crucible: lower estimate (0), manufacturer value (1), higher estimate (2)
    for Cc=0:2

        % Solves the problem for the 4 samples
        for sample=1:4
            if sample==1 % Ti_1200_180
                %Duration of the heat treatment (minutes)
                tht=180;
                %Heat treatment temperature (K)
                Tht=1200+273.15;
            elseif sample==2 % Ti_1275_180
                tht=180;
                Tht=1275+273.15;
            elseif sample==3 % Ti_1350_60
                tht=60;
                Tht=1350+273.15;
            elseif sample==4  % Ti_1350_12
                tht=12;
                Tht=1350+273.15;
            end

            tf=tht+60; % Adds cooling period (60 minutes)
            t=0:dt:tf; % Creates a vector for time (minutes)

            % Calculates the temperature profile (K)
            [T]=Tprofile(t,dt,Tht,Tamb,tht);

            for Tconst=0:1
            % Heat treatment with re-heating and cooling stages (0) or at constant temperature (1)

                    if Tconst==1 % For a heat treatment at constant temperature (Tht)
```

```
                    % Function that calculates the temperature
profile (K)
                    [T]=Tprofile(t,dt,Tht,Tamb,tht);

                    % Function that computes the diffusivity in
silicon along the temperature profile (m^2/s)
                    [D,~,~]=Ti(T,t,Tamb,Cc,Scenario);

                    % Mean diffusivity in silicon during heat
treatment
                    meanD=mean(D);
                    % Maximum diffusivity in silicon during
heat treatment
                    maxD=max(D);
                    % Adjusts the time vector for a constant
temperature(Tht) and diffusivity(maxD)
                    t=0:dt:tf*meanD/maxD;

                    % Resets the temperature vector for the
constant temperature assumption (Tht)
                    T=zeros(1,length(t));
                    T(:)=Tht;

                end

                % Function which sets the concentration and
diffusivity of the impurity in the crucible and the diffusivity in
silicon for the current temperature profile
                [D,Dc,Ccrucible]=Ti(T,t,Tamb,Cc,Scenario);

                % Determination of the maximum value of the
diffusivities, to calculate an adequate depth increment
                DM=max(max(D),max(Dc));
                % Defines the depth increment (micrometers)
based on von Neumann's stability condition
                dx=sqrt(DM*2.5*dt*60)*10^6;
                x=-x1:dx:x2;  % Creates the depth vector
(micrometers)
                xi=find(x>=0, 1 ); % Locates the position of the
interface in the vector
                x=x-x(xi); % Moves the interface to depth=0
(crucible/silicon thickness increases/decreases, respectively)

                % Solves the diffusion problem according to the
previously set parameters with explicit finite difference method
                [C,E]=Diffusion(x,dx,t,tht,dt,Cc,D,Dc,Tconst);

                % Sums uncertainty at each time step (Er),
estimates the amount of impurity in silicon (ntest), checks the
concentration balance, resulting from the method (nbal)
                [Er,ntest,nbal]=Resultparameters(E,C,x,t,tht,
Tconst);

                if Tconst==0
                    RT0=[Scenario,Ccrucible,Tht-273.15,tht,
dx,1,1,Tconst,n,Er(length(t)),nbal];
```

```
                    else
                        RT1=[Scenario,Ccrucible,Tht-273.15,tht,
dx,maxD,meanD,Tconst,n,Er(length(t)),nbal];
                    end %Combines results for the varying and
constant temperature profiles
                end

                if i==1
                    R1=[RT0;RT1];
                elseif i==2
                    R2=[RT0;RT1];
                elseif i==3
                    R3=[RT0;RT1];
                elseif i==4
                    R4=[RT0;RT1];
                end
            end %Groups results relative to each heat treatment

            if Cc==0
                RC0=[R1;R2;R3;R4];
            elseif Cc==1
                RC1=[R1;R2;R3;R4];
            elseif Cc==2
                RC2=[R1;R2;R3;R4];
            end
        end %Gathers results for the different Ti contents in the
crucible

        if Scenario==1
            RS1=[RC0;RC1;RC2];
        elseif Scenario==2
            RS2=[RC0;RC1;RC2];
        else
            RS3=[RC0;RC1;RC2];
        end
end %Gathers results for the different Scenarios

Results=[RS1;RS2;RS3]; % Groups results
```

Appendix D

MATLAB script for the analysis of unidimensional diffusion in the diffusion couples:

```
clc; close all; clear all;

Scenario=1;
Cc=2;
% Varying temperature profile. Scenario and crucible content (Cc) allocated to enable previous functions. These do not influence the results
Tamb=20+273.15; % Ambient temperature (K)
dt=1; % Time step (minutes)

for i=1:4
%(1) - Ti_1275_180
%(2) - Fe_1200_60
%(3) - Fe_1200_60 comparison of concentrations at 7.5 mm radius surface average and at 0 mm
%(4) - Fe_1200_60 with 20 mm radius of Si3N4|Si interface
    if i==1
        Imp=0;
    else
        Imp=1;
    end % Impurity: Ti (0) or Fe (1)

    if Imp==0
        tht=180; % Duration of the heat treatment (minutes)
        Tht=1275+273.15; % Temperature of the heat treatment (K)
        dx=250; % spacing for Ti (micrometers)
    else
        tht=60; % Duration of the heat treatment (minutes)
        Tht=1200+273.15; % Temperature of the heat treatment (K)
        dx=500; % spacing for Fe (micrometers) - due to higher diffusivity in silicon
    end
    tf=tht+60; % Adds cooling period (60 minutes)
    t=0:dt:tf; % Creates a vector for time (minutes)

    % Calculates the temperature profile (K)
    [T]=Tprofile(t,dt,Tht,Tamb,tht);

    tSi3N4=6*1000; % Thickness of the crucible sample (micrometers)
    tSi=3.5*1000; % Thickness of the mono-si sample (micrometers)
    x=-tSi3N4:dx:tSi; % Creates the depth vector (micrometers)

    if i==4
        LSi3N4=(40*1000)/2;    % Wider crucible width/radius (micrometers)
    else
        LSi3N4=(20*1000)/2; % Crucible width/radius (micrometers)
    end
    LSi=LSi3N4+(10*1000)/2; % Silicon width/radius (micrometers)
    y=0:dx:LSi; % Creates the radius vector (micrometers)
```

```
    CE=abs(y-LSi3N4); kc=find(CE==min(CE)); % Finds the position in
the y vector which corresponds to the crucible edge

    % Sets the concentration of impurity in the crucible and the
diffusivities (silicon and crucible) according to the temperature
profile
    if Imp==0 % For Ti
        [D,~,Ccrucible]=Ti(T,t,Tamb,Cc,Scenario);
        Dc=D*5; % Defines diffusivity in the crucible as 10 times the
diffusivity in silicon
    else % For Fe (diffusivity in the crucible = diffusivity in
silicon)
        [D,Dc,Ccrucible]=Fe(T,t,Tamb);
    end


    Dc(t>tht+1)=0; % Stops diffusion from the crucible when the couple
is disassembled (1 min after tht)

    % Solution of 2D diffusion problem
    [C,E]=Diffusion2D(x,y,dx,kc,t,dt,Ccrucible,D,Dc);

    % Creates new figure
    figure (i)

        % Sets a graph in the first row, of the figure, with 2 rows
and 1 column
        subplot(2,1,1)

            % Scatter plot of concentration across the interface
            semilogy(y/1000,C(find(x>=0, 1 ),:,length(t)),'b.')
            hold on

            % Axis labels
            xlabel('\bf Radius (mm)')
            ylabel('\bf Concentration (mol/m^3)')

            % GD-MS detection limits for Fe and Ti in silicon
(mol/m^3)
            FeDL=zeros(1,length(y)); FeDL(:)=3.75439*10^(-5);
            TiDL=zeros(1,length(y)); TiDL(:)=8.34309*10^(-6);

            if i==1 % Plot attributes for Ti_1275_180
                semilogy(y/1000,TiDL,'k--')   % Plots the GD-MS
detection limit for Ti
                ylim([1e-6 10*max(C(find(x>=0, 1 ),:,length(t)))]) %
y axis range
                title ('Ti profile along Si_3N_4|Si interface - 1275°C
- 180 min') % Graph title
            else % Plot attributes for Fe
                semilogy(y/1000,FeDL,'k--')   % Plots the GD-MS
detection limit for Fe
                ylim([1e-6 10*max(C(find(x>=0, 1 ),:,length(t)))]) %
y axis range
                title ('Fe profile along Si_3N_4|Si interface - 1200°C
- 60 min') % Graph title
```

```
            end
            hold off
            grid on % Adds grid to the graph
            legend('Diffusion-only    estimate','GD-MS    detection
limit'); % Adds legend to the graph

             YlogTicks=-6:1:0;
             LogTicks=10.^YlogTicks;
             TheLogTicks=LogTicks(LogTicks>=1e-6  &  LogTicks<=10*max(
C(find(x>=0, 1 ),:,length(t))));
             set(gca,'YTick',TheLogTicks)
             % Alters y axis ticks for better visualization

        % Sets a graph in the second row, of the figure, with 2 rows
and 1 column
        subplot(2,1,2)

            % Plots concentration discrepancy
            if i==1 % Ti_1275_180
             semilogy(x/1000,C(:,y==0,length(t))-
C(:,y==7500,length(t)),'r.')
            hold on
            % GD-MS detection limits for Ti in silicon (mol/m^3)
            TiDL=zeros(1,length(x)); TiDL(:)=8.34309*10^(-6);
            semilogy(x/1000,TiDL,'k--') % Plots the GD-MS detection
limit for Ti

           ylabel('\bf C0 - C7.5 (mol/m^3)') % y axis label
           ylim ([1e-15 1e-5]) % y axis range
           YlogTicks=-15:1:0;
           LogTicks=10.^YlogTicks;
           TheLogTicks=LogTicks(LogTicks>=1e-15 & LogTicks<=1e-5);
           set(gca,'YTick',TheLogTicks)
           % Alters y axis ticks for better visualization

            title ('Discrepancy between 0 and 7.5mm radius - silicon
sample') % Graph title
            legend('Concentration    difference','GD-MS    detection
limit'); % Adds legend to the graph

            elseif i==2 % Fe_1200_60
                semilogy(x/1000,C(:,y==7500,length(t))./C(:,y==0,
length(t)),'r.')
                ylabel('\bf C7.5 / C0') % y axis label
                title   ('Discrepancy   of   the   Fe   concentration
profiles') % Graph title

            elseif i==3 % Fe_1200_60 with surface average
                % Preallocation of variables
                Cmean=0;
                A=zeros(1,length(y==7000));
                for j=1:find(y==7000)
                    A(j)=(y(j+1)^2-y(j)^2)/7500^2;
                    Cmean=C(:,j,length(t))*A(j)+Cmean;   % Averaged
concentration near the sputtered surface (7.5 mm radius)
                end
```

```
                semilogy(x/1000,Cmean./C(:,y==0,length(t)),'k.')
                ylabel('\bf Csurf / Ccenter') % y axis label

                elseif i==4 % Fe_1200_60 with unidimensional diffusion
at 0 mm
                semilogy(x/1000,C(:,y==0,length(t))-C(:,y==LSi-
15000,length(t)),'k.')
                hold on
                %GD-MS detection limits for Fe in silicon (mol/m^3)
                FeDL=zeros(1,length(x)); FeDL(:)=3.75439*10^(-5);
                semilogy(x/1000,FeDL,'k--')   %   Plots   the   GD-MS
detection limit for Fe
                ylabel('\bf Concentration (mol/m^3)') % y axis label
                ylim ([1e-10 1e-4]) % y axis range

                YlogTicks=-10:1:0;
                LogTicks=10.^YlogTicks;
                TheLogTicks=LogTicks(LogTicks>=1e-20 & LogTicks<=1e-
4);
                set(gca,'YTick',TheLogTicks)
                % Alters y axis ticks for better visualization

                legend('Concentration  difference','GD-MS  detection
limit'); % Adds legend to the graph
            end
            xlabel('\bf Depth (mm)')% x axis label
            xlim([0 max(x)/1000]) % x axis range
            grid on % Add grid to the graph
end
```

Auxiliary functions

Functions previously featured in Appendix B are omitted.

1 `function [D,Dc,Ccrucible]=Fe(T,t,Tamb)`

```
% Stipulates diffusivities of Fe in the couple according to the
temperature profile, as well as the impurity content in the crucible

kb=0.000086173324; % Boltzmann's constant (eV/K)

% Preallocation of vectors
D1=zeros(1,length(T));
D2=zeros(1,length(T));
D=zeros(1,length(t));

%Sets the concentration in the crucible (mol/m^3)
Ccrucible=0.49; %highest estimate, has no influence in the results

% Diffusivity data in silicon according to the authors (m^2/s)
for i=1:length(t)
    if T(i)>=Tamb && T(i)<=1070+273.15
         % Nakashima, H. et al. (1992)
        D0=1.1*(10^-3)*(10^-4); %m^2/s
        Q=0.66; %eV
        D1(i)=D0*exp(-Q/(T(i)*kb));
    end
    if T(i)>=Tamb && T(i)<=1200+273.15
         % Weber, E.R. et al. (1983)
        D0=1.3*(10^-3)*(10^-4); %m^2/s
        Q=0.68; %eV
        D2(i)=D0*exp(-Q/(T(i)*kb));
    end
end

% Average of the diffusivities in silicon from literature (m^2/s)
for i=1:length(t)
  if T(i)>=Tamb && T(i)<=1070+273.15
  D(i)=max(D1(i),D2(i));
  end
  if T(i)>1070+273.15
  D(i)=D2(i);
  end
end

%By default attributes the diffusivity in silicon to the crucible
Dc=D;
```

```
2     function [C,E]=Diffusion2D(x,y,dx,kc,t,dt,Ccrucible,D,Dc)

% Preallocation of matrixes
C=zeros(length(x),length(y),length(t));
J=zeros(length(x),length(y),length(t));
E=zeros(length(x),length(y),length(t));
JE=zeros(length(x),length(y),length(t));

for k=1:kc
    C(x<0,k,1)=Ccrucible; % Sets the initial crucible concentration
end

for j=1:length(t)-1
for i=1:length(x)
for k=1:length(y)
             % Diffusion in the crucible
             if x(i)<0
                  % Back surface
                  if i==1
                  % Centre
                  if k==1
                       J(i,k,j)=Dc(j)*(C(i+1,k,j)+C(i,k+1,j)-
2*C(i,k,j))/(dx/(10^6))^2;
                       JE(i,k,j)=sqrt((Dc(j)*(E(i+1,k,j)-E(i,k,j)
)/(dx/(10^6))^2)^2+(Dc(j)*(E(i,k+1,j)-E(i,k,j))/(dx/(10^6))^2) ^2);
                  % Atmosphere/crucible boundary
                  elseif k==kc
                       J(i,k,j)=Dc(j)*(C(i+1,k,j)-C(i,k,j)+C(i,k-1,j)-
C(i,k,j))/(dx/(10^6))^2;
                       JE(i,k,j)=sqrt((Dc(j)*(E(i+1,k,j)-E(i,k,j)
)/(dx/(10^6))^2)^2+(Dc(j)*(E(i,k-1,j)-E(i,k,j))/(dx/(10^6))^2) ^2);
                  % Remaining back surface
                  elseif k<kc
                       J(i,k,j)=Dc(j)*(C(i+1,k,j)+C(i,k+1,j)+C(i,k-
1,j)-3*C(i,k,j))/(dx/(10^6))^2;
                       JE(i,k,j)=sqrt((Dc(j)*(E(i+1,k,j)-E(i,k,j)
)/(dx/(10^6))^2)^2+(Dc(j)*(E(i,k-1,j)-E(i,k,j))/(dx/(10^6))^2)^2
+(Dc(j)*(E(i,k+1,j)-E(i,k,j))/(dx/(10^6))^2)^2);
                  % Atmosphere
                  else
                       J(i,k,j)=0;
                       JE(i,k,j)=0;
                  end
% Remaining points in the crucible
             else
             % Centre
             if k==1
                  J(i,k,j)=Dc(j)*(C(i+1,k,j)+C(i-1,k,j)+  C(i,k+1,j)-
3*C(i,k,j))/(dx/(10^6))^2;
                  JE(i,k,j)=sqrt((Dc(j)*(E(i+1,k,j)-E(i,k,j))/
(dx/(10^6))^2)^2+(Dc(j)*(E(i-1,k,j)-E(i,k,j))/(dx/(10^6))^2)^2+
(Dc(j)*(E(i,k+1,j)-E(i,k,j))/(dx/(10^6))^2)^2);
             % Atmosphere/crucible boundary
             elseif k==kc
                  J(i,k,j)=Dc(j)*(C(i+1,k,j)+C(i-1,k,j)-
3*C(i,k,j)+C(i,k-1,j))/(dx/(10^6))^2;
```

```
                JE(i,k,j)=sqrt((Dc(j)*(E(i+1,k,j)-E(i,k,j))/
(dx/(10^6))^2)^2+(Dc(j)*(E(i-1,k,j)-E(i,k,j))/(dx/(10^6))^2)^2+
(Dc(j)*(E(i,k-1,j)-E(i,k,j))/(dx/(10^6))^2)^2);
            % Crucible bulk
            elseif k<kc
                J(i,k,j)=Dc(j)*(C(i+1,k,j)+C(i-1,k,j)-
4*C(i,k,j)+C(i,k+1,j)+C(i,k-1,j))/(dx/(1000000))^2;
                JE(i,k,j)=sqrt((Dc(j)*(E(i+1,k,j)-
E(i,k,j))/(dx/(10^6))^2)^2+(Dc(j)*(E(i-1,k,j)-E(i,k,j))/
(dx/(10^6))^2)^2+(Dc(j)*(E(i,k-1,j)-E(i,k,j))/(dx/(10^6))^2)^2+
(Dc(j)*(E(i,k+1,j)-E(i,k,j))/(dx/(10^6))^2)^2);
            % Atmosphere
            else
                J(i,k,j)=0;
                JE(i,k,j)=0;
            end
        end

%Diffusion in the interface
    elseif x(i)==0
        % Centre
        if k==1
            J(i,k,j)=(Dc(j)*(C(i-1,k,j)-C(i,k,j))+D(j)*
(C(i,k+1,j)+C(i+1,k,j)-2*C(i,k,j)))/(dx/(10^6))^2;
            JE(i,k,j)=sqrt((Dc(j)*(E(i-1,k,j)-E(i,k,j))/
(dx/(10^6))^2)^2+(D(j)*(E(i,k+1,j)-E(i,k,j))/(dx/(10^6))^2)^2+
(D(j)*(E(i+1,k,j)-E(i,k,j))/(dx/(10^6))^2)^2);
        % Remaining crucible/silicon interface
        elseif k<kc
            J(i,k,j)=(Dc(j)*(C(i-1,k,j)-C(i,k,j))+D(j)*(C(i,k-
1,j)+C(i+1,k,j)+C(i,k+1,j)-3*C(i,k,j)))/(dx/(10^6))^2;
            JE(i,k,j)=sqrt((Dc(j)*(E(i-1,k,j)-E(i,k,j))/
(dx/(10^6))^2)^2+(D(j)*(E(i,k-1,j)-E(i,k,j))/(dx/(10^6))^2)^2+
(D(j)*(E(i,k+1,j)-E(i,k,j))/(dx/(10^6))^2)^2+(D(j)*(E(i+1,k,j)-
E(i,k,j))/(dx/(10^6))^2)^2);
        % Silicon outer edge
        elseif k==length(y)
            J(i,k,j)=D(j)*(C(i,k-1,j)+C(i+1,k,j)-2*C(i,k,j))
/(dx/(10^6))^2;
            JE(i,k,j)=sqrt((D(j)*(E(i+1,k,j)-E(i,k,j))/
(dx/(10^6))^2)^2+(D(j)*(E(i+1,k,j)-E(i,k,j))/(dx/(10^6))^2)^2);
        % Atmosphere/silicon interface
        else
            J(i,k,j)=(D(j)*(C(i,k-1,j)+C(i+1,k,j)+C(i,k+1,j)-
3*C(i,k,j)))/(dx/(10^6))^2;
            JE(i,k,j)=sqrt((D(j)*(E(i,k-1,j)-E(i,k,j))/
(dx/(10^6))^2)^2+(D(j)*(E(i,k+1,j)-E(i,k,j))/(dx/(10^6))^2)^2+
(D(j)*(E(i+1,k,j)-E(i,k,j))/(dx/(10^6))^2)^2);
        end

    % Diffusion in silicon
    else
        % Silicon back surface
        if i==length(x)
            % Centre
            if k==1
```

```
                    J(i,k,j)=D(j)*(C(i-1,k,j)+C(i,k+1,j)-2*C(i,k,j))
/(dx/(10^6))^2;
                    JE(i,k,j)=sqrt((D(j)*(E(i-1,k,j)-(i,k,j))/
(dx/(10^6))^2)^2+(D(j)*(E(i,k+1,j)-E(i,k,j))/(dx/(10^6))^2)^2);
                % Edge
                elseif k==length(y)
                    J(i,k,j)=D(j)*(C(i-1,k,j)+C(i,k-1,j)-
2*C(i,k,j))/(dx/(10^6))^2;
                    JE(i,k,j)=sqrt((D(j)*(E(i-1,k,j)-E(i,k,j))/
(dx/(10^6))^2)^2+(D(j)*(E(i,k-1,j)-E(i,k,j))/(dx/(10^6))^2)^2);
                % Remaining points in the back surface
                else
                    J(i,k,j)=D(j)*(C(i-1,k,j)+C(i,k+1,j)+C(i,k-1,j)-
3*C(i,k,j))/(dx/(10^6))^2;
                    JE(i,k,j)=sqrt((D(j)*(E(i-1,k,j)-E(i,k,j))/
(dx/(10^6))^2)^2+(D(j)*(E(i,k+1,j)-E(i,k,j))/(dx/(10^6))^2)^2
+(D(j)*(E(i,k-1,j)-E(i,k,j))/(dx/(10^6))^2)^2);
                end
            % Remaining points in silicon
            else
                % Centre
                    if k==1
                        J(i,k,j)=D(j)*(C(i+1,k,j)+C(i-1,k,j)+
C(i,k+1,j)-3*C(i,k,j))/(dx/(10^6))^2;
                        JE(i,k,j)=sqrt((D(j)*(E(i+1,k,j)-E(i,k,j))
/(dx/(10^6))^2)^2+(D(j)*(E(i-1,k,j)-E(i,k,j))/(dx/(10^6))^2)^2+
(D(j)*(E(i,k+1,j)-E(i,k,j))/(dx/(10^6))^2)^2);
                    % Edge
                    elseif k==length(y)
                        J(i,k,j)=D(j)*(C(i+1,k,j)+C(i-1,k,j)+C(i,k-1,j)
-3*C(i,k,j))/(dx/(10^6))^2;
                        JE(i,k,j)=sqrt((D(j)*(E(i+1,k,j)-E(i,k,j))
/(dx/(10^6))^2)^2+(D(j)*(E(i-1,k,j)-E(i,k,j))/(dx/(10^6))^2)^2+
(D(j)*(E(i,k-1,j)-E(i,k,j))/(dx/(10^6))^2)^2);
                    % Bulk
                    else
                        J(i,k,j)=D(j)*(C(i+1,k,j)+C(i-1,k,j)+
C(i,k+1,j)+C(i,k-1,j)-4*C(i,k,j))/(dx/(10^6))^2;
                        JE(i,k,j)=sqrt((D(j)*(E(i+1,k,j)-E(i,k,j))
/(dx/(10^6))^2)^2+(D(j)*(E(i-1,k,j)-E(i,k,j))/(dx/(10^6))^2)^2
+(D(j)*(E(i,k+1,j)-E(i,k,j))/(dx/(10^6))^2)^2+(D(j)*(E(i,k-1,j)-
E(i,k,j))/(dx/(10^6))^2)^2);
                    end
                end
            end
        C(i,k,j+1)=C(i,k,j)+J(i,k,j)*dt*60;
        E(i,k,j+1)=sqrt((C(i,k,j+1)-C(i,k,j)-J(i,k,j)*dt*60)^2+(JE
(i,k,j)*dt*60)^2);
        % current truncation error + propagation of previous error
        end
    end
    end
    end
```

Appendix E

Information regarding the extrapolations of the Ti diffusivity estimates for a depth spacing of 0.8 μm in the simulated silicon sample, similar to the GD-MS sputtering data interval.

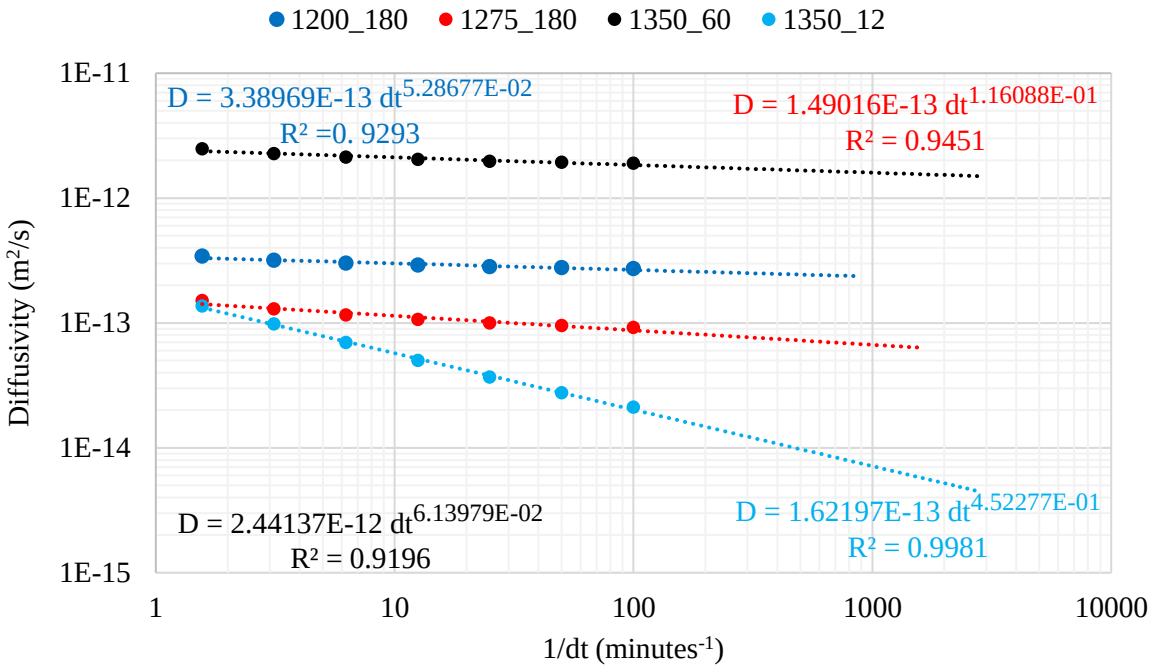

Figure 7.5 - Extrapolation of the diffusivity estimates at the GD-MS depth increment for scenario 2 with a Ti content in the crucible of 0.027 mol/m^3, by curve fitting a power function.

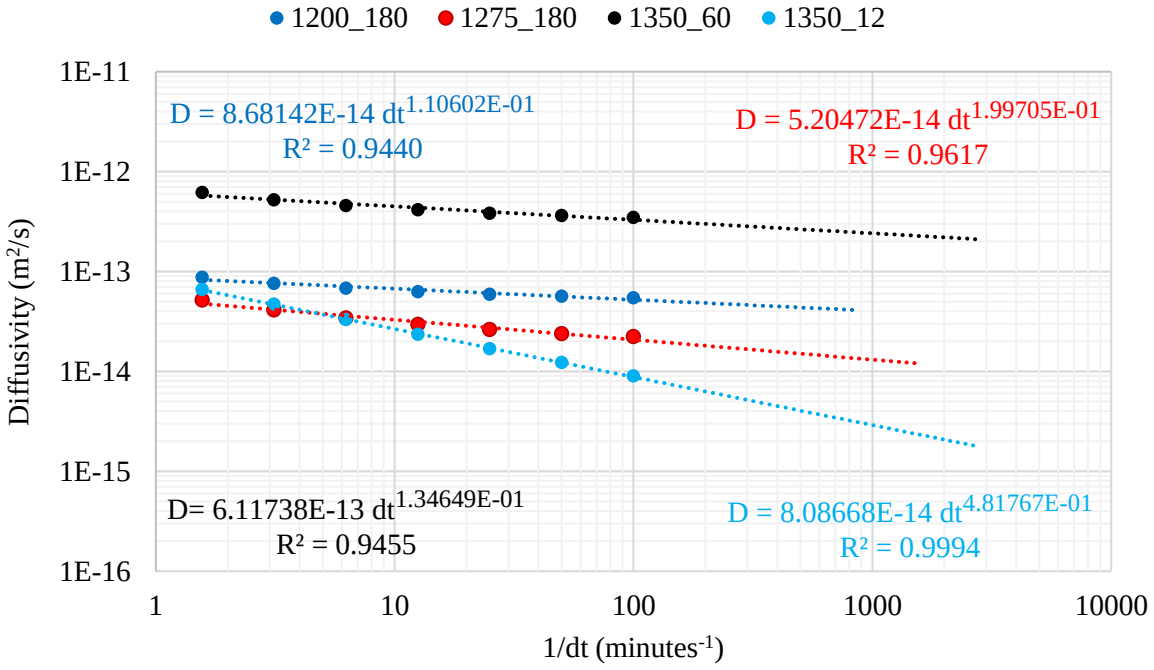

Figure 7.6 - Extrapolation of the diffusivity estimates at the GD-MS depth increment, for scenario 2 with a Ti content in the crucible of 0.054 mol/m^3, by curve fitting a power function.

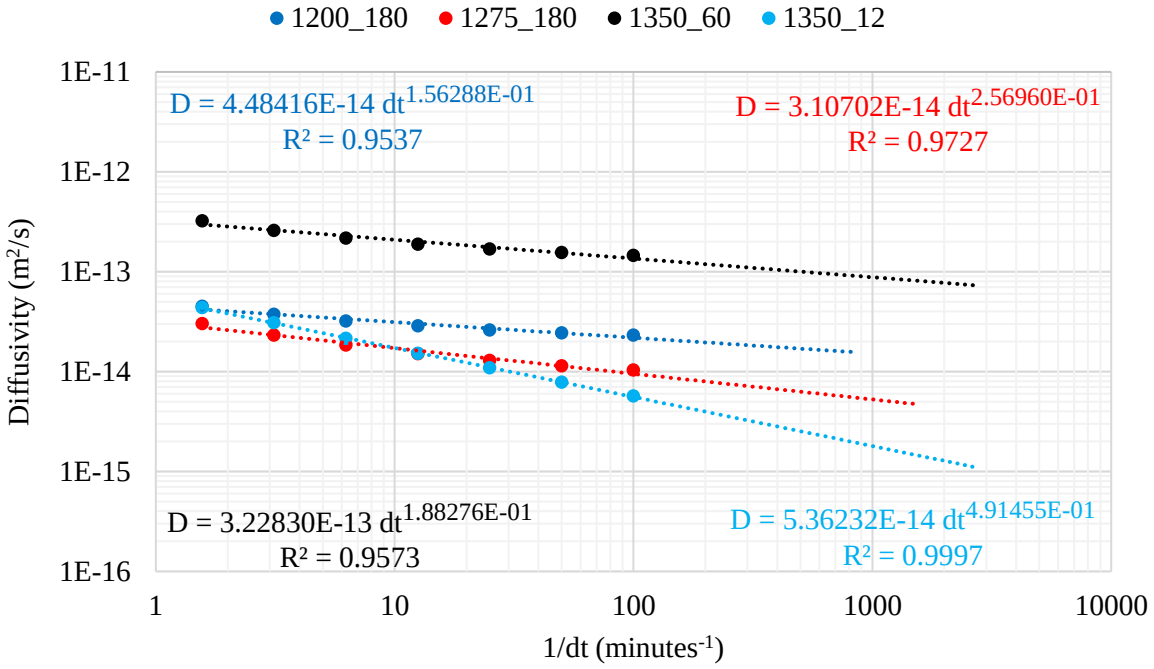

Figure 7.7 - Extrapolation of the diffusivity estimates at the GD-MS depth increment, for scenario 2 with a Ti content in the crucible of 0.082 mol/m^3, by curve fitting a power function.

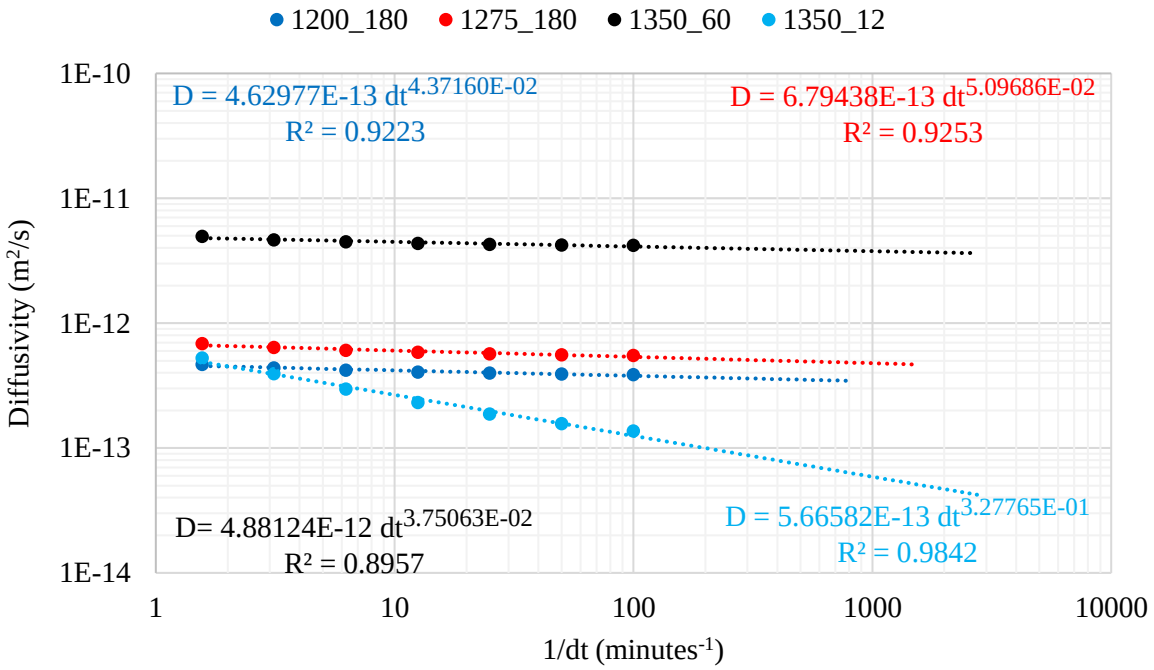

Figure 7.8 - Extrapolation of the diffusivity estimates at the GD-MS depth increment, for scenario 3 with a Ti content in the crucible of 0.027 mol/m^3, by curve fitting a power function.

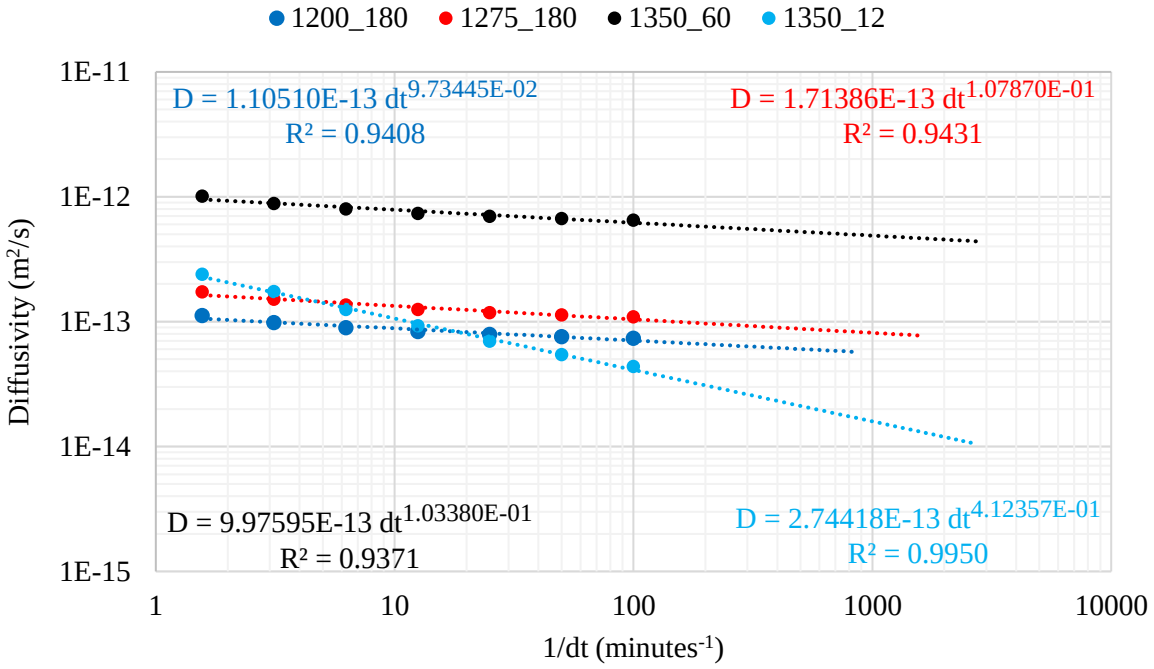

Figure 7.9 - Extrapolation of the diffusivity estimates at the GD-MS depth increment, for scenario 3 with a Ti content in the crucible of 0.054 mol/m^3, by curve fitting a power function.

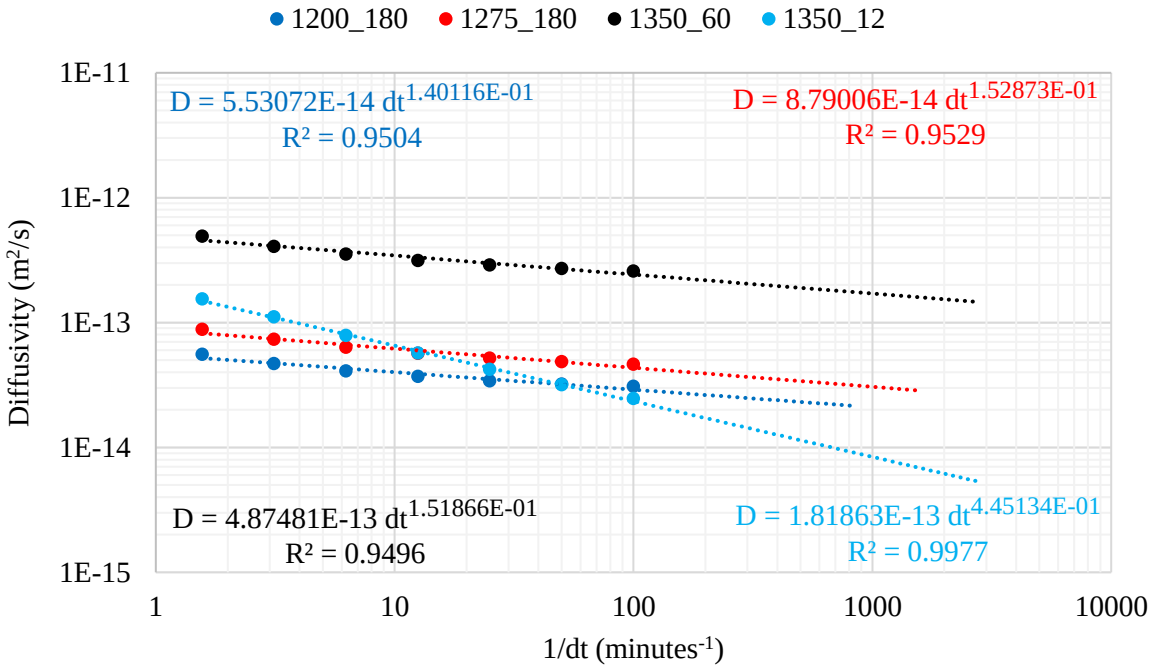

Figure 7.10 - Extrapolation of the diffusivity estimates at the GD-MS depth increment, for scenario 3 with a Ti content in the crucible of 0.082 mol/m^3, by curve fitting a power function.

Employing the dt value, which yields the 0.8 μm spacing (Table 5.3), to the previous equations, results in the following extrapolated diffusivities:

Table 7.5 - Extrapolated diffusion coefficients of each sample, for the GD-MS depth spacing of 0.8 μm, considering different amounts of Ti in the crucible and the three scenarios

Scenario	Ti content in the crucible (mol/m^3)	T_{ht} (ºC)	t_{ht} (min)	D (m^2/s)	$D_{extrapolation}$ (m^2/s)
1	0.027	1200	180	9.79×10^{-14}	7.85×10^{-14}
		1275	180	2.62×10^{-14}	1.45×10^{-14}
		1350	60	4.62×10^{-13}	2.94×10^{-13}
		1350	12	7.21×10^{-15}	1.44×10^{-15}
	0.054	1200	180	2.22×10^{-14}	1.49×10^{-14}
		1275	180	7.18×10^{-15}	3.01×10^{-15}
		1350	60	1.06×10^{-13}	4.85×10^{-14}
		1350	12	4.37×10^{-15}	8.33×10^{-16}
	0.082	1200	180	9.94×10^{-15}	5.86×10^{-15}
		1275	180	3.57×10^{-15}	1.29×10^{-15}
		1350	60	4.82×10^{-14}	1.80×10^{-14}
		1350	12	2.82×10^{-15}	5.31×10^{-16}
2	0.027	1200	180	2.72×10^{-13}	2.38×10^{-13}
		1275	180	9.18×10^{-14}	6.35×10^{-14}
		1350	60	1.90×10^{-12}	1.50×10^{-12}
		1350	12	2.11×10^{-14}	4.51×10^{-15}
	0.054	1200	180	5.48×10^{-14}	4.13×10^{-14}
		1275	180	2.24×10^{-14}	1.20×10^{-14}
		1350	60	3.49×10^{-13}	2.11×10^{-13}
		1350	12	9.02×10^{-15}	1.78×10^{-15}
	0.082	1200	180	2.33×10^{-14}	1.57×10^{-14}
		1275	180	1.04×10^{-14}	4.70×10^{-15}
		1350	60	1.46×10^{-13}	7.27×10^{-14}
		1350	12	5.69×10^{-15}	1.09×10^{-15}
3	0.027	1200	180	3.87×10^{-13}	3.45×10^{-13}
		1275	180	5.50×10^{-13}	4.67×10^{-13}
		1350	60	4.19×10^{-12}	3.63×10^{-12}
		1350	12	1.37×10^{-13}	4.23×10^{-14}
	0.054	1200	180	7.37×10^{-14}	5.74×10^{-14}
		1275	180	1.09×10^{-13}	7.76×10^{-14}
		1350	60	6.50×10^{-13}	4.40×10^{-13}
		1350	12	4.38×10^{-14}	1.05×10^{-14}
	0.082	1200	180	3.08×10^{-14}	2.16×10^{-14}
		1275	180	4.63×10^{-14}	2.86×10^{-14}
		1350	60	2.58×10^{-13}	1.46×10^{-13}
		1350	12	2.46×10^{-14}	5.36×10^{-15}

Arrhenius fits of these values were also done disregarding the sample treated during 12 minutes, as explained in 4.3.

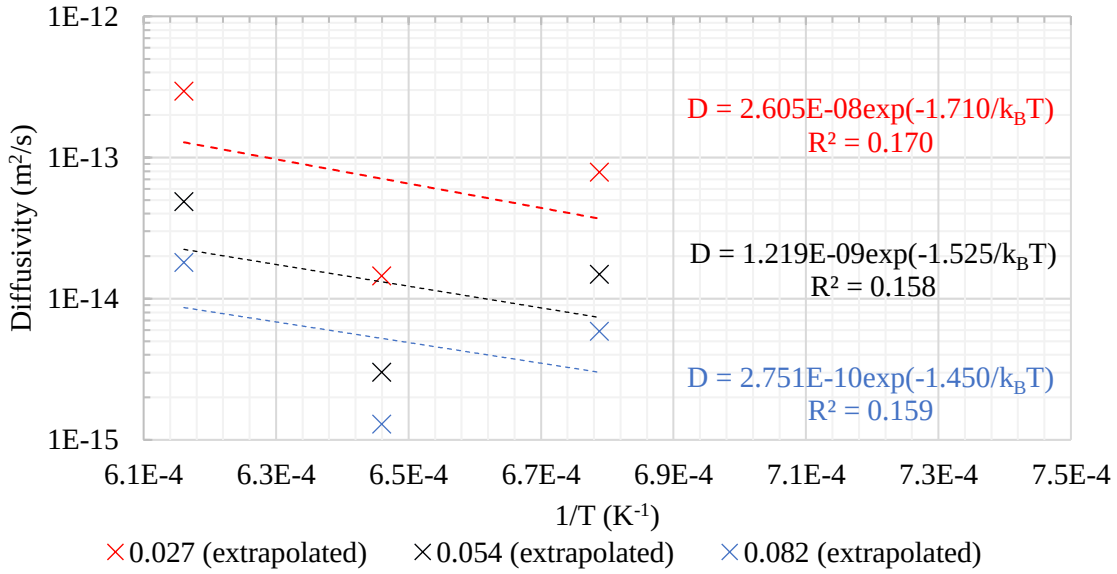

Figure 7.11 - Arrhenius fits of the extrapolated values at scenario 1 and the different Ti compositions in the crucible: low estimate (0.027 mol/m^3), proposed by manufacturer (0.054 mol/m^3) and high estimate (0.082 mol/m^3).

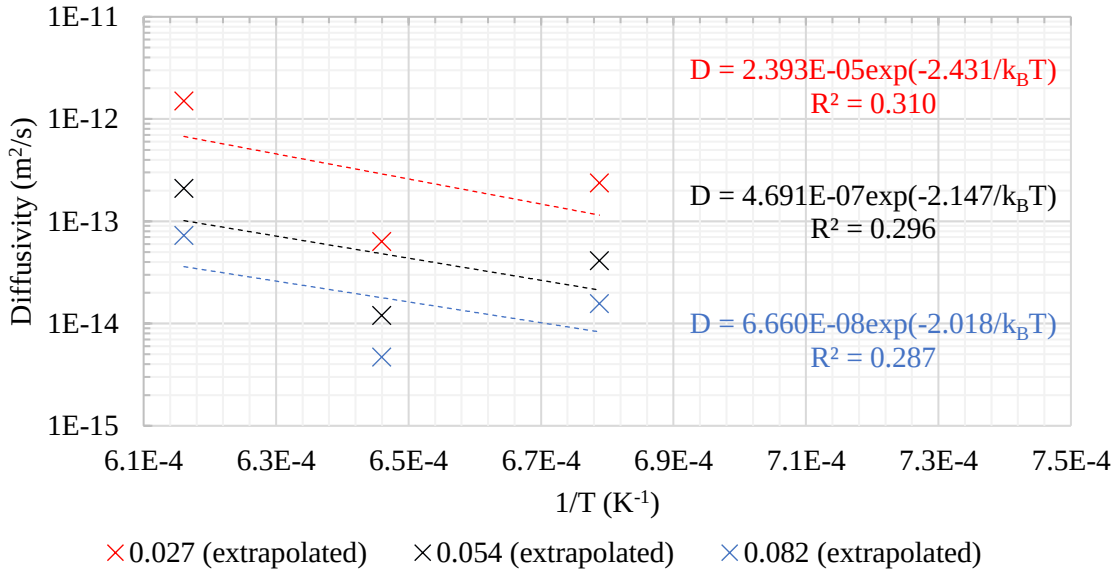

Figure 7.12 - Arrhenius fits of the extrapolated values at scenario 2 and the different Ti compositions in the crucible: low estimate (0.027 mol/m^3), proposed by manufacturer (0.054 mol/m^3) and high estimate (0.082 mol/m^3).

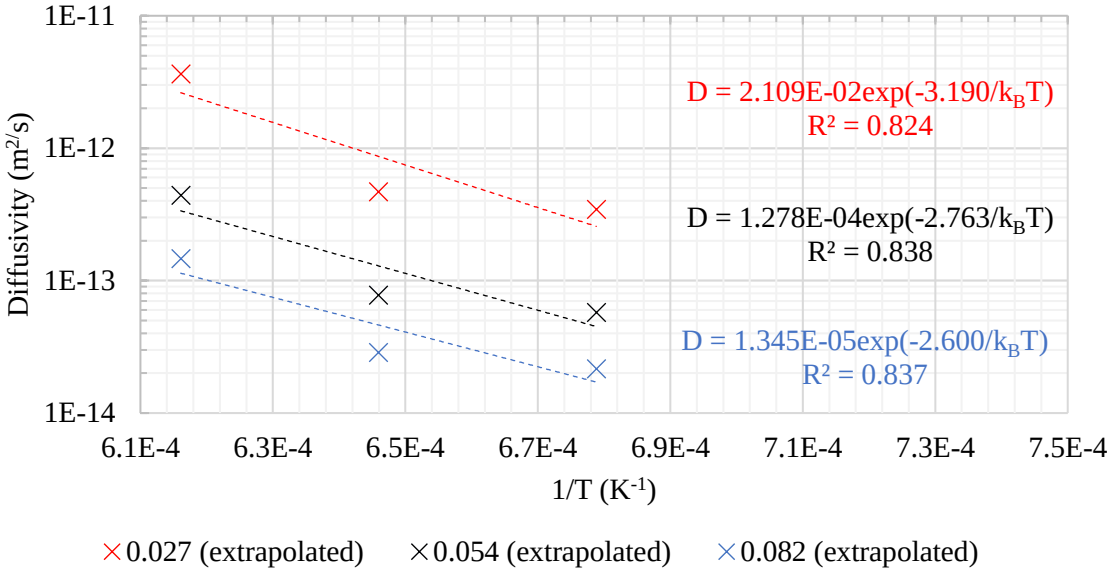

Figure 7.13 - Arrhenius fits of the extrapolated values at scenario 3 and the different Ti compositions in the crucible: low estimate (0.027 mol/m^3), proposed by manufacturer (0.054 mol/m^3) and high estimate (0.082 mol/m^3).

Applying the assumption of a heat treatment at a constant temperature for the method in Appendix B led to the following deviations, according to Appendix C. As seen previously in Table 5.2, the difference increases for shorter heat treatments and higher diffusivities, still in a manner that suggests diffusion coefficients close to the estimates:

Table 7.6 - Relative change of the estimates for Ti amount in silicon, for the varying profile in comparison with the constant temperature assumption, resulting from the extrapolations

Scenario	Ti content in the crucible (mol/m^3)	T_{ht} (ºC)	t_{ht} (min)	$\frac{n - n_{T=const}}{n_{T=const}}$ (%)
1	0.027	1200	180	-0.007%
		1275	180	-0.010%
		1350	60	-0.039%
		1350	12	-0.257%
	0.054	1200	180	0.033%
		1275	180	0.030%
		1350	60	0.112%
		1350	12	0.830%
	0.082	1200	180	0.055%
		1275	180	0.051%
		1350	60	0.205%
		1350	12	1.543%
2	0.027	1200	180	-0.112%
		1275	180	-0.112%
		1350	60	-0.406%
		1350	12	-2.507%
	0.054	1200	180	-0.082%
		1275	180	-0.084%
		1350	60	-0.317%
		1350	12	-2.117%
	0.082	1200	180	-0.066%
		1275	180	-0.068%
		1350	60	-0.263%
		1350	12	-1.895%
3	0.027	1200	180	-0.179%
		1275	180	-0.173%
		1350	60	-0.608%
		1350	12	-3.677%
	0.054	1200	180	-0.155%
		1275	180	-0.155%
		1350	60	-0.570%
		1350	12	-3.612%
	0.082	1200	180	-0.144%
		1275	180	-0.144%
		1350	60	-0.542%
		1350	12	-3.612%